

## Chapter-VI

### AC Conductivity Studies

---

*This chapter deals with the frequency dependent ac conductivity and the relaxation effect of three different series at different temperatures, frequency and composition range. Scaling of the conductivity spectra is also performed using scaling process. Dielectric and modulus spectra are also used to analyze the obtained results.*

## **6.1 INTRODUCTION:**

AC conductivity is one of the studies carried out on solids in order to characterize the bulk resistance of the crystalline samples. Measurement of ac conductivity can be done by different techniques. The currently used technique is the complex impedance spectroscopy which provides the information on electrical properties of materials and their interface with electronically conducting electrodes. It may be used to investigate the dynamics of bound or mobile charge in the bulk or interfacial regions of any kind of solid or liquid material: ionic, semiconducting, mixed electronic-ionic and even insulators (dielectrics). The complex impedance spectroscopy measurement of ac conductivity is based on studies made on the measurement of cell impedance/admittance over a range of temperatures and frequencies and analyzing them in complex impedance plane [1, 2]. This is particularly characterized by the measurement and analysis of  $Z$  (impedance),  $Y$  (admittance) and plotting of these functions in the complex plane, known as Nyquist diagrams.

In the past, Sluyter et. al. [3] have extensively used complex impedance spectroscopy technique to study the polarization phenomenon of aqueous electrochemical cells. Thereafter, it has been considered to be one of the most powerful tool to analyze electrochemical processes in the field of aqueous electrochemistry [4- 7]. For the first time, this technique had been applied by Bauerle [1] to study the basic polarization process in the cell of yttria stabilized zirconia (YSZ). Since then, complex impedance spectroscopy had been in use for characterizing a wide range of electrolyte and electrode materials, which include polymers, oxides, glasses, polycrystalline and composites.

Impedance spectroscopy has become a basic and ideal technique to characterize the solid electrolyte material [2] where the frequency dependent impedance data give the information about the bulk conductivity and the overall transport process of the solid electrolytes. The applied AC voltage and the resulting current across a cell have the form

$$V = V_{max} \sin (\omega t) \quad \dots\dots\dots(6.1)$$

$$I = I_{max} \sin (\omega t + \phi) \quad \dots\dots\dots(6.12)$$

where  $\phi$  is the phase angle and  $\omega=2\pi f$ ,  $f$  is the frequency of measurement. The phase angle  $\phi$  corresponds to the phase difference between the applied voltage and current. Thus, the magnitude of impedance is given by  $|Z| = V_{max}/I_{max}$ . The impedance is composed of a frequency independent resistive term  $R$  and a capacitive term  $1/j\omega C$ , where  $j = \sqrt{-1}$ . The absolute value  $|Z|$  and the phase angle  $\phi$  are related to real and imaginary parts of the impedance ( $Z'$  and  $Z''$ ) as follows:

$$Z' = |Z| \cos \phi \quad \dots\dots\dots(6.13)$$

$$Z'' = |Z| \sin \phi \quad \dots\dots\dots(6.14)$$

The projection of real and imaginary parts of impedance on the x and y axis is known as complex impedance plane (Fig.6.1) which is an implicit function of frequency. In ac, the resistance,  $R$ , is replaced by the impedance,  $Z$  and can be written as

$$Z^* = Z' - jZ'' \quad \dots\dots \quad (6.15)$$

where  $Z'$  is the real part and  $Z''$  the imaginary part of  $Z^*$ .

The impedance  $Z(\omega)$  has both magnitude  $|Z|$  and phase angle  $\phi$  and can be expressed in both polar as well as Cartesian forms.

In Polar form, Impedance  $Z(\omega)$  may be written as

$$Z(\omega) = |Z| \exp(-j\phi), \quad \dots\dots\dots (6.16)$$

where phase angle ( $\phi$ ) is expressed as  $\phi = \tan^{-1}\left(\frac{Z''}{Z'}\right)$ , magnitude

$$|Z| = [(Z')^2 + (Z'')^2]^{1/2} \text{ and } \exp(-j\phi) = \cos(\phi) - j\sin(\phi).$$

In Cartesian form,

$$Z(\omega) = |Z|[\cos(\phi) - j\sin(\phi)] = Z' - jZ'' \quad \dots\dots\dots (6.17)$$

The data is computed and displayed in the complex plane in the form of real and imaginary component as an implicit function of frequency and is called the *complex impedance plot*. Some complex impedance plots corresponding to R, C and RC circuit network, which form the basis for the conductivity measurements in the electrochemical cells, are shown in the Fig. 6.12. There are several other measured or derived quantities related to impedance which often play important roles in Impedance Spectroscopy. First is admittance ( $Y^*$ )

$$Y^* = 1/Z^* = Y' + jY'' \quad \dots\dots\dots (6.18)$$

The two other quantities complex dielectric constant or dielectric permittivity ( $\epsilon^*$ ) and the modulus function ( $M^*$ ) are usually defined as

$$\epsilon^* = 1/M^* = 1/(j\omega C_0 Z^*) = \epsilon' - j\epsilon'' \quad \dots\dots\dots (6.19)$$

$$M^* = j\omega C_0 Z^* = M' + jM'' \quad \dots\dots\dots (6.20)$$

In these expressions  $C_0 = \epsilon_0 \left(\frac{A}{t}\right)$  is the capacitance of the empty measuring cell of electrode area  $A$  and thickness  $t$ . The quantity  $\epsilon_0$  is the dielectric permittivity of free space,  $8.854 \times 10^{-12}$  F/m.

The modulus function  $M^* = 1/\epsilon^*$  was apparently first introduced by Schrama [8] and has been used appreciably by Mc Crum et.al. [9], Macedo et.al. [10] and

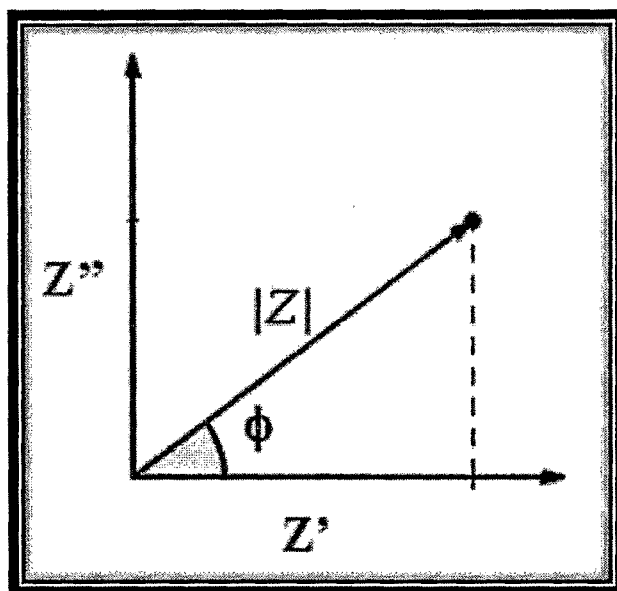


Fig. 6.1. Impedance plot in complex plane.

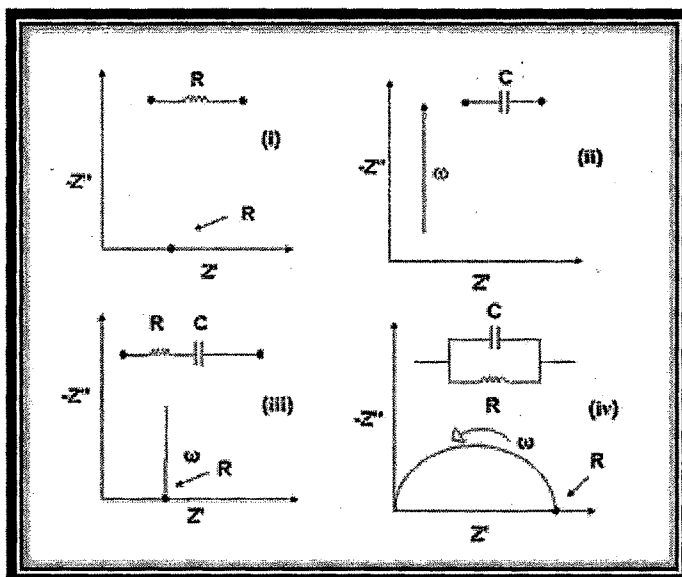


Fig.6.12. Complex Impedance plots for some elementary R, C and RC circuits.

Hodge et. al. [11, 12]. Cole and Cole [13] were the first to plot permittivity in the complex plane. AC Conductivity studies on many systems based on silver oxide such as AgI-Ag<sub>2</sub>O-SeO<sub>2</sub>-V<sub>2</sub>O<sub>5</sub> [14], AgI-Ag<sub>2</sub>O-B<sub>2</sub>O<sub>3</sub> [15], AgI-Ag<sub>2</sub>O-V<sub>2</sub>O<sub>5</sub> [16], AgI-Ag<sub>2</sub>O-P<sub>2</sub>O<sub>5</sub>-MoO<sub>3</sub> [17], AgI-Ag<sub>2</sub>O-B<sub>2</sub>O<sub>3</sub>-V<sub>2</sub>O<sub>5</sub> [18], AgI-Ag<sub>2</sub>O-B<sub>2</sub>O<sub>3</sub>-TeO<sub>2</sub> [19], PbI<sub>2</sub>-Ag<sub>2</sub>O-Cr<sub>2</sub>O<sub>3</sub> [20] have been studied widely. It is observed that the relaxation effect in these glasses is due to the motion of the mobile species i.e., Ag<sup>+</sup> ions, rather than by the rotation of the dipoles and is termed as conductivity relaxation. In order to obtain a better insight of the relaxation properties of the materials, typical impedance data of the Silver based Barium Vanado-Tellurite glasses has been analyzed under conductivity, permittivity and modulus formalisms over a range of frequency, temperature and composition.

## **6.2 CONDUCTIVITY FORMALISM:**

### **6.2.1 Complex Impedance Analysis:**

Ionic conductivity can be visualized as a series process involving consecutive hops of an ion over potential energy barriers along the direction of the electric field [10]. This can be modeled as a parallel RC circuit and the admittance of the circuit is given by

$$Y^* = (Z^*)^{-1} = R^{-1} + j \omega C \quad \dots\dots\dots (6.21)$$

or 
$$\frac{1}{Z} = \frac{1}{R} + j\omega C \quad \dots\dots\dots(6.22)$$

so that 
$$Z = \frac{R}{(1 + j\omega CR)} \quad \dots\dots\dots(6.23)$$

Simplifying the above expression (6.23) by using complex conjugate, gives

$$Z = \frac{R(1 - j\omega CR)}{1 + (\omega CR)^2} \quad \dots\dots\dots(6.24)$$

so that  $Z' = \frac{R}{1 + \omega^2 R^2 C^2} \quad \dots\dots\dots(6.25)$

and  $Z'' = \frac{\omega R^2 C}{1 + \omega^2 R^2 C^2} \quad \dots\dots\dots (6.26)$

when  $\omega=0$ ,  $Z'=R$  and  $Z''=0$  and when  $\omega=\infty$ ,  $Z'=0$  and  $Z''=0$ . Between these extreme values it can be seen that  $Z'$  and  $Z''$  comply with the following Eq.

$$\frac{R^2}{4} = \left( Z' - \frac{R}{2} \right)^2 + Z''^2 \quad \dots\dots\dots (6.27)$$

This is an equation of a circle with radius  $R/2$  and centre at  $(R/2, 0)$  as shown in Fig.6.13 (a). It represents the response of a resistor  $R$  in parallel with capacitor  $C$  which will be a perfect semicircle intersecting the real axis at  $(R, 0)$ .

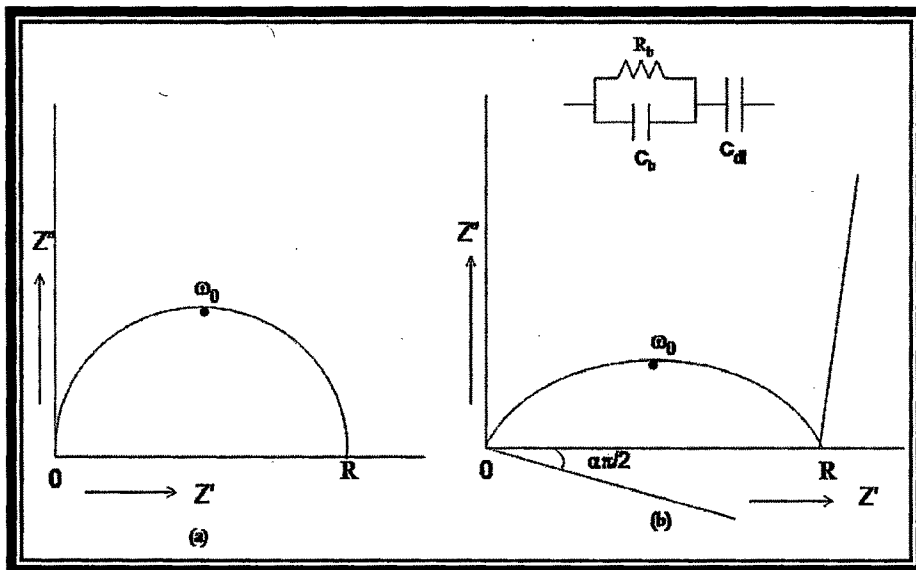


Fig. 6.13. Geometric response for an (a) ideal circuit (b) distributed elements.

The relaxation time  $\tau_0=1/\omega_0=RC$  is given by the inverse of frequency  $\omega_0$  at the top of the semicircle. A wide range of materials so reported [21] have shown a depressed semicircle in the impedance spectrum. In order to explain the depression of the semicircle, a new circuit element called *constant phase element* (CPE) has been introduced [2]. For cole-cole distribution of relaxation times the real and imaginary parts of impedance are given by

$$Z' = \frac{R \{ (1 + \omega \tau_0)^{-\alpha} \sin(\alpha \pi / 2) \}}{1 + 2(\omega \tau_0)^{1-\alpha} \sin(\alpha \pi / 2) + (\omega \tau_0)^{2(1-\alpha)}} \quad \dots\dots\dots(6.28)$$

$$Z'' = \frac{R \{ (\omega \tau_0)^{1-\alpha} \cos(\alpha \pi / 2) \}}{1 + 2(\omega \tau_0)^{1-\alpha} \sin(\alpha \pi / 2) + (\omega \tau_0)^{2(1-\alpha)}} \quad \dots\dots\dots(6.29)$$

$$\left( Z' - \frac{R}{2} \right)^2 + \left( Z'' - \frac{R \tan(\alpha \pi / 2)}{2} \right)^2 = r^2 \quad \dots\dots\dots(6.30)$$

$$r^2 = \left( \frac{R}{2} \right)^2 + \left( \frac{R}{2} \right)^2 (\tan(\alpha \pi / 2))^2 \quad \dots\dots\dots(6.31)$$

This is an equation of a circle with center at  $[R/2, R \tan (\alpha \pi / 2) / 2]$  with radius  $r$ . Thus, the impedance response of the above circuit or cole-cole distribution [13] would be an arc depressed below the real axis by an angle  $\alpha \pi / 2$  and intersecting it at  $(R, 0)$  as shown in Fig. 6.13 (b). The co-ordinates at the top of the arc are  $R/2$  and  $R/2 [(\cos \alpha \pi / 2) / (1 + \sin \alpha \pi / 2)]$ .

Complex Impedance measurements were carried out to determine the electrical conductivity and the ac behavior of the present glasses over a range of temperature and frequencies. Fig.6.14 shows the complex impedance plot obtained for the first series  $x$  (BaO:1.5 Ag<sub>2</sub>O)-(95-x) V<sub>2</sub>O<sub>5</sub>-5 TeO<sub>2</sub> with  $x=25\%$  of the modifier at different temperatures which clearly shows two semicircles.

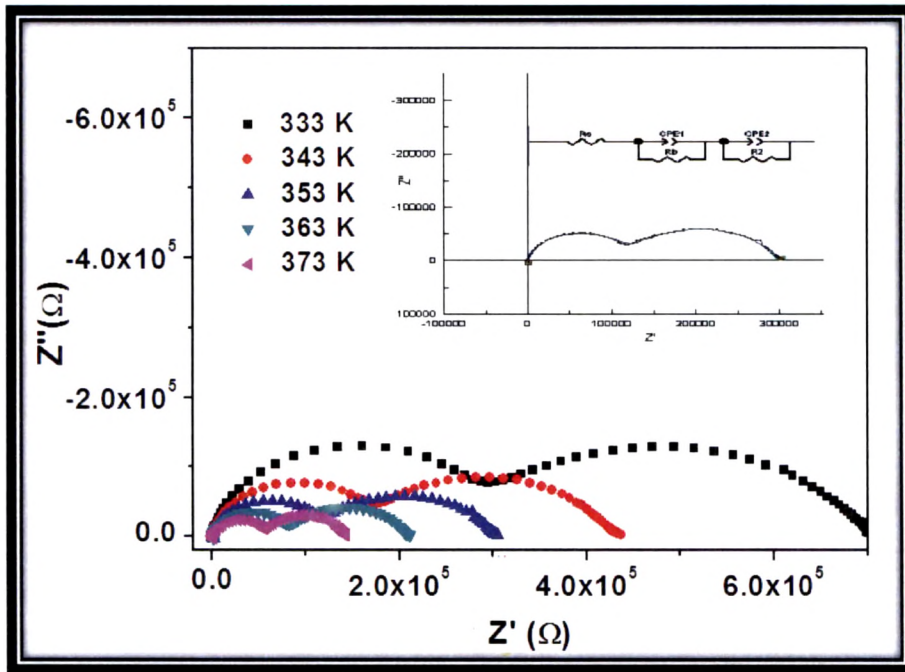


Fig. 6.14: Plot of  $Z'$  vs.  $Z''$  for  $x=25$  mol % at different temperatures for first series.

The high frequency depressed semicircle is a parallel combination of bulk resistance ( $R_b$ ) and constant phase element (CPE) in series with another parallel combination of CPE and resistance for second semicircle at low frequency [22, 23]. The value of  $R_s$  is very low in the range of  $10^{-4}$ . The equivalent circuit is shown in the inset of Fig.6.14. The element CPE is considered as a leaky capacitor (i.e., hybrid between a resistor and a capacitor) and the admittance of CPE [24, 25] is defined as

$$Y_{CPE} = A_0 (j\omega)^n \quad \dots\dots\dots(6.32)$$

Here  $j$  is the imaginary unit,  $A_0$  is the prefactor of the CPE and  $n$  is its exponent. The exponent  $n$  of the CPE may vary between 0 and 1 and is usually found around

0.8 [26]. When  $n=0$ ,  $A_0=1/R$  and for  $n=1$ ,  $A_0=C$ .

The above equation can also be written as

$$Y_{CPE} = A\omega^n + jB\omega^n \dots\dots\dots(6.33)$$

where the parameters  $A$  and  $B$  are given by  $A=A_0 \cos(n\pi/2)$  and  $B=A_0 \sin(n\pi/2)$ .

The necessity of using constant phase elements (CPEs) [27] rather than ordinary capacitors, to fit the spectra, is consequence of the fact that the centers of experimental semicircles lie below the  $Re(Z)$  axis which revealed that the associated relaxations of ions are of non-Debye in nature. It is observed that with the increase in temperature, the intercept of the low frequency arc on the real axis shifts towards the origin i.e., the bulk resistance of the sample decreases with increase of temperature and thus conductivity increases. This bulk conductivity is calculated from the sample dimensions and bulk resistance ( $R_b$ ) obtained from

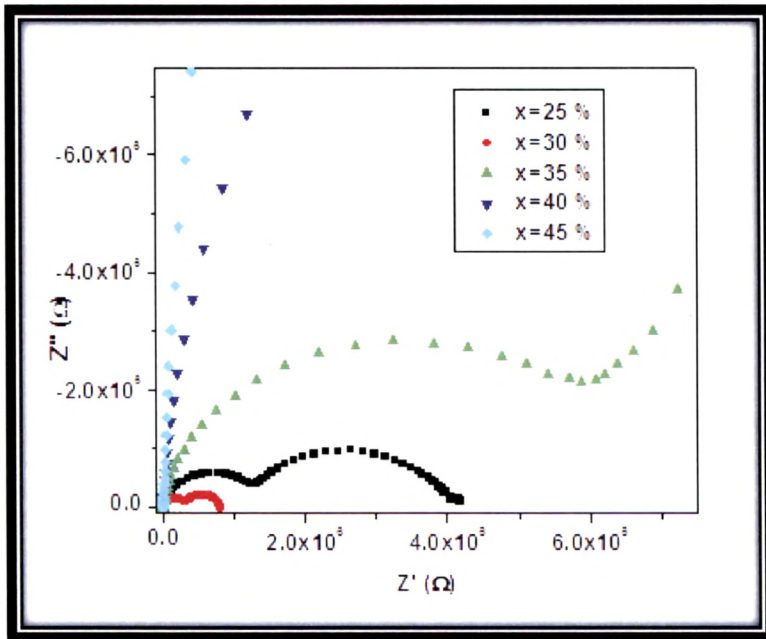
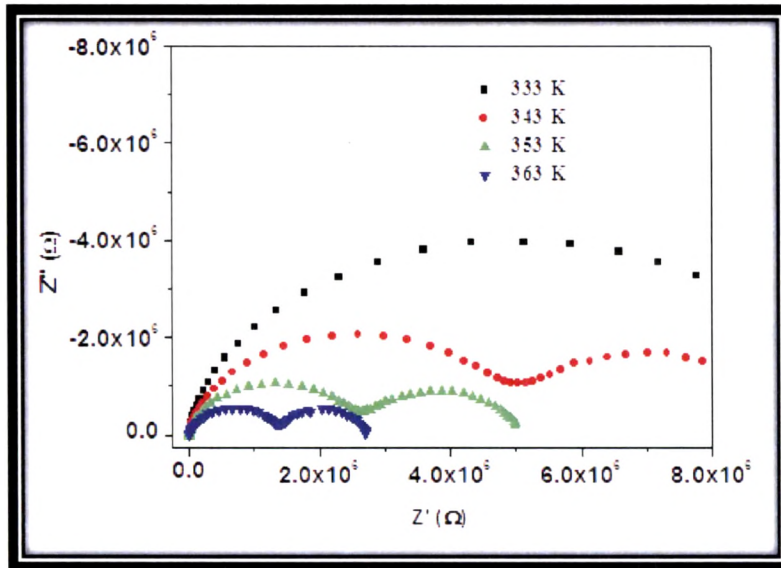


Fig. 6.15: Impedance plot for all the samples of first series.

analyzed data. Impedance plot for all samples of first series is shown in Fig. 6.15. In this series, for  $x=25-35$  mol % samples, the impedance plots consist of two semicircle at higher as well as at lower frequency region, while for  $x=40$  and  $45$  mol % two semicircles exist only for temperature above  $353$  K. From the figure, it is clear that the resistance of the samples increases continuously with increasing modifier content except for  $x=30$  mol %, where the resistance of the sample decreases and shows slightly high dc conductivity with respect to  $x=25$  mol % sample, whereas for other samples, dc conductivity decreases continuously due to increasing resistance of the sample.

Figs. 6.16 and 6.17 show the impedance plot of second series  $10 \text{ BaO}-y \text{ Ag}_2\text{O}-(85-y)\text{V}_2\text{O}_5-5 \text{ TeO}_2$  for  $y=35$  mol% and  $y=50$  mol % of  $\text{Ag}_2\text{O}$  at different temperatures respectively. The impedance of the glass with  $y=35$  mol % of  $\text{Ag}_2\text{O}$  contains two arcs. The first one is related to the bulk conductivity and the second



**Fig.6.16: Impedance plot for  $y=35$  % sample for second series.**

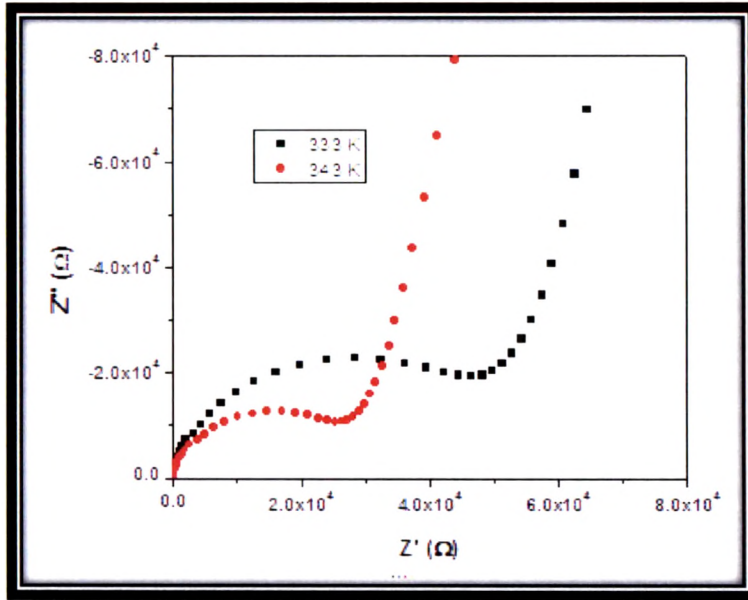


**Fig. 6.17: Impedance plot for  $y=50$  % sample for second series.**

arc is due to the interfacial phenomenon on the boundary of glass silver electrode. The impedance plot of the glass with  $y=50$  mol % of  $\text{Ag}_2\text{O}$  consists of one arc and a spur at low frequencies. The spur is due to the interfacial polarization and is a proof of ionic conductivity appearance. The centers of arcs are displaced below the real axis. The reason for that is the presence of a distribution in relaxation times. The bulk resistance values are determined from the real axis intercept at the low frequency side. The Figure shows that the real axis intercept of the impedance plot is shifted towards the origin with increase of temperature, i.e., the resistance value decreases with increase of temperature. Fig. 6.18 shows the impedance plot obtained for all samples of the second series which shows that resistance increases clearly for  $y=20$  % to  $y=30$  %, above which it decreases with the addition of

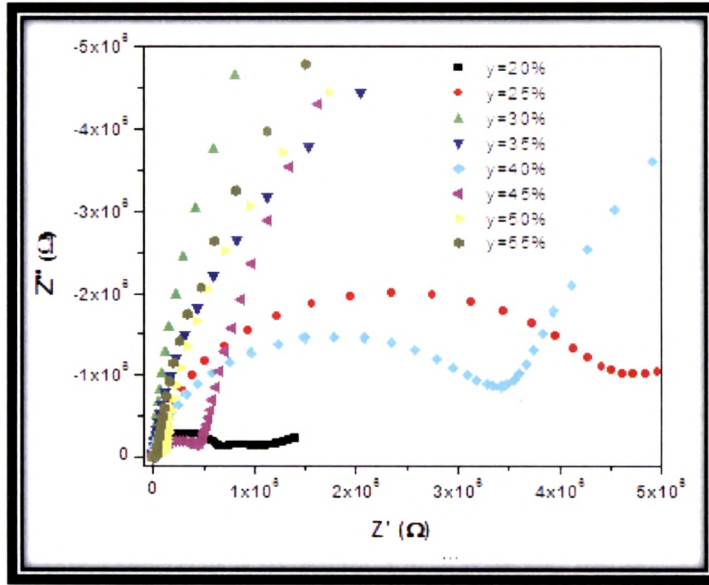


**Fig. 6.18: Impedance plot for all samples of second series.**

$\text{Ag}_2\text{O}$  in the system as seen from the shifting of the intercept towards origin. In this series all samples show two semicircles except for  $y=30$  and  $35$  mol %, in which two semicircles are observed at temperature above  $333$  K. This is due to the low conductivity of the samples. It is clear from the figure that the system with  $y=55$  mol % has a lower side intercept on the real axis and is regarded as the highest conducting system in the second series. It is also evident from transport number studies (Fig. 4.25) that the dominance of  $t_e$  over  $t_{\text{Ag}}$  is observed upto  $30$  mol% where conductivity of the samples decreases afterwards the dominance of  $t_e$  is taken over by  $t_{\text{Ag}}$ , where conductivity starts increasing, leaving a minima at around  $y=30$  mol%.

Similarly, in the third series  $5 \text{ BaO}-z \text{ Ag}_2\text{O}-35 \text{ V}_2\text{O}_5-(60-z) \text{ TeO}_2$ , where the

amount of  $\text{TeO}_2$  is varied in the samples, and the amount of  $\text{BaO}$  is also reduced to 5 mol%, the impedance spectrum for  $z= 55$  mol % of  $\text{Ag}_2\text{O}$  at different temperature is shown in Fig. 6.19. The Figure shows a continuous decrease in the value of resistance with the increase of temperature. The high frequency semicircle arises from the bulk relaxation and the low frequency spike is due to the interfacial effects. With the increase of temperature, the size of the semicircle decreases as expected and the real axis intercept of the plot shifts towards the origin. Fig. 6.20 shows the characteristic impedance plots obtained for all the samples of the third series. In third series  $z= 25$  mol% sample shows one semicircle in all the studied temperature range. For  $z= 30$  mol% sample, two semicircles appear at temperature above 313 K while rest of the samples show two semicircles even at room temperature and above. Figure shows a continuous

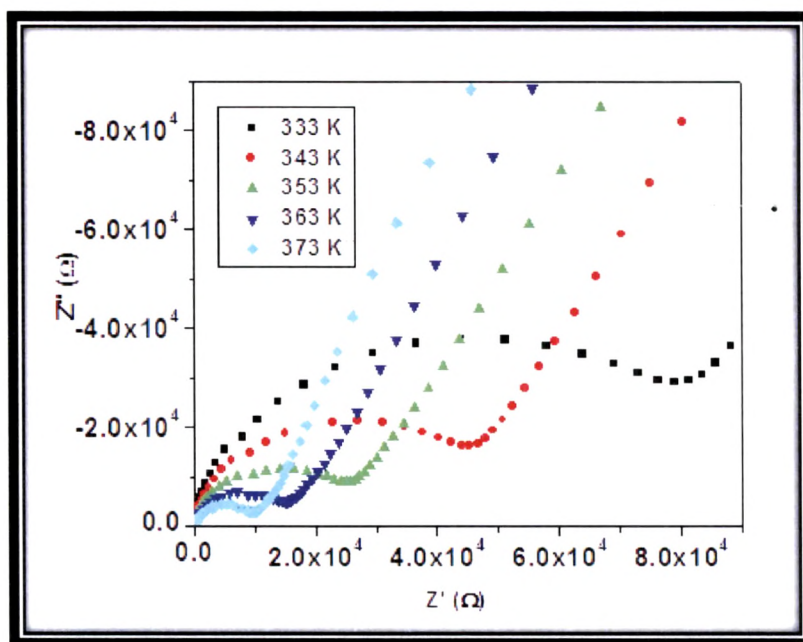
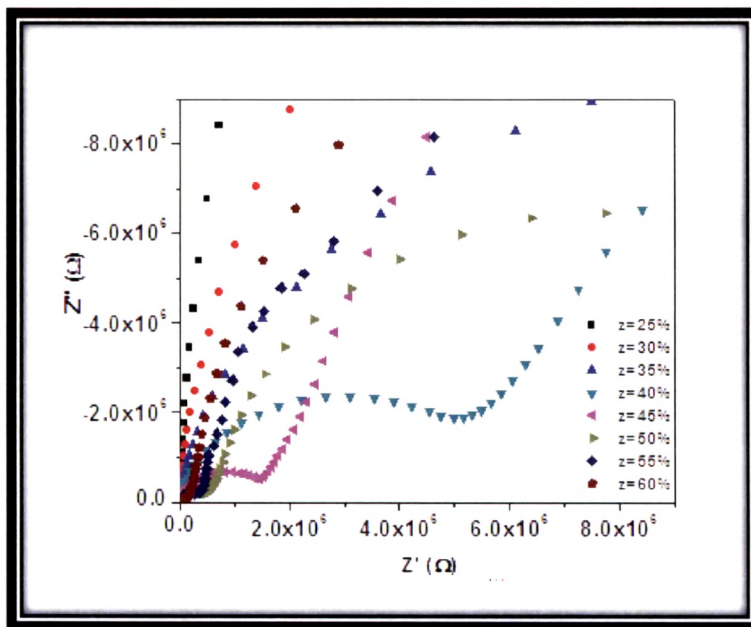


Fig. 6.19: Impedance plot for  $z=55\%$  sample of third series.



**Fig. 6.20: Impedance plot for all samples of third series.**

change in the value of the resistance with increasing  $\text{Ag}_2\text{O}$  mol % in this series and the system with  $z = 60$  mol % has a lower side intercept on the impedance spectrum and is regarded as the highest conducting system in this series. The silver ion transport number ( $t_{\text{Ag}}$ ) is observed to be higher than electronic transport number ( $t_e$ ) for all the samples of this series. From the Fig.4.26, it is clear that the dominance of  $t_{\text{Ag}}$  over  $t_e$  increases with the increase of  $\text{Ag}_2\text{O}$  content as conductivity also increases continuously with modifier  $\text{Ag}_2\text{O}$ .

### **6.2.2 Frequency dependent conductivity studies:**

Conductivity is a complex quantity and can be represented by

$$\sigma^* = \sigma' + j \sigma'' \quad \dots\dots\dots(6.34)$$

$$= \frac{t}{A} \left[ \frac{1}{R} + j\omega C \right] \quad \dots\dots\dots(6.35)$$

$$= \frac{t}{A} [Y' + jY''] \quad \dots\dots\dots (6.36)$$

where  $t$  is the thickness and  $A$  is the area of the sample respectively. Thus, the admittance data has direct relevance to extract real and imaginary parts of conductivity. If we consider parallel  $R$ - $C$  element, the conductivity should be independent of frequency and is equal to  $\left( \frac{t}{A} \times \frac{1}{R} \right)$ .

Frequency dependent conductivity spectra for the glass system of first series  $x$  (BaO: 1.5 Ag<sub>2</sub>O)-(95- $x$ ) V<sub>2</sub>O<sub>5</sub>-5 TeO<sub>2</sub> with  $x= 25$  mol % and 40 mol % of the modifier ratio at different temperatures are shown in Figs. 6.21 and 6.22. Similar behavior is also reported for other silver based ionic conductors [28-32]. The conductivity is found to be increasing with increase of temperature. It is observed that at low frequencies variation of conductivity is due to electrode polarization effects at the electrode-glass interfaces [28]. More and more charge accumulation starts occurring at electrode and glass interface when frequency is decreased which leads to a drop in conductivity at low frequencies. In the intermediate frequency region, the conductivity is almost independent of frequency and is identical to dc conductivity obtained from the complex impedance plots (zero frequency value of first semicircle). In the high frequency region, mobility of charge carriers, Ag<sup>+</sup> is high near to relaxation times and hence conductivity increases with frequency. It is also observed that as the temperature increases, the frequency at which the dispersion becomes prominent shifts to higher frequency region [33, 34]. Fig. 6.23 shows the conductivity versus frequency plot for all

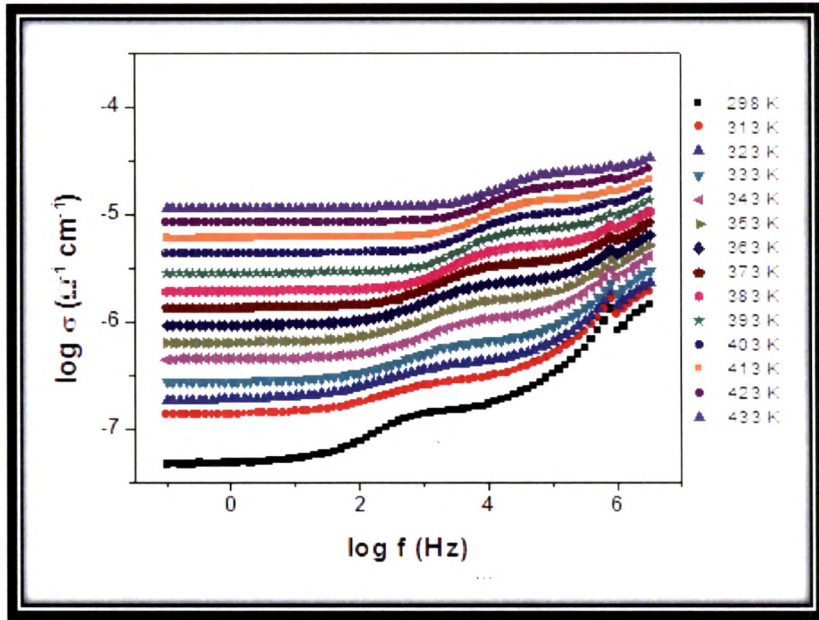


Fig. 6.21. Conductivity spectra for x=25 % sample of first series at different temperatures.

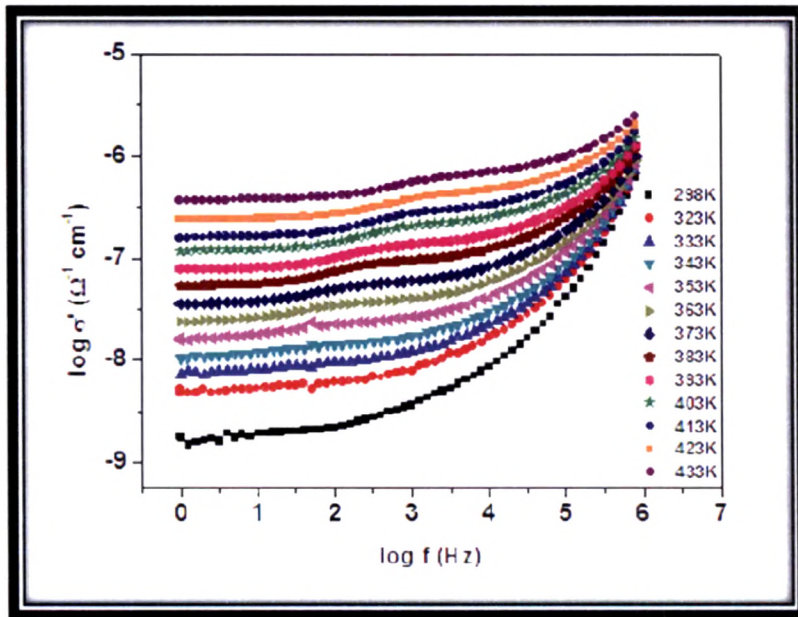
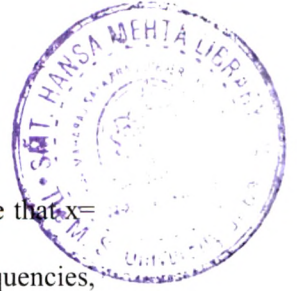


Fig.6.22. Conductivity spectra for x=40 % sample of first series at different temperatures.



samples of first series at room temperature. It is observed from the figure that  $x=$  25, 30 and 35 mol % samples show electrode polarization in low frequencies, frequency independent plateau region in mid frequency and frequency dispersion at higher frequencies while for  $x=$  40 and 45 mol% samples, low frequency dispersion is not available at room temperature because of the high resistivity of the samples. Figure also shows that the conductivity is found to decrease non linearly with the increase in modifier ratio except for  $x=30$  mol % sample which shows highest conductivity. Nishida et. al. [35] have studied the AgI containing glasses. At 30 mol %  $Ag_2O$ , their sample shows minimum conductivity and after that conductivity starts increasing due to reverse change occurring in the glass matrix from the one dimensional chain structure composed of  $VO_4$  tetrahedra to a

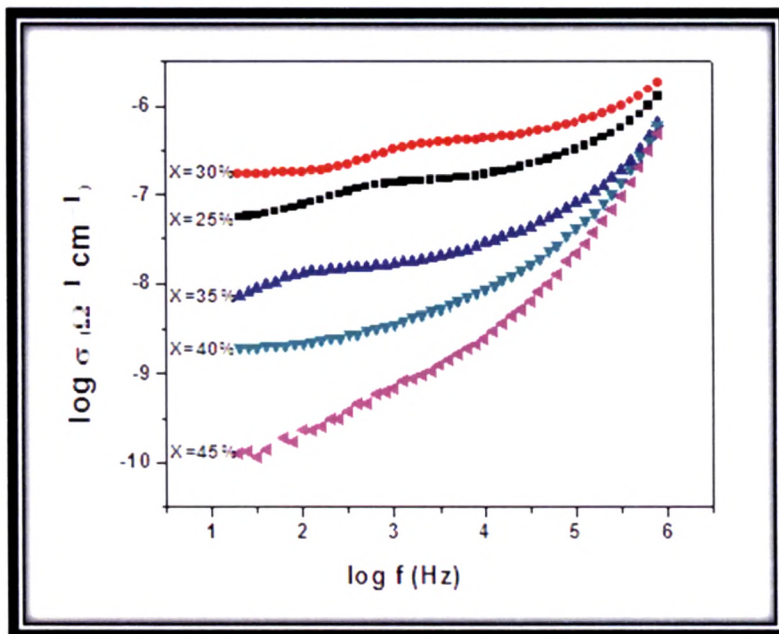


Fig. 6.23. Conductivity spectrum for all the samples of first series.

two or three-dimensional network structure composed of  $\text{VO}_4$  tetrahedra when the  $\text{Ag}_2\text{O}/\text{V}_2\text{O}_5$  ratio is greater than unity and for the same series, Mossbauer spectrum shows minimum in their quadrupole splitting. It is clear that the ac conductivity  $\sigma_{ac}(\omega)$  for all the samples exhibit the same characteristics of the curve with different conductivity values depending on the glass composition.

The conductivity plot for the second series  $10 \text{ BaO}-y \text{ Ag}_2\text{O}-(85-y) \text{ V}_2\text{O}_5-5 \text{ TeO}_2$  with  $y=40$  mol % at different temperatures is shown in Fig.6.24. The figure shows that the conductivity of the system increases with increase in temperature and the dispersion region obtained at higher frequencies are shifted to still higher range with temperature as expected for this kind of systems. The conductivity spectra for different compositions of this series at room temperature are shown in Fig.6.25. In this series, low frequency dispersion is not observable at room temperature for  $y=30$  and  $35$  mol % samples due to their high resistivity while for rest of the samples low frequency dispersion due to electrode polarization is clearly visible. In the mid frequency region, the conductivity plot is found to be almost independent of frequency approaching the dc conductivity and at high frequency region, conductivity increases continuously because at that frequency, the charge carrier gets excitation energy from the electrical signal. Due to this excitation energy, the mobility of the charge carrier increases, the relaxation time decreases and thus, the conductivity increases [36]. High frequency dispersion shifts to higher frequencies with increasing temperature. The frequency dispersion effects are present in all the samples which are clear from the figure. It is also visible that the conductivity decreases non-linearly with increasing modifier up to  $30$  mol %  $\text{Ag}_2\text{O}$ . After that conductivity increases with increasing modifier

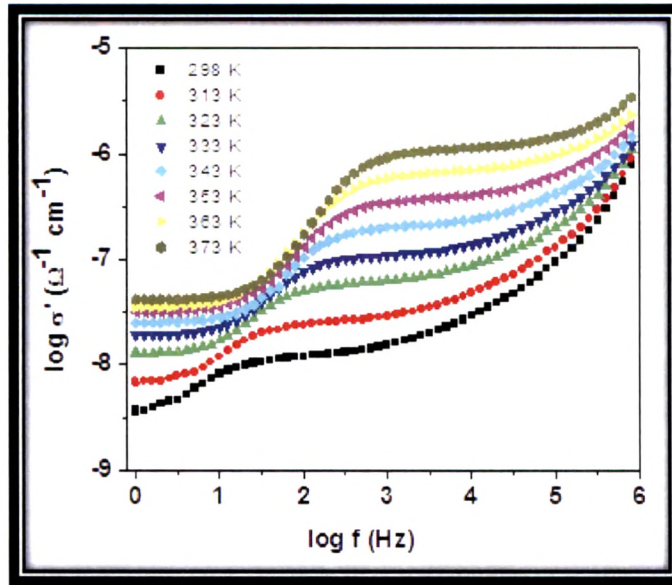


Fig.6.24. Conductivity spectra at different temperatures for  $y=40\%$  sample of second series.

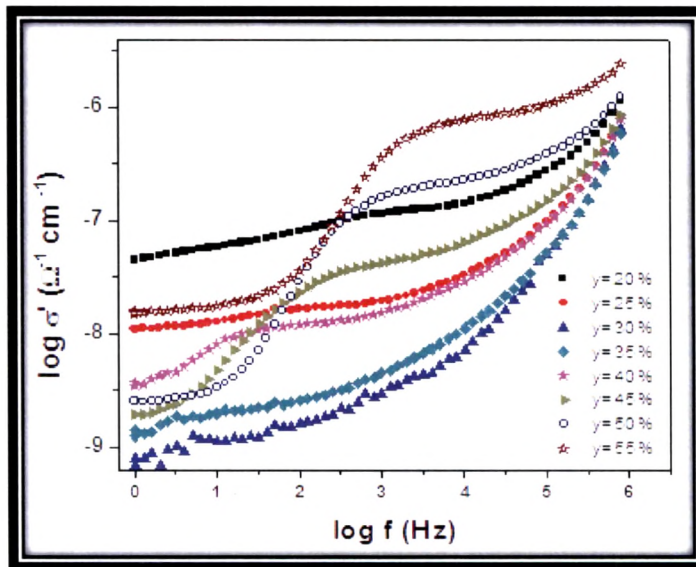


Fig.6.25. Conductivity spectra all samples of second series at 298 K.

content. Montani et. al. [37] have shown a deep minimum in the isotherm of conductivity in their silver based vanado-tellurite glass system and the explanation for this minimum was given assuming the existence of two kinds of independent migrating paths. One kind of path consisting of an electronic transfer in the chain  $V^{+4}-V^{+5}$  and the other kind of path made by the regular position of non-bridging oxygen along the network-former chains allowing the ion-displacement. This explanation is an alternative to the existence of an ion-polaron effect (chapter 5) as proposed by Bazan [38]. This transition is also expected due to the variation of dominance of ionic transport over electronic as observed in Fig.4.25.

The conductivity spectra obtained for  $z=25$  and  $35$  mol % of third series  $5BaO-zAg_2O-35V_2O_5-(60-z)TeO_2$  at various temperatures are shown in Figs.6.26 and 6.27. Here also the conductivity increases with the increase in temperature. For  $z=35$  mol % of  $Ag_2O$ , it is observed that at low frequencies, dispersion arises due to electrode polarization and mid frequency dispersion corresponds to the dc conductivity. At higher frequencies, conductivity increases due to the increase of mobility of charge carriers. It is clear that the high frequency dispersion shifts to higher frequency region with increasing temperature. However, for  $z=25$  mol % sample of  $Ag_2O$ , the low frequency dispersion is not observed in the frequency range measured, which may be due to the high resistivity of the sample. The conductivity spectra for all the samples of third series are shown in Fig.6.28 which clearly shows that the conductivity increases with increasing modifier content and a maximum conductivity is obtained for the system with  $z= 60$  mol % sample since the amount of  $BaO$  (kept at 5 %) and  $V_2O_5$  (at 35 %) are quite low as compared to other series. Here, the low frequency dispersion is not available for  $z= 25$  and  $30$  mol % samples.

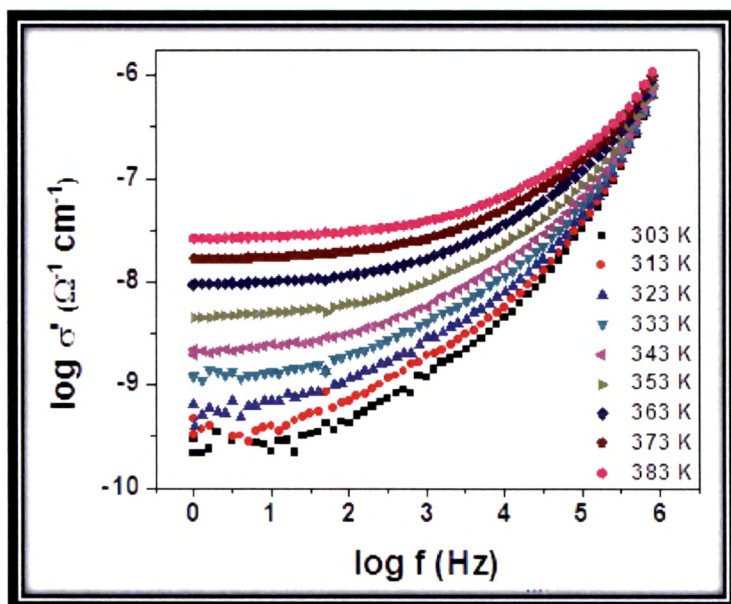


Fig.6.26. Conductivity spectra for  $z=25$  % sample of third series at different temperatures.

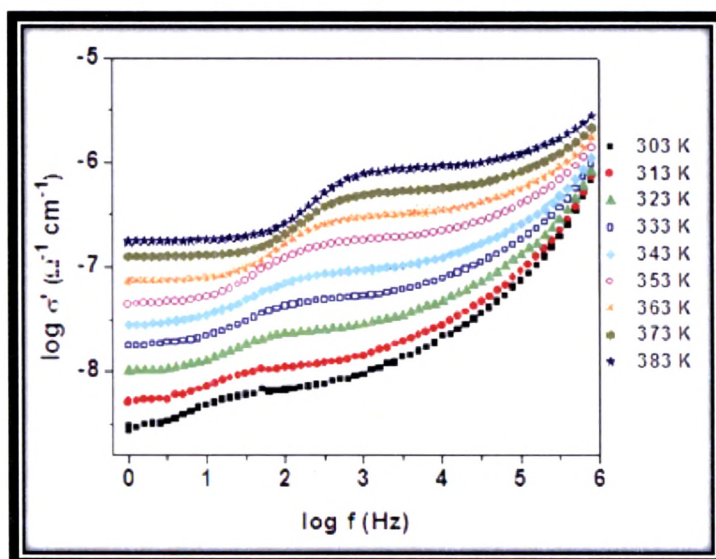
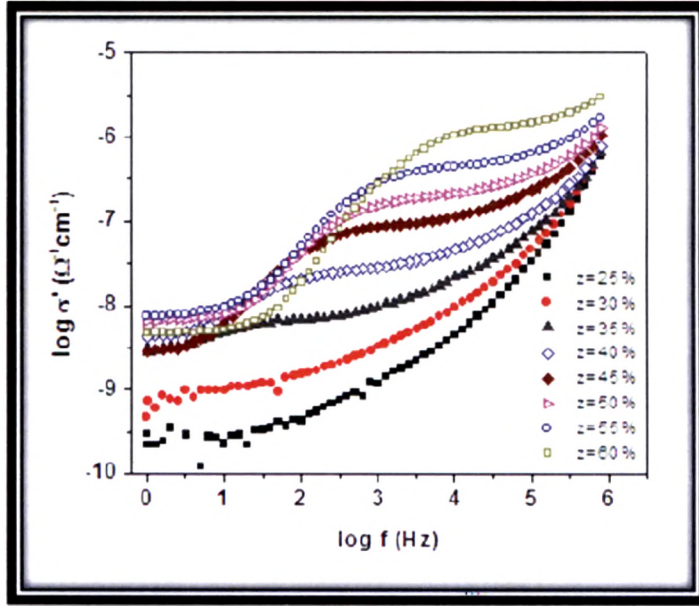


Fig.6.27. Conductivity spectra for  $z=35$  % sample of third series at different temperatures.



**Fig.6.28: Conductivity spectra for all samples of third series at 303 K.**

The frequency dependence of conductivity is a sum of dc conductivity due to the movement of free charges and polarization conductivity due to the movement of bound charges. With decreasing frequency, the conductivity  $\sigma(\omega, T)$  decreases and approaches the direct current conductivity  $\sigma_{dc}$ . The low conductivity value at low frequencies is related to the accumulation of ions due to the slow periodic reversal of the electric field. In the high frequency region, the power law nature  $\sigma(\omega) \propto \omega^b$  is observed and the conductivity sharply increases with frequency. The variation of conductivity with frequency may be expressed to the well known power law of ac behavior which indicates a non-random process, wherein the ion motion is correlated [39-42] given by the following equation,

$$\sigma(\omega) = \sigma_{dc} + A\omega^b \quad \dots\dots\dots(6.37)$$

where  $\sigma(\omega)$  is the conductivity at a particular frequency,  $\sigma_{dc}$  is the dc conductivity at zero frequency,  $A$  is a constant and  $n$  is the frequency exponent lies in the range of  $0 < n < 1$ . The above expression is known as the *power law of ac behavior*. Because the power law of ac behavior is observed in wide range of materials, Jonscher called it "*Universal Behavior*" [21, 43]. The Eq. 6.37 is accepted universally for considering the sample conductivity, hopping charges, frequency dependence of conductivity etc. The frequency exponent  $n$  was calculated from the slope of the plot  $\log(\sigma' - \sigma_{dc})$  versus  $\log \omega$ , which is a straight line. Since the calculated values of the exponent  $n$  lie in the range 0.6-0.9, the correlation motion is sub-diffusive and indicates a preference on the part of ions that has hopped away to return to where it started. The exponent is a measure of degree of interaction with the environment. Jonscher [44] had shown that a non zero  $n$  in the dispersive region of conductivity is due to the energy stored in the short range collective motion of ions. A higher  $n$  implies that large energy is stored in such collective motions. The magnitude of  $n$  appears to be associated with high degree of modification.

Fig. 6.29 shows the variation of power law exponent for the series  $x$  (BaO:1.5 Ag<sub>2</sub>O)-(95-x)V<sub>2</sub>O<sub>5</sub>-5TeO<sub>2</sub> at  $x= 40$  mol % at different temperatures. It is observed that the value of frequency exponent  $n$  is unity at cryogenic temperatures [45] while, in most of the systems it was evident that the  $n$  value decreases with temperature and then level off in the neighborhood of 0.5 [46] but in our case figure clearly shows that frequency exponent  $n$  increases with temperature. Some glasses investigated by Ganguli et. al. [47] have exhibited similar trend of increasing  $n$  as a function of temperature. No full explanation of this behavior is

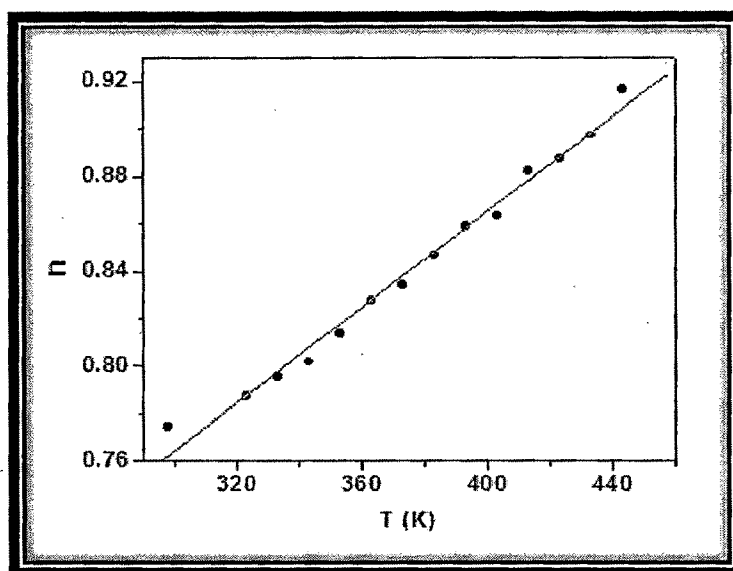


Fig.6.29. Variation of the parameter  $n$  with temperature for  $x=40$  mol % sample of first series.

known. In the second series  $10 \text{ BaO-y Ag}_2\text{O- (85-y) V}_2\text{O}_5\text{- 5TeO}_2$ , where BaO and  $\text{TeO}_2$  are kept constant at 10 and 5 mol % respectively, frequency exponent  $n$  is independent of temperature, as it is clear from Fig. 6.30. The increasing trend of  $n$  (similarly as in first series) with temperature is also visible in third series  $5 \text{ BaO-z Ag}_2\text{O- 35 V}_2\text{O}_5\text{- (60-z) TeO}_2$ , where  $\text{Ag}_2\text{O}$  is increasing with respect to  $\text{TeO}_2$ , as shown in Fig. 6.31. The value of frequency independent dc conductivity ( $\sigma_{dc}$ ), frequency exponent  $n$  and constant  $A$  at room temperature for all the samples of three different series are given in Table.6.1 (a), (b) and (c). The  $n$  values clearly show that they are independent of composition but lies in the range of 0.65-0.78. In the jump diffusion model [48], the frequency exponent is determined by the

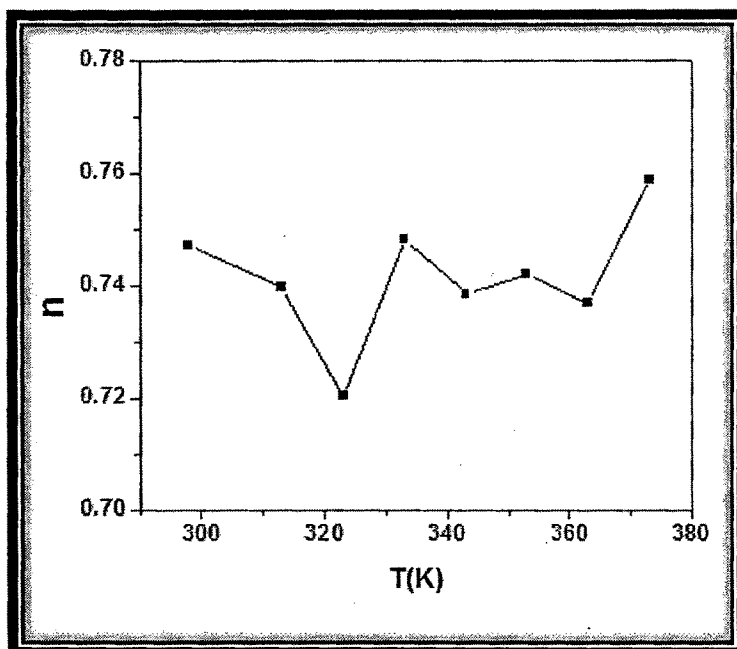


Fig.6.30. Variation of the parameter  $n$  temperature for  $y=25$  mol % sample of second series.

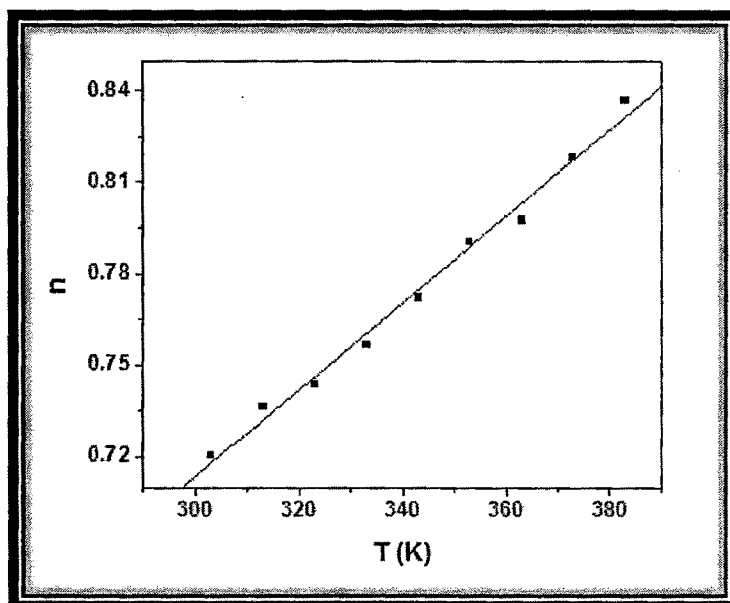


Fig.6.31. Variation of the parameter  $n$  with temperature for  $z=45$  % sample of third series.

**Table.6.1 (a): Values of the dc conductivity, frequency dependent conductivity parameters  $A$  and  $n$  for the system  $x(\text{BaO}:1.5\text{Ag}_2\text{O})-(95-x)\text{V}_2\text{O}_5-5\text{TeO}_2$  at 298K.**

$x$	$\sigma_{dc} (\Omega^{-1}\text{cm}^{-1})$	$A(\Omega^{-1}\text{cm}^{-1}\text{rad}^{-n})$	$n$
25	$1.39 \times 10^{-7}$	$5.47 \times 10^{-12}$	0.78
30	$3.87 \times 10^{-7}$	$1.23 \times 10^{-11}$	0.75
35	$1.41 \times 10^{-8}$	$3.40 \times 10^{-12}$	0.75
40	$1.92 \times 10^{-9}$	$1.66 \times 10^{-12}$	0.77
45	$6.96 \times 10^{-11}$	$2.14 \times 10^{-12}$	0.65

**Table.6.1 (b): Values of the dc conductivity, frequency dependent conductivity parameters  $A$  and  $n$  for the system  $10\text{BaO}-y\text{Ag}_2\text{O}-(85-y)\text{V}_2\text{O}_5-5\text{TeO}_2$  at 298K.**

$y$	$\sigma_{dc} (\Omega^{-1}\text{cm}^{-1})$	$A(\Omega^{-1}\text{cm}^{-1}\text{rad}^{-n})$	$n$
20	$1.137884 \times 10^{-7}$	$4.96 \times 10^{-12}$	0.78
25	$1.635065 \times 10^{-8}$	$4.16 \times 10^{-12}$	0.75
30	$1.269768 \times 10^{-9}$	$1.95 \times 10^{-12}$	0.76
35	$2.310623 \times 10^{-9}$	$3.95 \times 10^{-12}$	0.71
40	$1.149307 \times 10^{-8}$	$5.29 \times 10^{-12}$	0.74
45	$3.689176 \times 10^{-8}$	$1.10 \times 10^{-11}$	0.70
50	$1.904101 \times 10^{-7}$	$8.53 \times 10^{-12}$	0.75
55	$7.412371 \times 10^{-7}$	$1.24 \times 10^{-11}$	0.76

**Table.6.1 (c): Values of the dc conductivity, frequency dependent conductivity parameters  $A$  and  $n$  for the system  $5\text{BaO-zAg}_2\text{O-35V}_2\text{O}_5\text{-(60-z)TeO}_2$  at 303 K.**

$z$	$\sigma_{dc} (\Omega^{-1}\text{cm}^{-1})$	$A(\Omega^{-1}\text{cm}^{-1}\text{rad}^{-n})$	$n$
25	$2.15583 \times 10^{-10}$	$2.07 \times 10^{-12}$	0.71
30	$1.11639 \times 10^{-9}$	$4.52 \times 10^{-12}$	0.70
35	$6.19767 \times 10^{-9}$	$7.13 \times 10^{-12}$	0.69
40	$2.37316 \times 10^{-8}$	$1.04 \times 10^{-11}$	0.69
45	$8.20149 \times 10^{-8}$	$1.06 \times 10^{-11}$	0.72
50	$1.78043 \times 10^{-7}$	$1.07 \times 10^{-11}$	0.73
55	$4.04742 \times 10^{-7}$	$8.78 \times 10^{-12}$	0.76
60	$1.11222 \times 10^{-6}$	$1.31 \times 10^{-11}$	0.76

fractional mismatch between a neighboring ion position after a central ion hop and a local potential minimum before the hop and suggested a universal value of  $n$  to be 0.5-0.6. Diffusion controlled relaxation model [49] predicts  $n=0.5$ ; whereas the coulomb interacting lattice gas model [50, 51] predicts a limiting value of  $n$  is 0.75. All these models predict that the ac conductivity should be thermally activated with activation energy less than that for dc conductivity.

Regarding the general behavior of  $\sigma(\omega)$ , there is a critical frequency,  $\omega_h$ , at which the conductivity deviates from the frequency independent part and obeys the above mentioned power relation (Eq.6.37). Almond and West [52] suggested a simple way to calculate the hopping frequency from Eq. (6.37), by knowing the value of  $A$ ,  $n$  and  $\sigma_{dc}$ , at the frequency where  $\sigma(\omega) = 2\sigma_{dc}$ . Using Jonscher's empirical expression, Eq. (6.37) can be written as [43, 53]

$$\sigma_{(\omega)} \propto \omega \left[ \left( \frac{\omega}{\omega_h} \right)^{n_1-1} + \left( \frac{\omega}{\omega_h} \right)^{n_2-1} \right] \quad \dots\dots\dots (6.38)$$

where  $n_1$  and  $n_2$  are empirical constants of the material and  $\omega_h$  is the hopping frequency. For materials, which show a frequency independent region of conductivity  $n_1=0$  and  $n_2=n_1$  i.e.,

$$\sigma_{(\omega)} \propto (\omega_h + \omega_h^{1-n} \omega^n) \quad \dots\dots\dots(6.39)$$

$$\sigma_{(\omega)} = K' \omega_h + K' \omega_h^{1-n} \omega^n \quad \dots\dots\dots (6.40)$$

where  $K'$  is a constant which depends on the concentration of the mobile charge carriers and by comparing Eq. (6.37) and (6.40), the hopping rate is given by

$$\omega_h = [\sigma_{dc}/A]^{1/n} \quad \dots\dots\dots (6.41)$$

Temperature dependence of  $\omega_h$  for all glass samples of first series calculated using Eq. 6.41 follows the Arrhenius nature and is shown in Fig. 6.32. The plots of  $\omega_h$

against  $1000/T$  for second and third series glass samples are shown in Figs.6.33 and 6.34. The hopping frequency  $\omega_h$  is found to be thermally activated in the mentioned range of temperature and is represented by

$$\omega_h = \omega_0 \exp(-E_h/K_B T) \quad \dots\dots\dots (6.42)$$

where  $E_h$  is the free energy of migration and  $\omega_0$  is the effective attempt frequency. Since  $\text{Ag}^+$  ions are the mobile species in these series,  $\omega_h$  has been identified as the hopping rate of  $\text{Ag}^+$  ions.

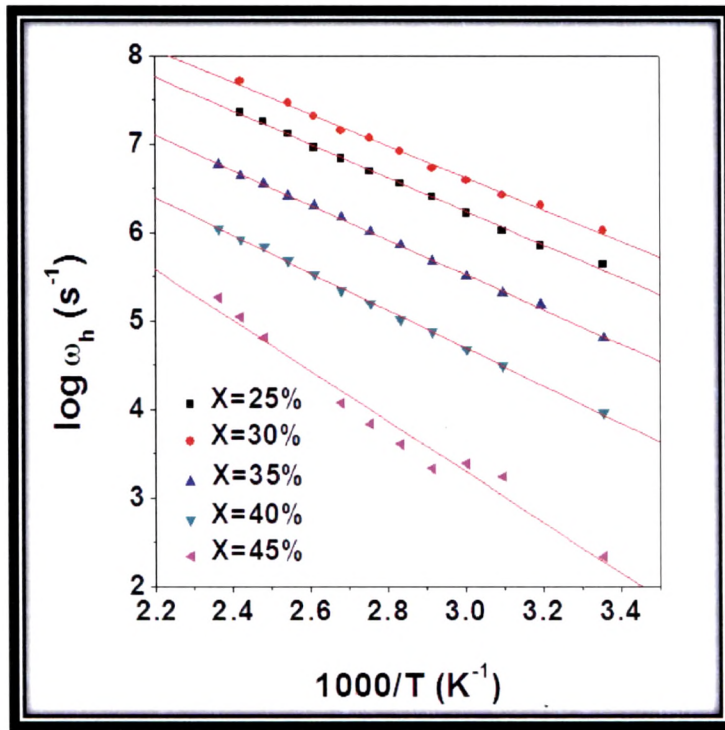


Fig. 6.32.  $\log \omega_h$  vs.  $1000/T$  for all samples of first series.

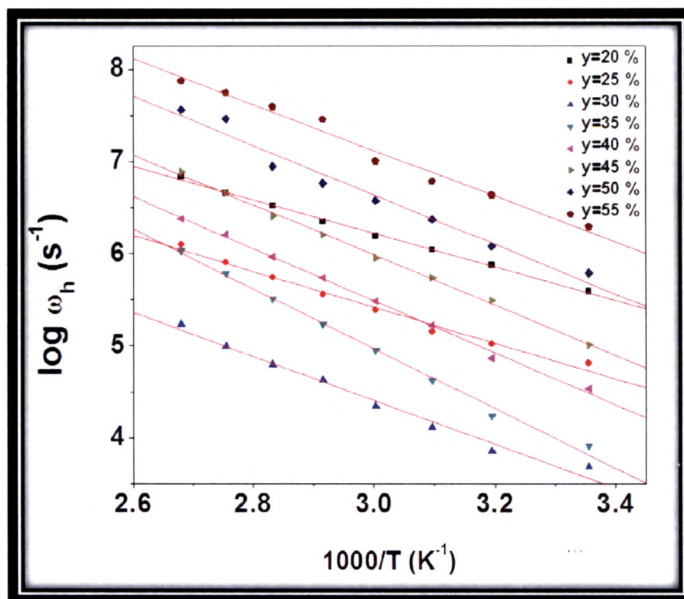


Fig.6.33.  $\log \omega_h$  vs.  $1000/T$  plot for all samples of second series.

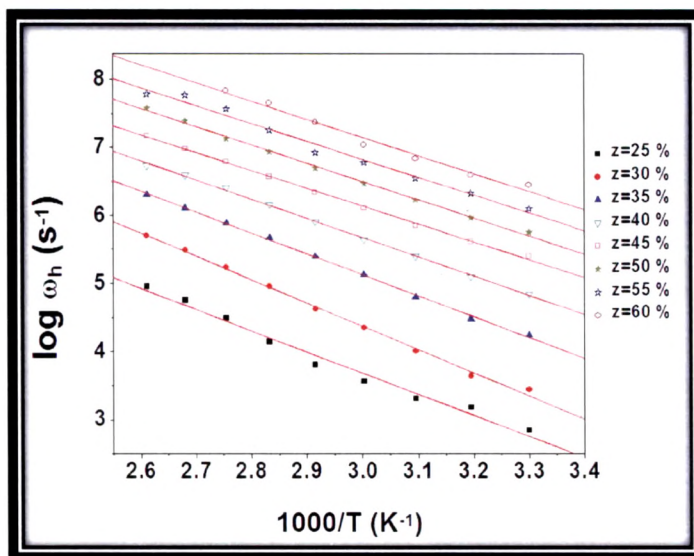


Fig.6.34.  $\log \omega_h$  vs.  $1000/T$  for all samples of third series.

The variation of  $\log \omega_h$  and  $E_h$  (activation energy) with increasing modifier content in first series  $x$  (BaO:1.5 Ag<sub>2</sub>O)-(95-x) V<sub>2</sub>O<sub>5</sub>-5 TeO<sub>2</sub> is shown in Fig. 6.35. It clearly shows that the values of hopping frequency  $\omega_h$  continuously decreases with increasing modifier content except for 30 mol % sample which shows slightly high conductivity, while the activation energy  $E_h$  increases with increasing modifier content. Fig. 6.36 shows the plot of  $\log \omega_h$  and  $E_h$  versus Ag<sub>2</sub>O mol % for the system 10 BaO-y Ag<sub>2</sub>O-(85-y) V<sub>2</sub>O<sub>5</sub>-5 TeO<sub>2</sub> (second series). In this series, it is observed from the figure that upto 30 mol% of Ag<sub>2</sub>O, where BaO is fixed at 10 mol %, there is a decrease in  $\omega_h$  (hopping frequency) and after 30 mol % of Ag<sub>2</sub>O,  $\omega_h$  values are continuously increasing. The reason for this

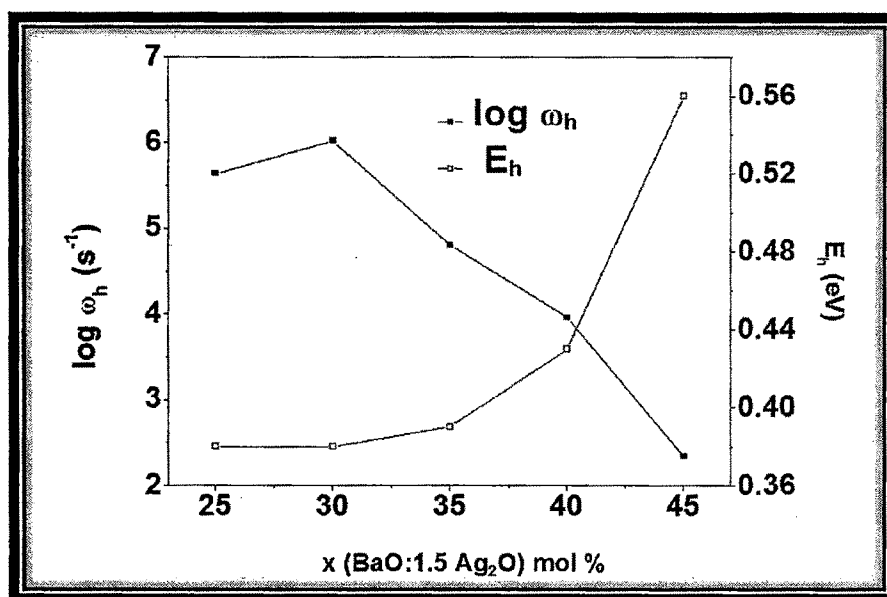


Fig.6.35. Variation of  $\log \omega_h$  and  $E_h$  with modifier content for first series.

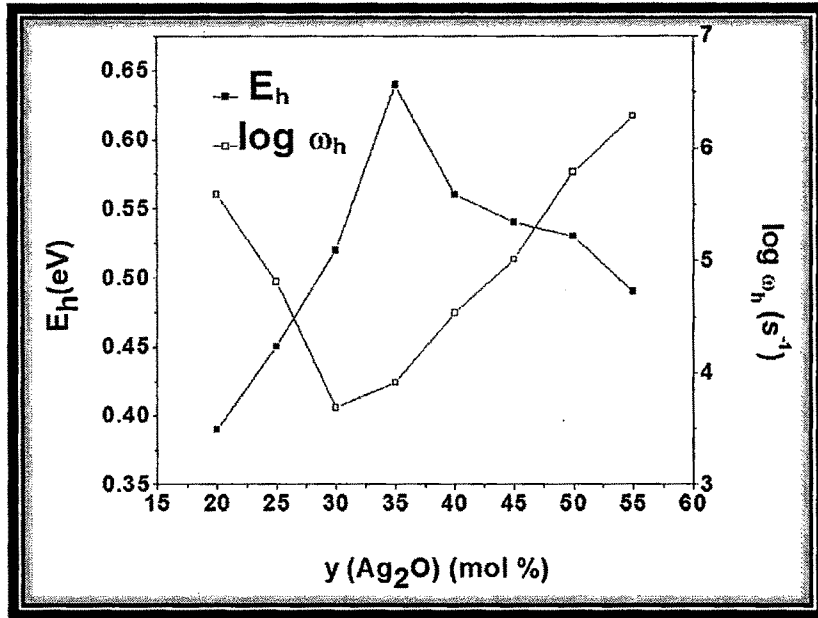


Fig.6.36. Variation of  $\log \omega_h$  and  $E_h$  with  $\text{Ag}_2\text{O}$  mol % for second series.

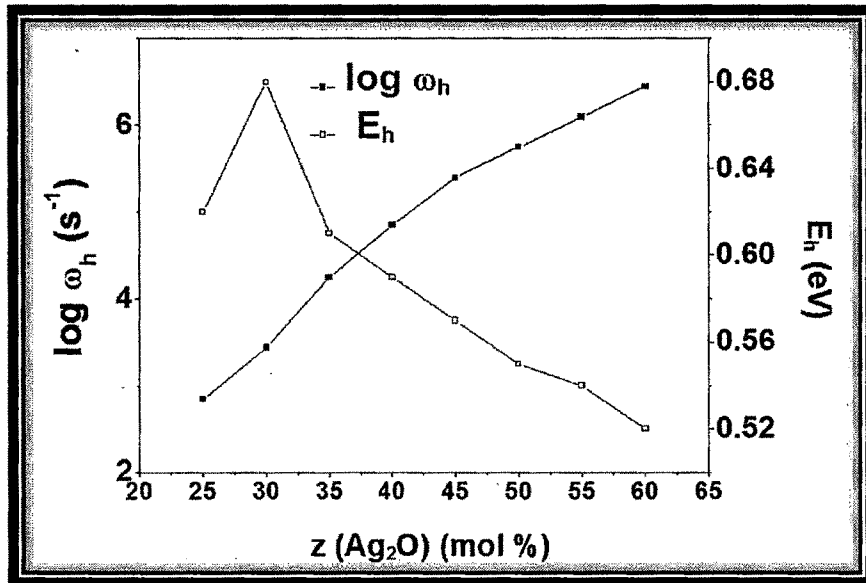


Fig.6.37. Variation of  $\log \omega_h$  and  $E_h$  with modifier content for third series.

behavior is the change of mechanism for the electrical transport process at  $y=30$  mol % of  $\text{Ag}_2\text{O}$ . Upto 30 mol % of  $\text{Ag}_2\text{O}$ , electronic conductivity dominates and after 30 mol %, as  $\text{Ag}_2\text{O}$  increases continuously, ionic conductivity dominates in the system and a deep minimum in the isotherm of conductivity is observed. This transition is also evident from the EMF measurement Fig.4.25. The activation energy obtained in this system increases upto 35 mol % and then decreases continuously. The variation of hopping frequency ( $\omega_h$ ) and activation energy ( $E_h$ ) with modifier ( $\text{Ag}_2\text{O}$ ) content is shown in Fig. 6.37 for the system  $5 \text{ BaO-zAg}_2\text{O}-35 \text{ V}_2\text{O}_5-(60-z) \text{ TeO}_2$  (third series). In this series, hopping frequency increases continuously with increasing  $\text{Ag}_2\text{O}$  content as the conductivity of the samples also increases in the same manner and the activation energy decreases continuously except for  $z = 30$  mol % where it gives highest value. We have also observed that the activation energy calculated from the hopping frequency and that of the conduction process are close to each other for all the glass samples in three different series which indicates that the ions in these glasses also have to overcome the same barrier while conducting by hopping as well as relaxing. The hopping frequency also assists in the estimation of the mobile ion concentration factor  $K'$  of a conductor. Almond [54] has suggested that by knowing the values of  $\omega_h$  and  $\sigma_{dc}$ , mobile ion concentration factor can be calculated by the relation

$$K' = \sigma_{dc} T / \omega_h \quad \dots\dots\dots(6.43)$$

where  $\sigma_{dc}$  is the dc conductivity,  $T$  is the temperature and  $\omega_h$  is the hopping rate of the mobile ions and is found to be a thermally activated quantity. Fig. 6.38 shows the variation of mobile ion concentration factor  $K'$  with temperature for  $x=35$

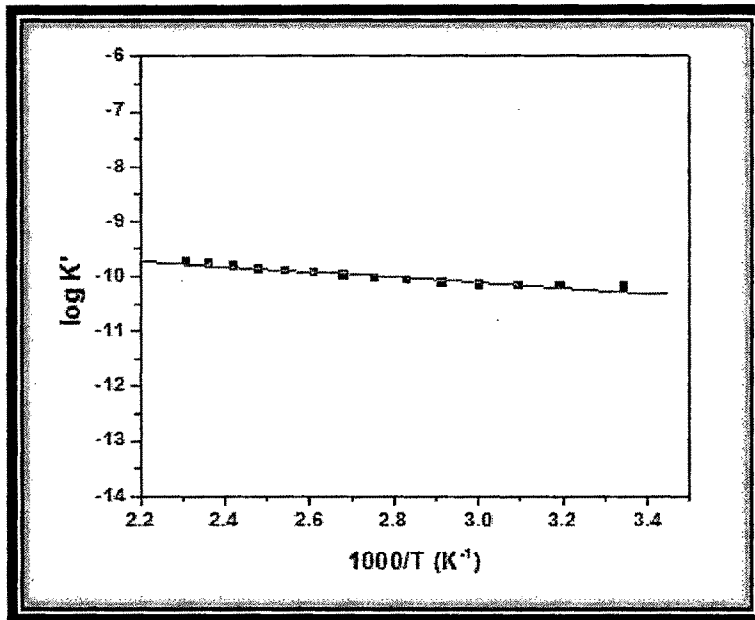


Fig. 6.38.  $\log K'$  vs.  $1000/T$  for  $x=35\%$  sample of first series.

mol% of first series calculated from above equation, which is found to be constant with increasing temperature. Similar temperature dependence of mobile ion concentration factor  $K'$  is shown in Fig. 6.39 for  $y=45$  mol % of the system  $10 \text{ BaO}-y \text{ Ag}_2\text{O}- (85-y) \text{ V}_2\text{O}_5-5 \text{ TeO}_2$  (second series) and Fig. 6.40 shows the plot for  $z=30$  mol % of the system  $5 \text{ BaO}-z \text{ Ag}_2\text{O}- 35 \text{ V}_2\text{O}_5- (60-z) \text{ TeO}_2$  (third series). These plots show the temperature independence of the mobile ion concentration factor  $K'$ . Thus, in the presently studied systems, mobile ion concentration factor is not thermally activated and the variation of conductivity arises due to the temperature dependence of the hopping rate of mobile ions. Such behavior is also reported for other systems [55, 56]. Similarly, variation of mobile ion concentration factor  $K'$  with composition is also discussed for different series. The

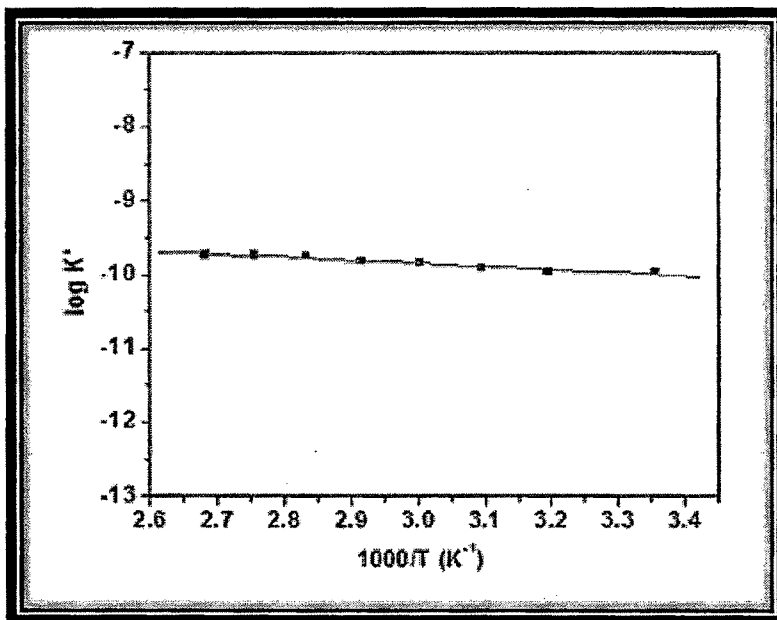


Fig.6.39.  $\log K'$  vs.  $1000/T$  for  $y=45\%$  sample of second series.

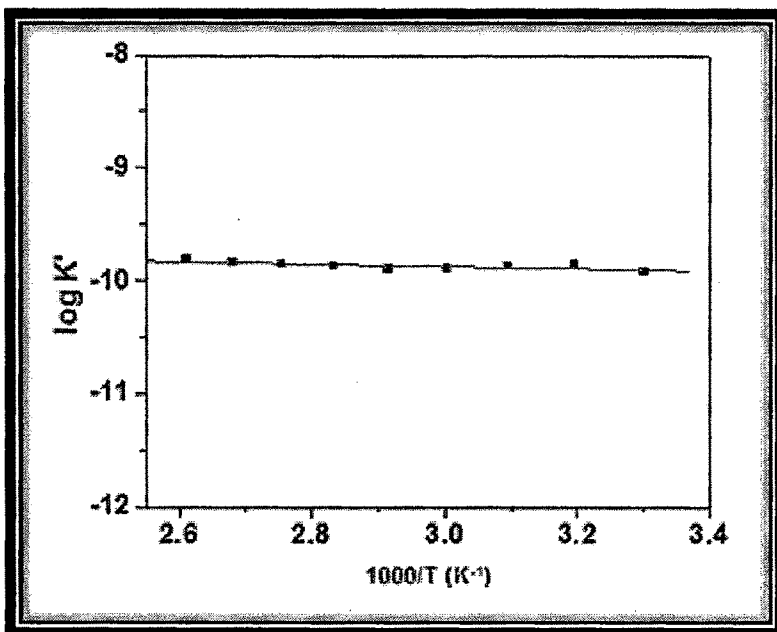


Fig.6.40.  $\log K'$  vs.  $1000/T$  for  $z=30\%$  sample of third series.

plot of  $\log K'$  versus modifier content for three different series is given in Figs. 6.41, 6.42 and 6.43 respectively. It is clear from the figures that the  $K'$  values are almost constant with the modifier increase. It means that the  $K'$  values are constant with composition. Thus, the mobile ion concentration factor is not responsible for conductivity increase and the variation in conductivity may be due to the mobility of the ions. The dc conductivity of most of the ionic conductors is determined by the expression obtained from the theory of random walk [52].

$$\sigma_{dc} = K\omega_h \quad \dots\dots\dots (6.44)$$

where  $K$  is the constant of proportionality defined as [57]

$$K = \left( \frac{Ne^2 a^2}{kT} \right) \gamma c(1-c)\omega_h \quad \dots\dots\dots (6.45)$$

where  $\gamma$  is a geometrical factor which includes correlation factor,  $c$  is the concentration of mobile ions on  $N$  equivalent lattice sites per unit volume,  $a$  is the hoping distance,  $e$  is the electronic charge,  $k$  is the Boltzmann's constant,  $T$  is the

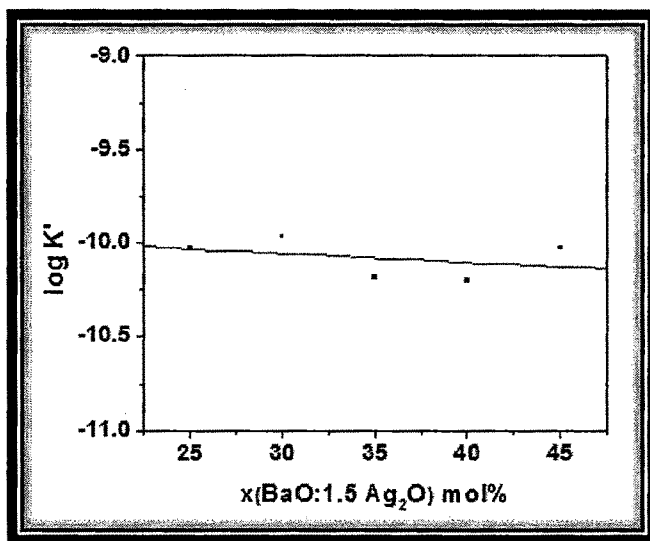


Fig.6.41. Variation of  $\log K'$  with composition in first series.

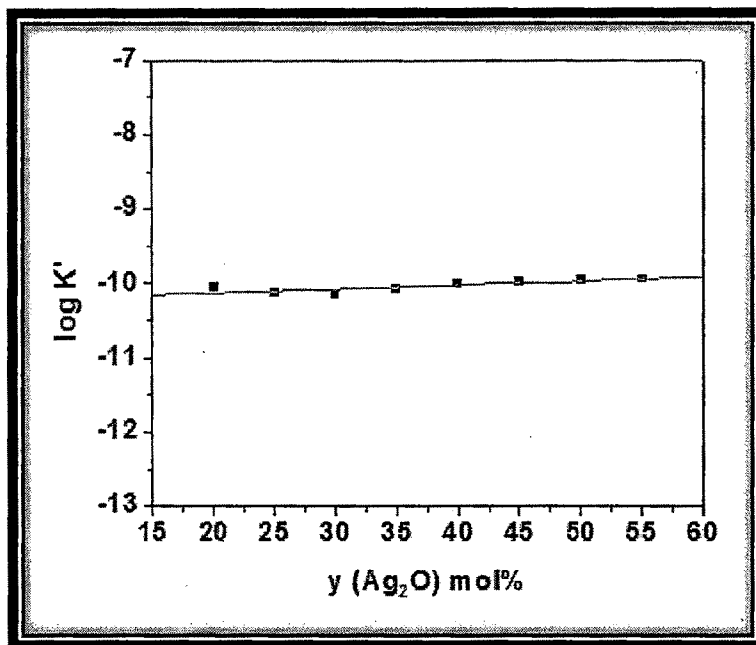


Fig.6.42. Variation of  $\log K'$  with composition in second series.

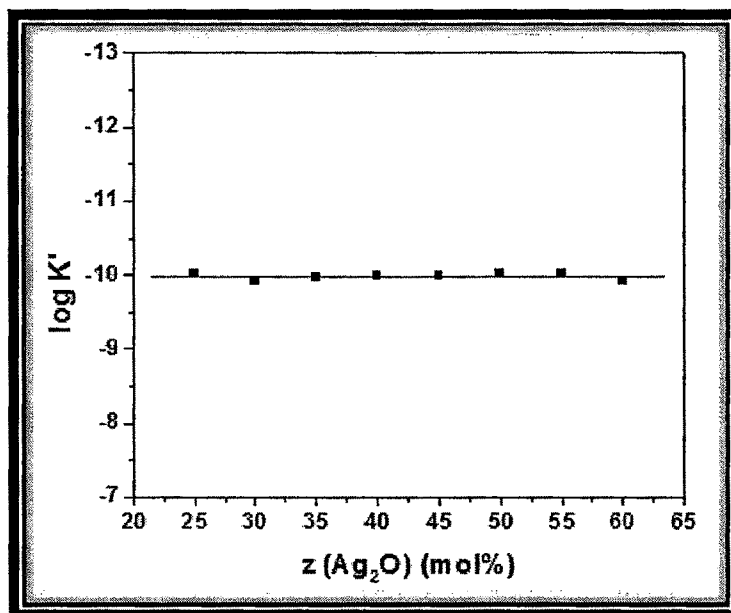


Fig. 6.43. Variation of  $\log K'$  with composition in third series.

absolute temperature and  $\omega_h$  is the hopping rate of mobile ions. As observed from Eq. 6.44 that dc conductivity depends on carrier concentration and hopping rate. In super ionic conductor carrier concentration is not thermally activated and the variation of conductivity arises only due to the temperature dependence of hopping frequency  $\omega_h$  [34]. Therefore, it can be concluded that as the hopping frequency increases with the temperature, the conductivity should increase as is observed in the present glass systems.

### **6.2.3 Scaling of conductivity spectra:**

Scaling is an important feature in any data evaluation. The ability to scale different conductivity isotherms so as to collapse all to one common curve indicates that the process can be separated into a common physical mechanism modified only by thermodynamic scales. The study of the conductivity spectra of several glasses at different temperatures leads to a scaling law which results in a time temperature superposition [39, 40]. In this regard the following expression has been used to describe the real part of the ac conductivity in glasses [58, 59]

$$\sigma'(\omega) = \sigma_{dc} \left[ 1 + \left( \frac{\omega}{\omega_h} \right)^n \right]^{-1}, \quad 0 < n < 1 \quad \dots\dots(6.46)$$

where  $\sigma_{dc}$  is the dc conductivity,  $\omega_h$  is the hopping frequency of the charge carriers and  $n$  is the dimensionless frequency exponent. Eq. (6.46) can be obtained from the imaginary part of the complex dielectric susceptibility [21]. Recently renewed interest has developed regarding the scaling observed in the frequency dependence of the ionic conductivity of an ion containing glasses [60, 61, 62]. In this formalism different scaling parameters were used for the frequency axis,

while the conductivity axis was scaled by the dc conductivity [39, 41, 42, 63, 64, 65]. Roling et. al. [39] have considered (i)  $\sigma_{dc} T$  and (ii)  $\sigma_{dc} T/x$  as a scaling factors and composition, where  $x$  is the mole fraction of mobile (alkali) ions and  $T$  is the absolute temperature. They have also made use of the Barton-Nakajima-Namikawa (BNN) relation [66] while defining the crossover frequency from dc behavior to the dispersive conductivity. Sidebottam [63] has extended the above scaling approach to the case where the alkali content is very low by making use of the fact that the ion hopping length changes with the alkali content. He has used  $(\sigma_{dc}/\epsilon_0 \Delta\epsilon)$  for the scaling frequency, where  $\epsilon_0$  is the permittivity of free space and  $\Delta\epsilon = (\epsilon_s - \epsilon_\infty)$  is the permittivity change from the unrelaxed baseline  $\epsilon_\infty$  to fully relaxed level  $\epsilon_s$ . This scaling frequency is equivalent to some numerical factor times the crossover or hopping frequency according to the Barton-Nakajima-Namikawa (BNN) relaxation [66]. In the present case, we have scaled the conductivity spectra following a newly developed scaling approach, known as Ghosh's scaling model [42], given by the relation

$$\frac{\sigma'}{\sigma_{dc}} = F\left(\frac{\omega}{\omega_h}\right) \dots\dots\dots (6.47)$$

The dynamics of the carriers is described by a universal function  $F$ , which is independent of temperature. Here  $\omega_h$  is used as scaling parameter for the frequency axis and is expected to be more appropriate for scaling the conductivity spectra of ionic conductors, since it takes into account the dependence of the conductivity spectra on structure and the possible changes of the hopping distance experienced by the mobile ions [42].

Now it is interesting to note whether the conductivity spectra merge into a single

master curve when the conductivity axis is scaled with respect to  $\sigma_{dc}$  and the frequency axis with respect to  $\omega_h$ . To observe this, we have scaled the conductivity spectra at different temperatures for  $x=35$  mol% of first series  $x(\text{BaO}:1.5\text{Ag}_2\text{O})-(95-x)\text{V}_2\text{O}_5-5\text{TeO}_2$  which is shown in Fig.6.44. The scaled conductivity spectra of second series for  $y=40$  mol% and that of third series for  $z=30$  mol% sample are given in Figs. 6.45 and 6.46 respectively. The perfect superimposition of the plot at different temperatures suggests that the ion transport in these glasses follow a common mechanism throughout the temperature range studied. The conductivity spectra at different temperatures of the other glass compositions also superimposed perfectly.

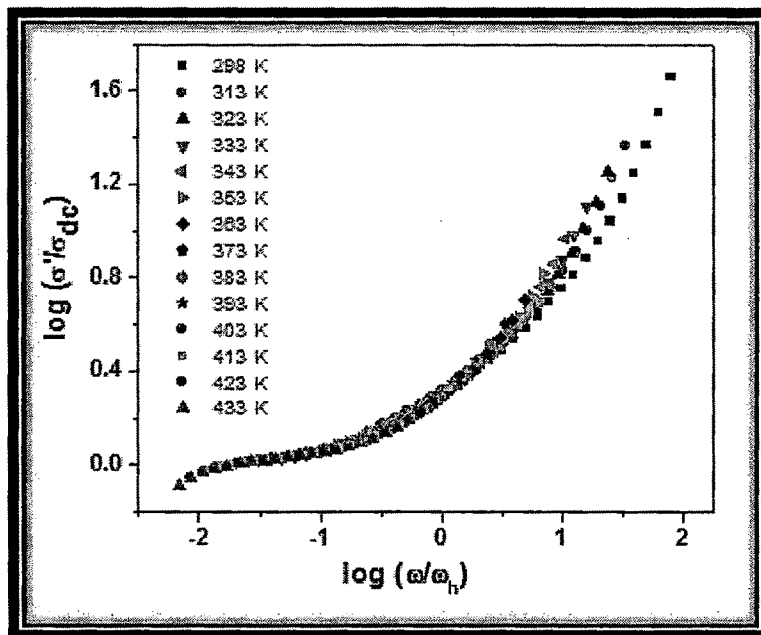


Fig.6.44. Conductivity scaling of  $x=35$  % sample of first series at different temperatures.

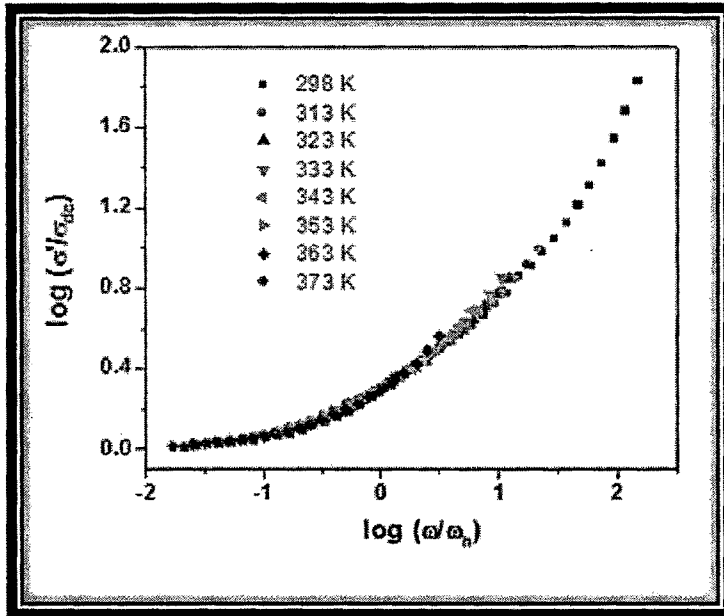


Fig.6.45. Conductivity scaling of y=40 % sample of second series at different temperatures.

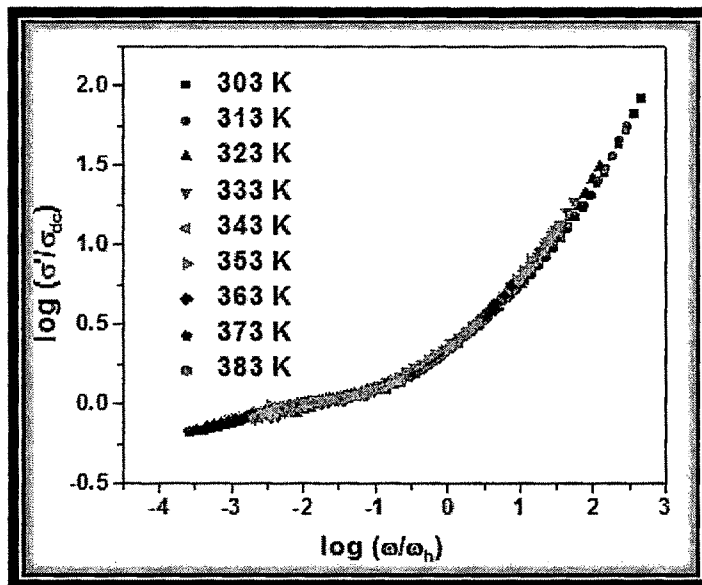


Fig.6.46. Conductivity scaling of z=30 % sample of third series at different temperatures.

The compositional dependence of the scaled conductivity spectra for different series is also discussed. The scaled conductivity spectra for different glass compositions of all series at a particular temperature are given in Figs. 6.47, 6.48 and 6.49 respectively. It is observed from these figures that the spectra for all the samples of three series superimpose on a single curve, indicating that the relaxation mechanism is independent of compositions also. Similar compositional scaling behavior in AgI based superionic glasses is also discussed by Ghosh [67]. The results support the scaling formalism of the conductivity spectra for a large number of oxide glasses [41, 63] but contradict the scaling results for some oxide glasses [42, 68].

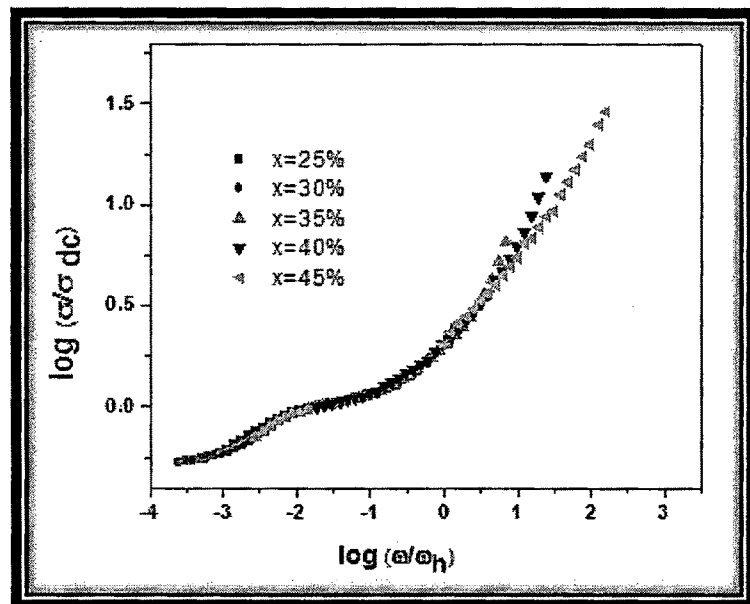


Fig.6.47. Conductivity scaling of all samples of first series at 353 K.

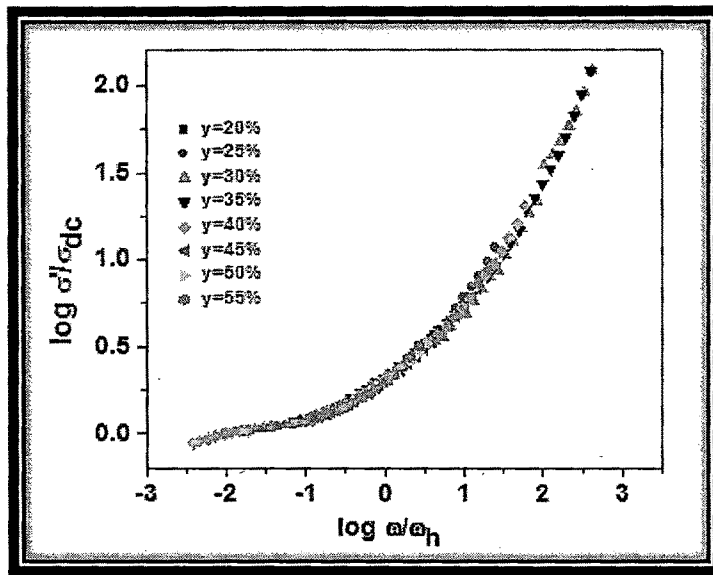


Fig.6.48. Conductivity scaling of all samples of second series at 298 K.

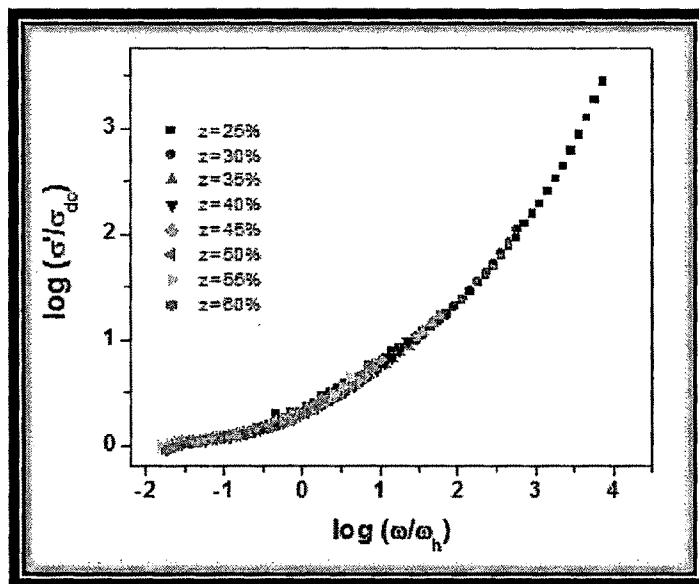


Fig. 6.49. Conductivity scaling of all samples of third series at 303 K.

### 6.3 Dielectric Analysis:

Dielectric properties of semiconducting oxide glasses are of increasing importance as the field of solid state electronics continues to expand rapidly. For most applications, the most important properties are the dielectric constant  $\epsilon'$  and the dielectric loss factor, i.e.,  $\tan \delta$ , because most of the new devices in many applications are continually increasing the frequency range and the range of environmental condition particularly the temperature.

Dielectric polarization arises due to the existence of atomic and molecular forces and appears whenever charges in a material are somewhat displaced with respect to one another under the influence of an electric field. In a capacitor, the negative charges (-ve) within the dielectric are displaced toward the positive electrode (+ve), while the positive charges shift in the opposite direction. As charges are not free to move in an insulator, restoring forces are activated which either do work, or cause work to be done on the system i.e., energy is transferred. On charging a capacitor, the polarization effect opposing the applied field draws charges onto the electrodes, storing energy. On discharge, this energy is released. A result of the above interaction is that, certain materials, which possess easily polarizable charges, will greatly influence the degree of charge which can be stored in a capacitor. The proportional increase in storage ability of a dielectric with respect to vacuum is defined as the dielectric constant of the material [69, 70]. The degree of polarization ' $P$ ' is related to the dielectric constant  $K$  and the electric field strength  $\bar{E}$  as follows

$$P = \epsilon_0 (K-1) \bar{E} \dots\dots\dots(6.48)$$

where  $\epsilon_0$  is the permittivity of free space, (a constant).

The total polarization of a dielectric arises from four sources of charge displacement: (a) electronic displacement ( $P_e$ ), (b) ionic displacement ( $P_i$ ), (c) orientation of permanent dipoles ( $P_d$ ) and (d) space charge displacement ( $P_s$ ). The total contribution of polarization to the dielectric constant is therefore a summation of the above

$$P_t = P_e + P_i + P_d + P_s \dots\dots\dots(6.49)$$

The schematic representation of polarization mechanisms with different charge displacement in dielectric materials is shown in Fig. 6.50 (i-iv) [69].

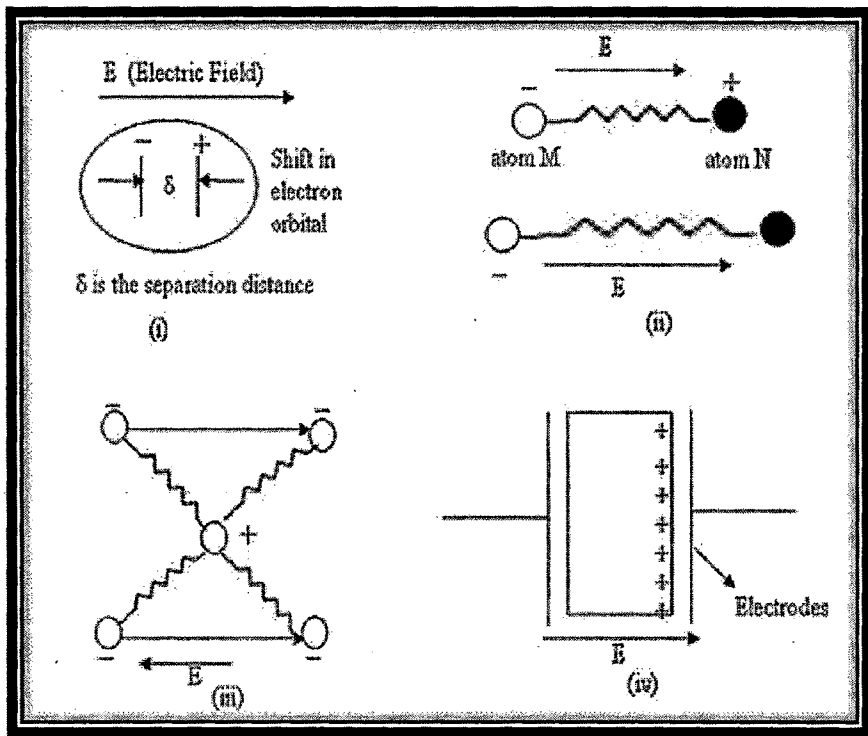


Fig. 6.50. Schematic representation of polarization mechanism in dielectric materials: (i) Electronic polarization (ii) Atomic or ionic polarization (iii) Dipoles polarization (iv) Space charge polarization.

**Electronic Displacement:** This effect is common in all materials, as it involves distortion of the center of charge symmetry of the basic atom. Under the influence of an applied field, the nucleus of an atom and the negative charge center of the electrons shift, creating a small dipole. This polarization effect is small, despite the vast number of atoms within the material, because the moment arm of the dipoles is very short, perhaps only a small fraction of an Angstrom ( $1 \text{ \AA} = 10^{-10} \text{ m}$ ) (Fig. 6.50 (i)).

**Ionic Polarization:** Ionic displacement is common in certain materials, which consists of crystal lattices occupied by cations and anions. Under the influence of an electric field, dipole moments are created by the shifting of these ions towards their respective (opposite) polarity of the field. The displacement, or moment arm of the dipoles can be relatively large in comparison to the electronic displacement, (although still much less than one Angstrom unit), and therefore can give rise to high dielectric constants in some ceramics (Fig. 6.50 (ii)).

**Dipole Orientation:** This is a phenomenon involving rotation of permanent dipoles under an applied field. Although permanent dipoles exist in ceramic compounds, such as in  $\text{SiO}_2$ , which has no center of symmetry for positive and negative charges, dipole orientation is not found to occur, as the dipole is restricted from shifting by the rigid crystal lattice, reorientation of the dipole is precluded as destruction of the lattice would ensue. Dipole orientation is more common in polymers which by virtue of their atomic structure permit reorientation. Note that this mechanism of permanent dipoles is not the same as that of induced dipoles of ionic polarization (Fig. 6.50 (iii)).

**Space charge Polarization:** This mechanism is extrinsic to any crystal lattice. The phenomenon arises due to charges which exist due to contaminants or

irregular geometry of the interfaces of polycrystalline ceramics, and is therefore an extraneous contribution. These charges are partly mobile and migrate under an applied field (Fig. 6.50 (iv)).

**Effect of Frequency on Polarization:** The mechanisms of polarization have varying time response capability to an applied field frequency, and the net contribution of polarization to the dielectric constant is therefore frequency dependent. Electronic displacement responds rapidly to the field reversals, and no lag of the polarization contribution occurs up to  $10^{17}$  Hz. As is expected, ions, which are larger and must shift within the crystal structure, are less mobile, and have a less rapid response. The polarization effect of ionic displacement decreases at  $10^{13}$  Hz. At this frequency, the ionic displacement begins to lag the field reversals, increasing the loss factor and less contribution to the dielectric constant. At higher frequency, the field reversals are such that the ions no longer “see” the field (the natural frequency of ions is less than the applied frequency) and no polarization (or loss factor) contribution is made by ionic displacement. Dipole orientation and space charge polarization have slower frequency responses [69]. The total net effect is illustrated in Fig. 6.51. The peaks which occur near the limiting frequency for ionic and electronic polarization are due to the resonance points, where the applied frequency equals the natural frequency of the material. The variation of the polarization mechanism with frequency is reflected when measuring dielectric constant of a capacitor. As expected, capacitance value, i.e., dielectric constant, always decreases with increased frequency, for all ceramic materials, although with varying degrees depending upon which type of polarization mechanism is dominant in any particular dielectric type.

The dielectric relaxation as well as conductivity relaxation can be explained and

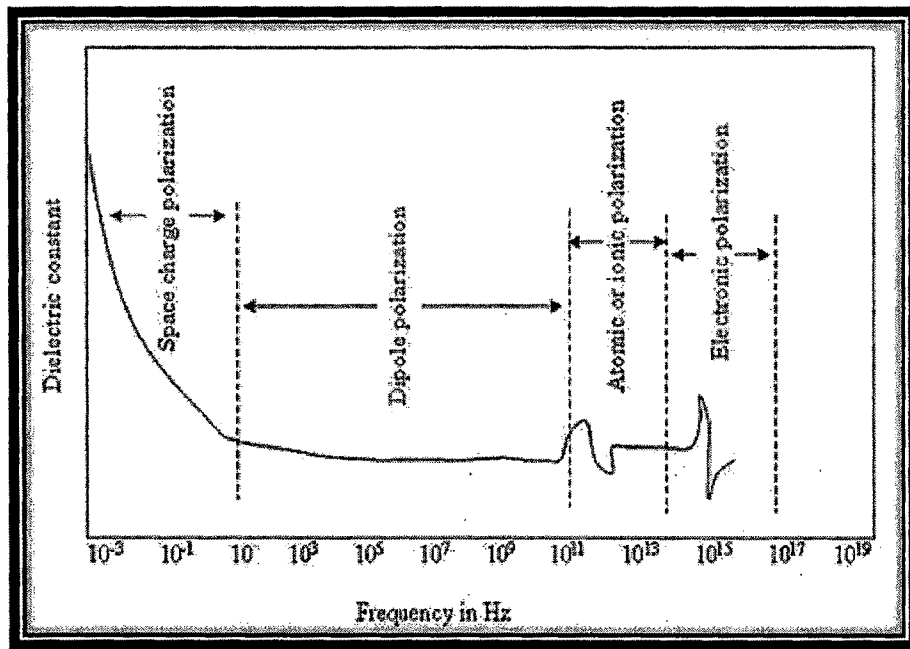


Fig. 6.51. Frequency dependence of polarization mechanism in dielectric materials.

understood easily through ionic conduction studies in solids. At sufficiently higher temperature, all materials are liable to show increasing movements of ions, either intrinsic to their lattice as in the case of ionic solids, or extrinsic due to impurity in purely covalent lattice including many polymers. This is normally expected to lead to dc conduction, although in many cases there is evidence of low frequency dispersion in data which on superficial analysis may be considered to represent dc conduction [69-71]. There are numerous materials which conduct predominantly by motion of ions, the extreme examples being the so-called fast ion conductor or superionic conductors. Ordinary ionic conduction relies on the formation of lattice

defects under the action of thermal excitation, thus creating vacancies through which ion motion may proceed under the action of external electric field [72]. This leads to Arrhenius temperature dependence with an activation energy given by the energy of formation of a defect.

In order to understand the structure and properties of solids including superionic solids, information about the motion of the mobile ions is necessary. This is contained in the dielectric spectra in the wide frequency range, for which relaxation of the ion motion and network motion contribute. Generally, relaxation is a process which occurs in dielectric having low electrical conductivity. This process mainly applies to linear systems where a response and stimulus are proportional to one another in equilibrium [73, 74]. The details of formulations for measuring the dielectric parameters are discussed below in brief. According to Maxwell equation the permittivity of a medium is defined as:  $\bar{D} = \epsilon \bar{E}$ , where  $\bar{D}$  is the displacement vector and ' $\bar{E}$ ' is applied electric field. The displacement vector is also equal to the surface charge per unit area. Consider a parallel plate capacitor of area  $A$ , separated by a distance ' $t$ ' (in vacuum). If a potential ' $V$ ' be applied to it and the charge carried by ' $Q$ ' then the electric field strength is  $V/t$  in Volt/m units. Hence, permittivity can be written as:

$$\epsilon = \frac{\bar{D}}{\bar{E}} = \left(\frac{Q}{A}\right)\left(\frac{V}{t}\right) = \left(C \frac{t}{A}\right) \dots\dots\dots(6.50)$$

One of the most important dielectric parameter widely used is relative dielectric constant or relative permittivity, which is defined as  $\epsilon' = \frac{\epsilon}{\epsilon_0}$ . Then by using Eq.

6.50, we have

$$\epsilon' = \frac{Ct}{\epsilon_0 A} \dots\dots\dots(6.51)$$

From the measurement of the capacitance, dielectric constant can be determined using above equation (6.51). The relative permittivity is usually known as permittivity and is always greater than unity. Suppose a parallel plate capacitor has a capacitance of  $C_0$  in air, then its capacitance, when the space between the plates is filled by a medium of permittivity  $\epsilon'$ , is given by following equation [75].

$$\epsilon' = \left( \frac{C}{C_0} \right) \dots\dots\dots(6.52)$$

Assume that a dielectric material is subjected to an alternative electric field as given below:

$$\bar{E} = \bar{E}_0 \cos \omega t \dots\dots\dots(6.53)$$

The induced current in the dielectric does not change exactly at the same time i.e., the current and voltage are maximum and minimum at different times. The current is found to lead the potential in phase. In a similar way the electrical displacement is also not in same phase with applied electric field ( $\bar{E}$ ).

The expression for displacement vector ' $\bar{D}$ ' is

$$\bar{D} = \bar{D}_0 \cos (\omega t - \delta) \dots\dots\dots(6.54)$$

$$= \bar{D}_0 \cos \omega t \cos \delta + \bar{D}_0 \sin \omega t \sin \delta$$

$$= \bar{D}_1 \cos \omega t + \bar{D}_2 \sin \omega t \dots\dots\dots(6.55)$$

where  $\bar{D}_1 = \bar{D}_0 \cos \delta$ ,  $\bar{D}_2 = \bar{D}_0 \sin \delta$  and  $\delta$  is phase angle.

It is clear from the Equations that  $\bar{D}_0$  is proportional to  $\bar{E}_0$  and the ratio  $\frac{\bar{D}_0}{\bar{E}_0}$  is generally frequency dependent. So dielectric permittivity ( $\epsilon'$ ) and dielectric loss ( $\epsilon''$ ) can be written as

$$\epsilon'(\omega) = \left( \frac{\bar{D}_0}{E_0} \right) \cos \delta \quad \dots\dots\dots(6.56)$$

and 
$$\epsilon''(\omega) = \left( \frac{\bar{D}_0}{E_0} \right) \sin \delta \quad \dots\dots\dots (6.57)$$

The energy absorbed by the dielectric material can be measured using factor  $\sin \delta$ . It is well known that, in a capacitor the dielectric medium usually has a resistance ( $R$ ) and impedance ( $Z$ ), which are related to the phase angle. It is considered that for ( $R$ ) to be very large than loss factor, it can be written as:

$$\sin \delta \approx \tan \delta = \left( \frac{1}{\omega} \right) RC \quad \dots\dots\dots(6.58)$$

$\tan \delta$  is also known as tangent loss. The complex permittivity is given by

$$\epsilon^* = \epsilon' - j \epsilon'' \quad \dots\dots\dots(6.59)$$

where  $\epsilon'$  and  $\epsilon''$  are real and imaginary parts of dielectric permittivity. The real and imaginary parts of complex permittivity can be measured using impedance data by the following Eqn.

$$\epsilon^* = \frac{1}{j\omega C_0 Z^*} \quad \dots\dots\dots(6.60)$$

where  $Z^*$  is complex impedance,  $C_0 = \epsilon_0 \left( \frac{A}{t} \right)$ , where  $A$  is the area of the sample,  $t$  is the thickness of the sample and  $\epsilon_0$  is permittivity of vacuum.

In Debye like or single relaxation dispersion, the frequency dependence of  $\epsilon_p^*$  is given by

$$\epsilon_p^* = \epsilon_\infty + (\epsilon_s - \epsilon_\infty) \left( \frac{1}{1 + j\omega\tau} \right) \quad \dots\dots\dots(6.61)$$

where  $\epsilon_\infty$  is the high frequency value and  $\epsilon_s$  is the low frequency value of dielectric

constant.  $\tau$  is the dielectric relaxation time, which is the measure of the nominal time scale on which ion jump can take place. Separation of real and imaginary parts give equally familiar expression for the dielectric relaxation constant,  $\epsilon'$  and dielectric loss  $\epsilon''$ .

$$\epsilon' = \epsilon_{\infty} + \left( \frac{\epsilon_s - \epsilon_{\infty}}{1 + \omega^2 \tau^2} \right) \dots\dots\dots(6.62)$$

$$\epsilon'' = \frac{(\epsilon_s - \epsilon_{\infty}) \omega \tau}{1 + \omega^2 \tau^2} \dots\dots\dots(6.63)$$

The dielectric response obtained from many systems departs significantly from ideal Debye behavior and shows the dispersion and distribution of relaxation times which is determined by the hopping charge carriers [21]. Experimental evidences [21, 76] show that the universal dielectric response has a fractional power law dependence on frequency

$$\epsilon^*_{(\omega)} = A.(j\omega)^{n-1} \dots\dots\dots(6.64)$$

with  $0 < n < 1$ , where  $A$  is constant. The Kramer-Kronig transformation of above Eq. is independent of frequency and the ratio

$$\frac{\epsilon''_{(\omega)}}{\epsilon'_{(\omega)}} = \cot\left(\frac{n\pi}{2}\right) = \text{constt.} \dots\dots\dots(6.65)$$

which is a general property of the so called universal dielectric response in complete contrast with the Debye behavior for which the ratio is equal to  $\omega \tau$  [43].

The dielectric relaxation studies for a number of glass system have been studied widely [76-79]. In general, the dielectric relaxation spectra of a material provide the measure of the dynamic and relaxation behavior of the electric dipoles present in the system. The real part of the permittivity  $\epsilon'$  has the same significance as that

of ordinary dielectric constant of the material. It measures the elastically stored energy in the material during each cycle of the applied alternating field and the energy returned to the field at the end of each cycle. The term  $\epsilon''$  corresponds to the dielectric loss factor. Figs.6.52, 6.53 and 6.54 represent variation of dielectric constant ( $\epsilon'$ ) with log frequency for  $x=30$  mol % of first series,  $y=45$  mol% of second series and for  $z=60$  mol% of third series respectively. Observing the data

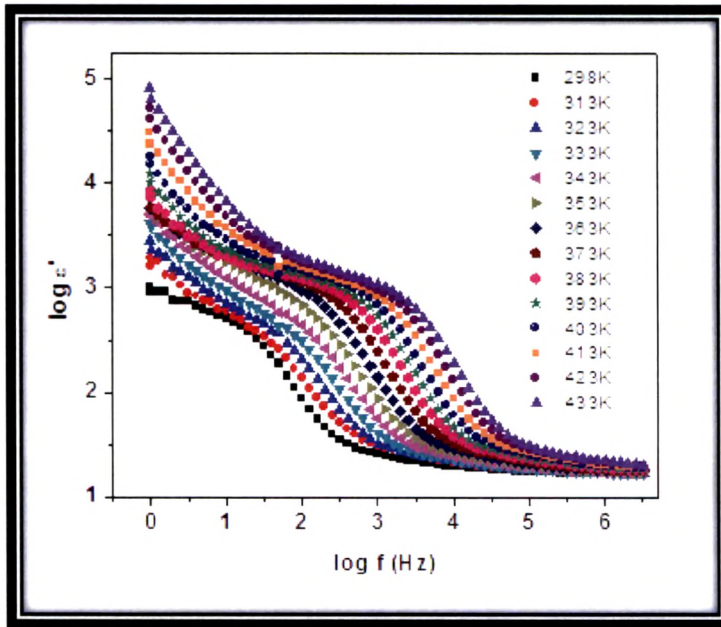


**Fig. 6.52. Plot of  $\log \epsilon'$  versus  $\log f$  for  $x=35$  % sample of first series at different temperatures.**

on dielectric properties, it is clear that dielectric constant decreases with increase of frequency and saturates at higher frequencies i.e. approaching  $\epsilon(\infty)$  which is due to the rapid polarization occurring in the glasses [80]. The experimental

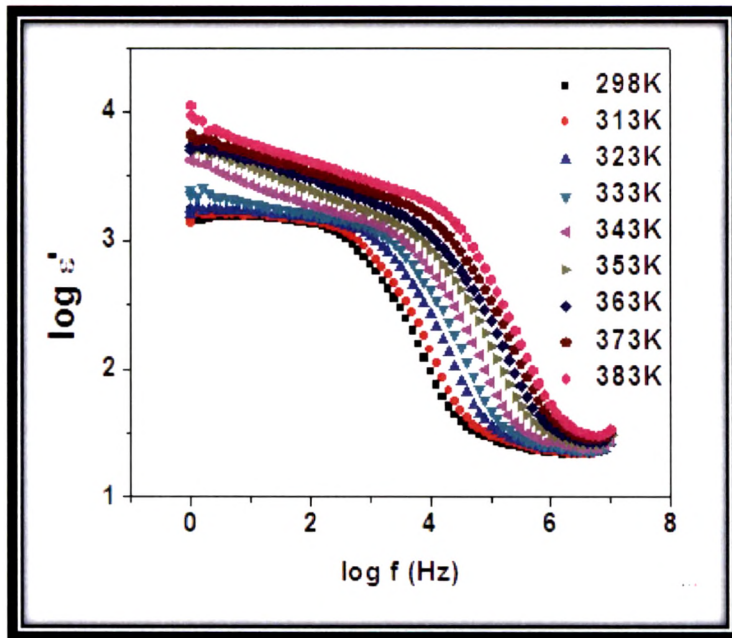


Fig. 6.53. Plot of  $\log \epsilon'$  versus  $\log f$  for  $\gamma=45\%$  sample of second series at different temperatures.

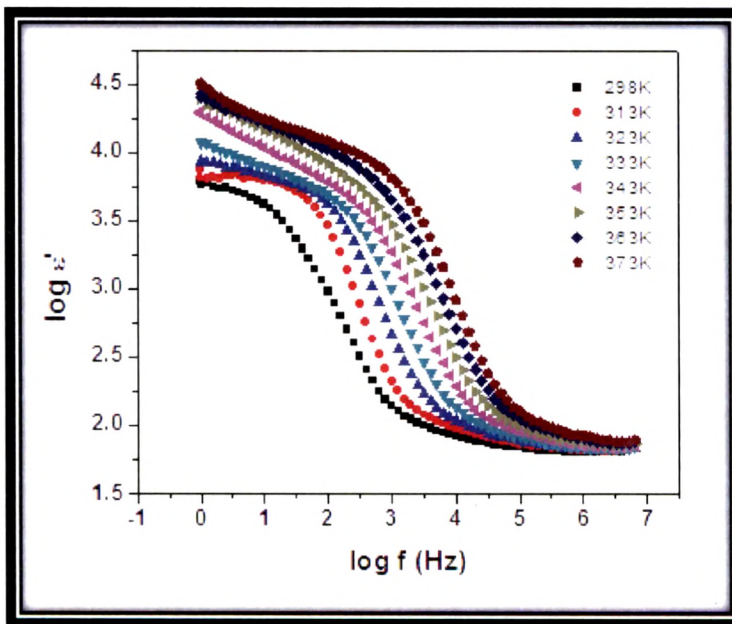


Fig. 6.54. Plot of  $\log \epsilon'$  versus  $\log f$  for  $z=60\%$  sample of third series at different temperatures.

results obtained in the present study for dielectric permittivity can be explained by Stevel's model on dielectric relaxation in glasses [10]. Since the conduction of  $\text{Ag}^+$  ions can be visualized as a series of jumps by ions along the lattice sites. If all the sites are equivalent, the ions spend equal amount of time at each site during the conduction process. This is not the case when the sites are not equal. Thus, the charge carriers tend to pile up at high free energy barriers resulting in an increase of capacitance at low frequency. Thus the variation of  $\epsilon'$  at mid frequencies is due to the long range diffusion of  $\text{Ag}^+$  ions involving series of jumps over barriers of varying height. Low frequency dispersion is due to electrode polarization. At higher frequencies, the periodic reversal of field takes place so rapidly that there are no excess ionic jumps in the field direction. The capacitive effect at the high free energy barriers site disappears at high frequencies and results in the low value of dielectric constant. These are in conformity with the observation made by earlier workers [81-84]. Similar features of dielectric dispersion spectrum are also shown by all the other samples of three different series. When the temperature is raised the frequency dispersion in the dielectric constant shifts towards higher frequency side. This frequency dispersion can be attributed due to the interfacial polarization, structural inhomogeneities and space charge polarization in the present vanado-tellurite glass material.

In order to get details about dielectric relaxation in vitreous ionic conductors, it is necessary to subtract a contribution  $\sigma_{dc}/\omega\epsilon_0$  from  $\epsilon^*$  [10] because dielectric relaxation peaks are suppressed due to the polarization of mobile species present in the material. Hence the frequency dispersion of the remaining part of the complex permittivity ( $\epsilon^*$ ) can be written as

$$\epsilon^* = \epsilon' - j\epsilon''_{corrected} = \epsilon' - j \left[ \epsilon'' - \frac{\sigma_{dc}}{\omega\epsilon_0} \right] \dots\dots\dots (6.66)$$

where  $\epsilon''_{corrected}$  is the actual value of dielectric loss for a simple Debye like or single relaxation process. The experimental results show that  $\epsilon^*$  occurs over a broader frequency range than predicted by Eq. 6.61 and this is accounted for by distribution of relaxation time. The present systems do not have any polar molecules, but have dc conductivity. Hence dielectric relaxation due to ionic motions is termed as “migration losses” [85]. Normally, in ionic crystals free energy barriers are of uniform height, while in glassy materials there will be variation in free energy barriers from site to site. Hence conduction can be visualized as a series of jumps of ions along the lattice sites. At lower frequencies, ions (here  $Ag^+$  ions) hop easily out of the sites with low free energy barriers in the electric field direction and tend to accumulate at sites with high free energy barriers. This leads to a net polarization of the ionic medium and gives a contribution  $\epsilon_s - \epsilon_\infty$  to the static value of  $\epsilon'$ . Thus, the variation of  $\epsilon'$  with frequency for the present glass systems at mid frequencies is due to long range ionic diffusion of  $Ag^+$  ions involving a series of jumps over barriers of varying height. At higher frequencies ( $\omega \gg 1/\tau$ ), where  $1/\tau$  is the jump frequency out of low free energy barriers sites), the periodic reversal of the field takes place so rapidly that there are no excess ionic jumps in the field direction, and the polarization due to charge pile up at high free energy barrier sites disappears and the observed value of  $\epsilon'$  falls to  $\epsilon_\infty$ .

Fig. 6.55 shows the typical variation of  $\log [\epsilon'' - \sigma_{dc}/\omega\epsilon_0]$  with frequency for x= 35 mol % sample of first series at different temperature range, whereas for y= 35

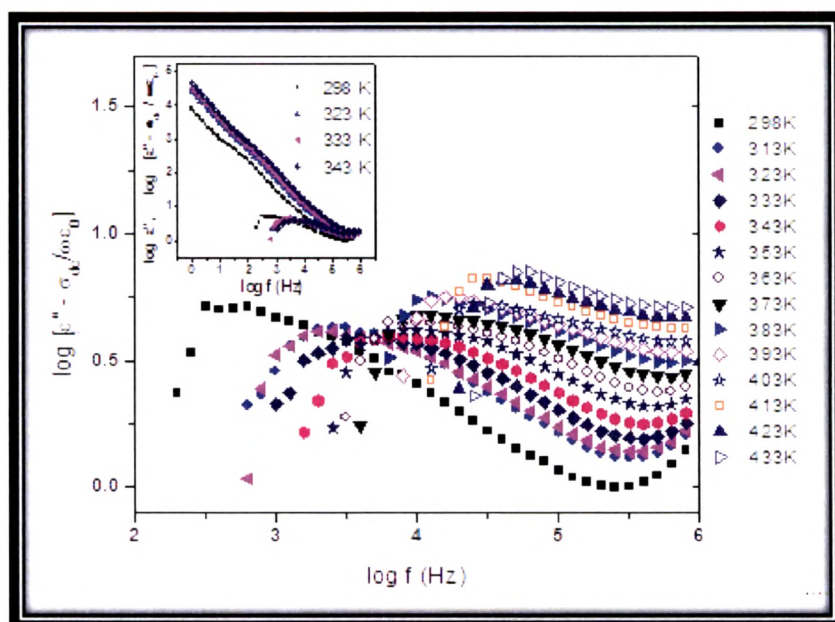


Fig.6.55. Plot of  $\log [\epsilon'' - \sigma_{dc} / \omega \epsilon_0]$  with frequency for  $x=35$  mol% sample of first series.

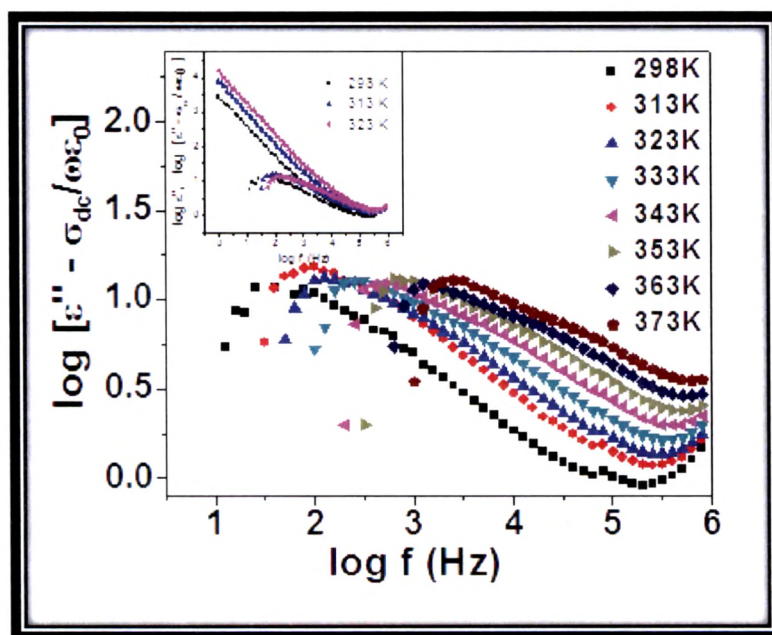


Fig.6.56. Plot of  $\log [\epsilon'' - \sigma_{dc} / \omega \epsilon_0]$  with frequency for  $y=35$  mol% sample of second series.

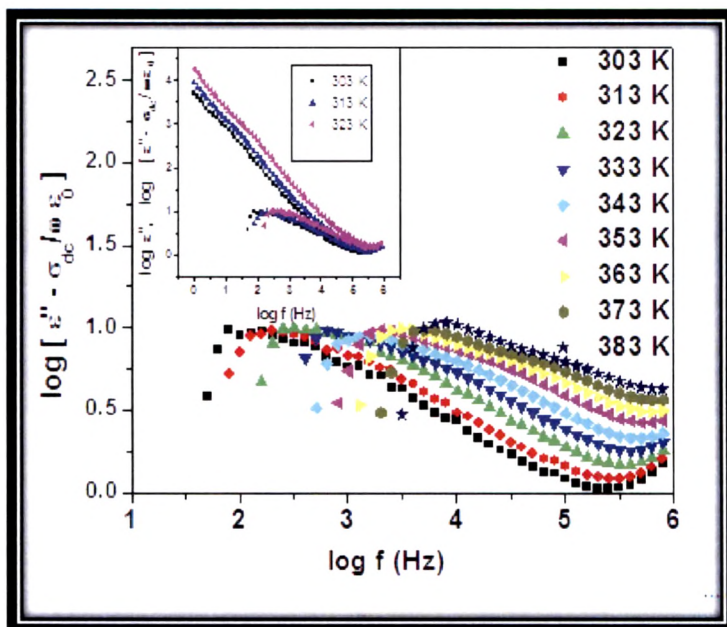


Fig.6.57. Plot of  $\log [\varepsilon'' - \sigma_{dc} / \omega \varepsilon_0]$  with frequency for  $z=35$  mol% sample of third series.

mol% (second series) and for  $z= 35$  mol% (third series) of  $\text{Ag}_2\text{O}$ , it is shown in Figs. 6.56 and 6.57 respectively. Inset figure shows the variation of  $\log \varepsilon''$  and  $\log [\varepsilon'' - \sigma_{dc} / \omega \varepsilon_0]$  versus  $\log$  frequency of the respective samples. It is seen from these plots that  $\varepsilon''$  depends on inverse of frequency or  $1/\omega$  and increases with increase in temperature. Similar behavior is also reported by Kaushik et.al. [81] and Chowdari et.al. [82, 83] for other  $\text{Ag}^+$  ion conducting glasses.

The observed dielectric relaxation loss in the radio frequency range can be attributed to combination of dipole relaxation loss and conduction loss. Both losses together often termed as migration losses. Conduction losses depend on dc conductivity  $\sigma_{dc}$  according to formula

$$\varepsilon''_{\sigma_{dc}} = \frac{\sigma_{dc}}{\omega \varepsilon_0} \dots\dots\dots(6.67)$$

These losses arise under the influence of an electric force. The mobile ions move through the glassy network and in doing so, the ions give off part of the energy obtained from the electric force to the network in the form of heat. Conduction loss increases with increase in temperature since  $\sigma_{dc}$  increases with increase in temperature and also shifts to lower frequencies at lower temperatures. From the known value of dc conductivity  $\sigma_{dc}$ , the actual value of dielectric loss  $\varepsilon''_{corrected}$  at various frequencies and different temperatures is calculated using the following expression

$$\varepsilon''_{corrected} = \varepsilon'' - \left( \frac{\sigma_{dc}}{\omega \varepsilon_0} \right) \dots\dots\dots(6.68)$$

Hence, to separate the contribution of conduction losses from migration losses, we have to subtract  $\sigma_{dc}/\omega\varepsilon_0$  from  $\varepsilon''$ . After subtracting dc contribution, all the plots have shown a peak, whose maximum shifts to higher frequencies with increasing temperature. Now the contribution from dipole relaxation loss is clearly visible ( $\varepsilon''_{corrected}$  is much smaller compared to  $\varepsilon''$ ).

The observed variation in  $\varepsilon'$  and  $\varepsilon''$  with frequency could also be attributed to the formation of a space charge region at the electrode-glass ( $\omega^{n-1}$ ) variation or the non-Debye type behavior where the space charge regions with respect to frequency is explained in terms of ion diffusion [2, 86].

Figs.6.58 (a) and (b) show the temperature dependence of real ( $\varepsilon'$ ) and imaginary ( $\varepsilon''$ ) part of permittivity for  $x= 35$  mol % sample of first series  $x(\text{BaO}:1.5 \text{ Ag}_2\text{O})-(95-x) \text{ V}_2\text{O}_5-5 \text{ TeO}_2$  for different values of frequencies within the interval of  $10^2$

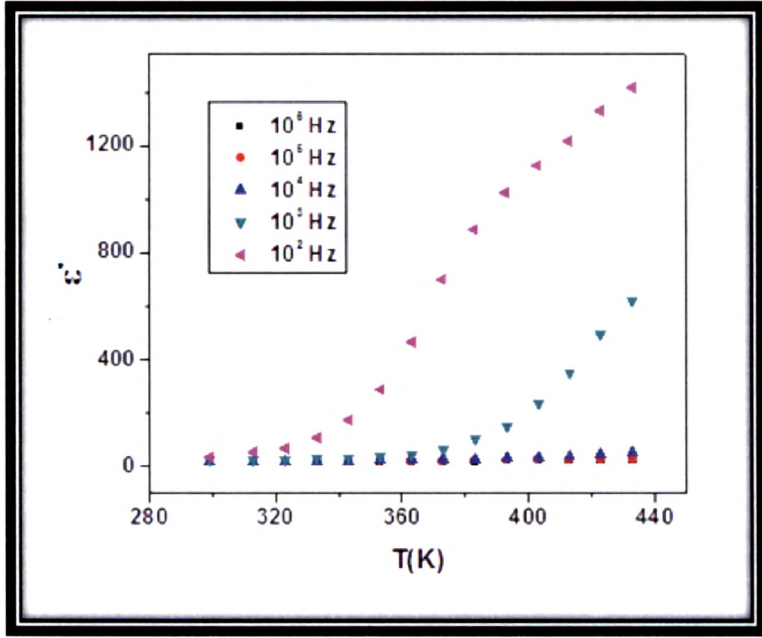


Fig.6.58. (a):  $\epsilon'$  versus  $T$  (K) for  $x=35\%$  sample of first series.

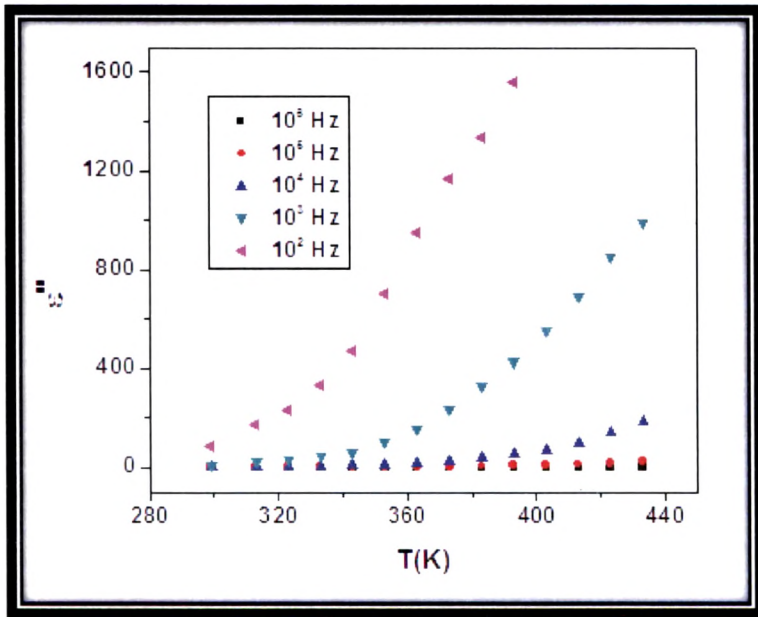


Fig.6.58. (b):  $\epsilon''$  versus  $T$  (K) for  $x=35\%$  sample of first series.

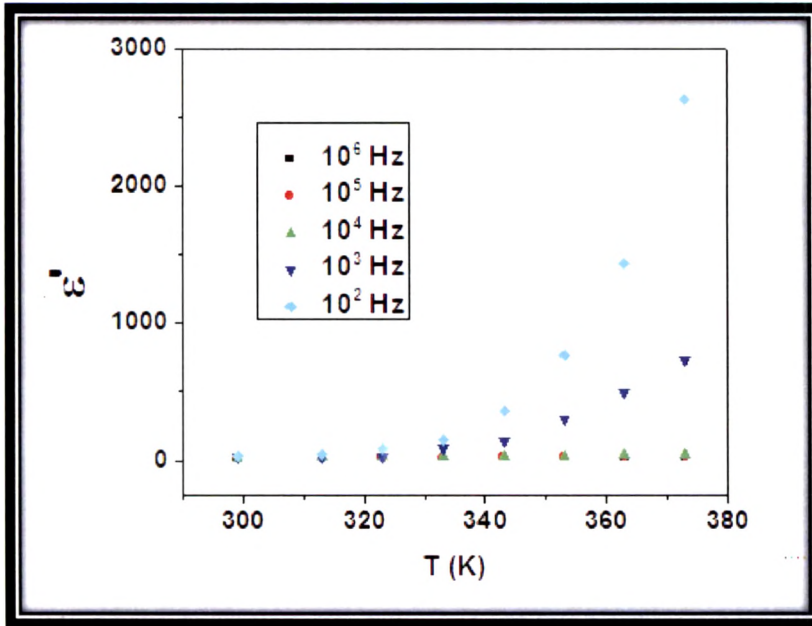


Fig.6.59. (a):  $\epsilon'$  versus  $T$  (K) for  $y=40\%$  sample of second series.

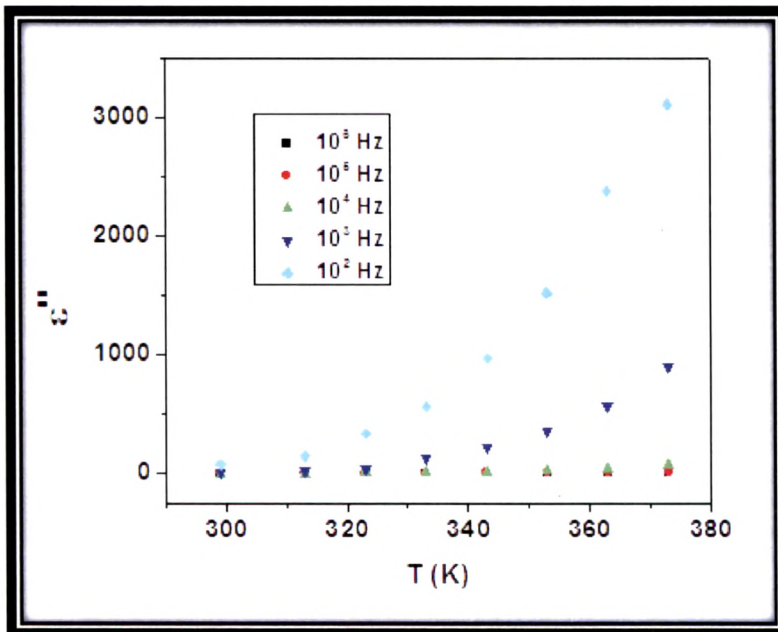


Fig.6.59. (b):  $\epsilon''$  versus  $T$  (K)  $y=40\%$  sample of second series.

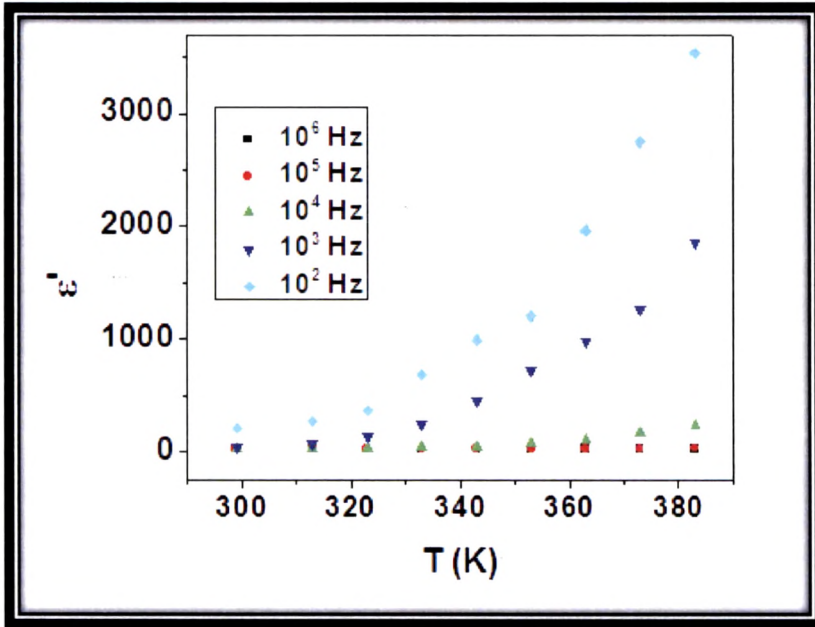


Fig.6.60. (a):  $\epsilon'$  versus  $T$  (K) for  $z=50$  % sample of third series.

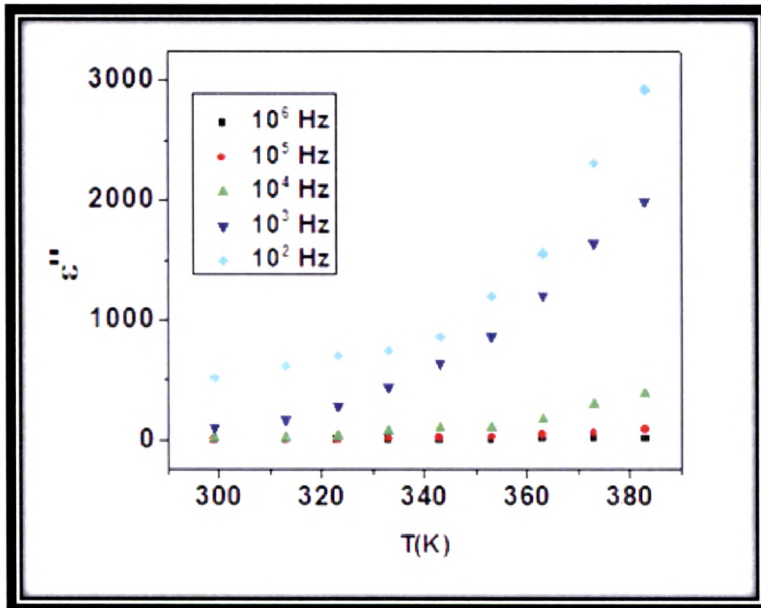


Fig.6.60. (b):  $\epsilon''$  versus  $T$  (K) for  $z=50$  % sample of third series.

to  $10^6$  Hz. It is clear that at low frequencies i.e., below  $10^3$  Hz, both  $\epsilon'$  and  $\epsilon''$  sharply rises with increase in temperature while for higher frequencies i.e., above  $10^3$  Hz, the increase in both real and imaginary values of permittivity are very less pronounced compared to low frequencies. At higher frequencies, within our temperature interval range the charge carriers ( $\text{Ag}^+$ ) are not sufficiently free to follow the changing electric field and therefore, the  $\epsilon'$  and  $\epsilon''$  quantities remain nearly constant, while for low frequencies, with the increase in temperature, the mobile ions are free to hop themselves parallel to the applied field, which lead to the rise in the permittivity [55]. Such behavior of permittivity is also observed in second and third series glass samples as shown in Figs. 6.59 (a & b) and 6.60 (a & b). However, a low value of  $\epsilon'$  and  $\epsilon''$  is observed in the glass samples of the first series where both the modifiers are changing i.e. BaO and  $\text{Ag}_2\text{O}$ . Temperature dependence of dielectric constant was also reported for other silver Vanadotellurite glasses of various compositions by Jayaseelan et.al. [23]. The plot of log of dielectric constant  $\epsilon'$  versus modifier content of first series glass samples at different frequencies at 373 K temperature is shown in Fig.6.61. It is observed that at low frequencies, i.e., from  $10^1$  to  $10^3$  Hz, the dielectric constant decreases with the increase in the mol% of the modifier content except for  $x=30$  mol% sample while at higher frequencies i.e., from at  $10^4$ - $10^6$  Hz, the measured dielectric constant is almost independent of the composition. Due to the decrease in conductivity the dielectric constant is found to decrease with the increase in the modifier content. The plot of dielectric constant versus modifier  $\text{Ag}_2\text{O}$  content, for the glass samples of second and third series at 298 K for the frequency 320 Hz is shown in Fig.6.62. It is observed that for the second series, the dielectric constant

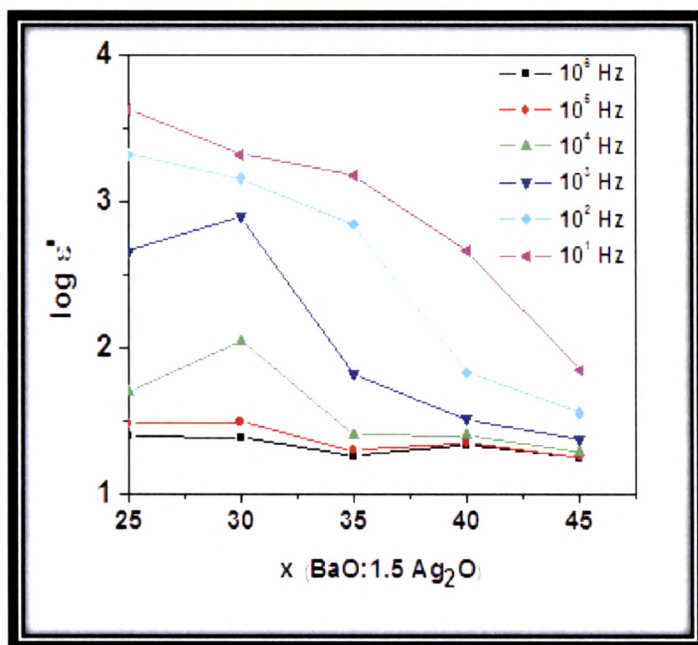


Fig.6.61. Variation of log  $\epsilon'$  versus modifier content for first series.

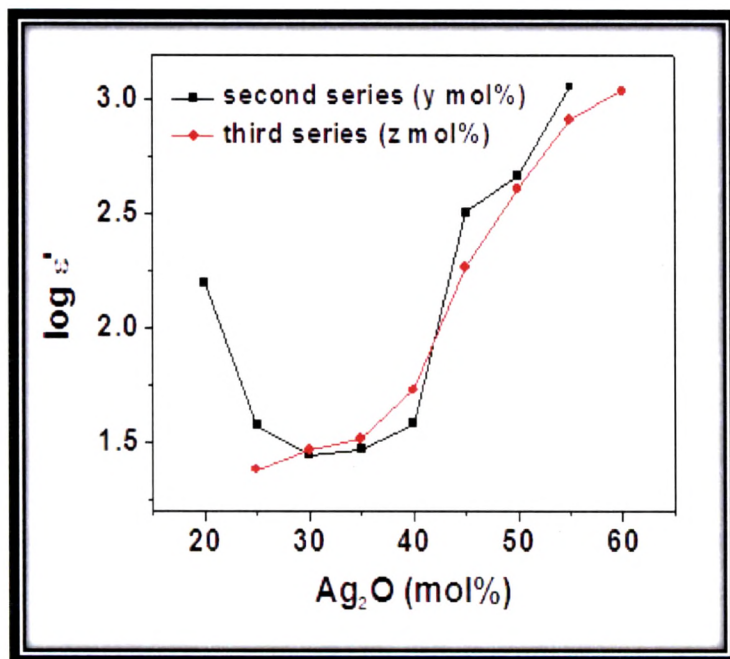


Fig.6.62. Variation of log  $\epsilon'$  vs. Ag<sub>2</sub>O mol % at frequency 320 Hz .

clearly decreases and shows the minimum value at  $y=30$  mol% and above which it increases, because of the reason that the conductivity also shows the minimum at  $y=30$  mol% due to the change of mechanism for electric transport process from electronic to ionic one whereas in the third series, it increases continuously with increasing  $\text{Ag}_2\text{O}$  content because the conductivity of the samples increases continuously in this series.

The tangent of loss angle represents the ratio of the energy dissipated per radian in the dielectric to the energy stored at the peak of polarization. It is given by the relation

$$\tan \delta = \frac{\varepsilon''(\omega)}{\varepsilon'(\omega)} \quad \dots\dots\dots(6.69)$$

One practical advantage of  $\tan \delta$  as a figure of merit of a dielectric material consists in its independence of the geometry of the sample. It is the ratio of two parameters which both contain the same geometrical factor.

The dielectric loss angle,  $\tan \delta$  versus log frequency at different temperature for  $x= 35$  mol % glass sample is plotted and shown in Fig. 6.63, for the series  $x(\text{BaO}:1.5\text{Ag}_2\text{O})-(95-x)\text{V}_2\text{O}_5-5\text{TeO}_2$ . Figure shows that  $\tan \delta$  decreases with increasing frequency and a peak is observed in the mid frequency range, after that it again starts decreasing and becomes constant in the high frequency region. At low frequencies  $\tan \delta$  increases with increase of temperature while for high frequencies, it is constant with temperature. Larger value of  $\tan \delta$  at low frequency range is due to the migration of ions, which is the main source of dielectric loss at low frequencies. The dielectric loss at low frequencies characterized by high value is due to the contribution of ion jump and dc conduction loss of ions in addition to

the electron polarization loss. As the frequency is further increased, ion migration is mitigated and a rapid decrease in dielectric loss is observed. In the mid frequency range, peak in  $\tan \delta$  is observed due to dipole or interfacial polarization, associated with the increase in both capacitance and loss factor. Further increasing the frequency,  $\tan \delta$  decreases and becomes constant in high frequency range, due to ion vibrations, which is the only source of dielectric loss in higher frequency

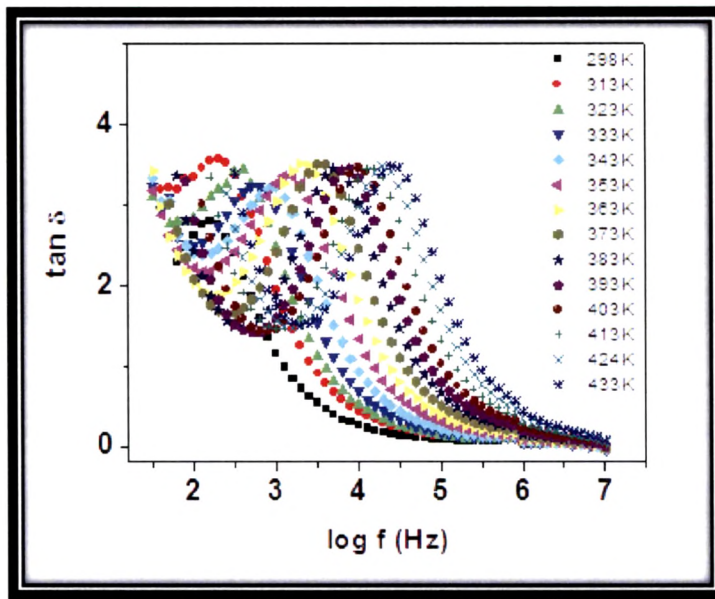


**Fig.6.63.**  $\tan \delta$  versus  $\log f$  at different temperatures for  $x=35\%$  sample of first series.

range. Similar variation of  $\tan \delta$  with frequency is also shown for the glass samples of second and third series in Figs.6.64 and 6.65. However, in third series the maximum of  $\tan \delta$  increases with temperature after 353 K. Such behavior was also reported by other workers in other systems [87-89] which is the indicative of

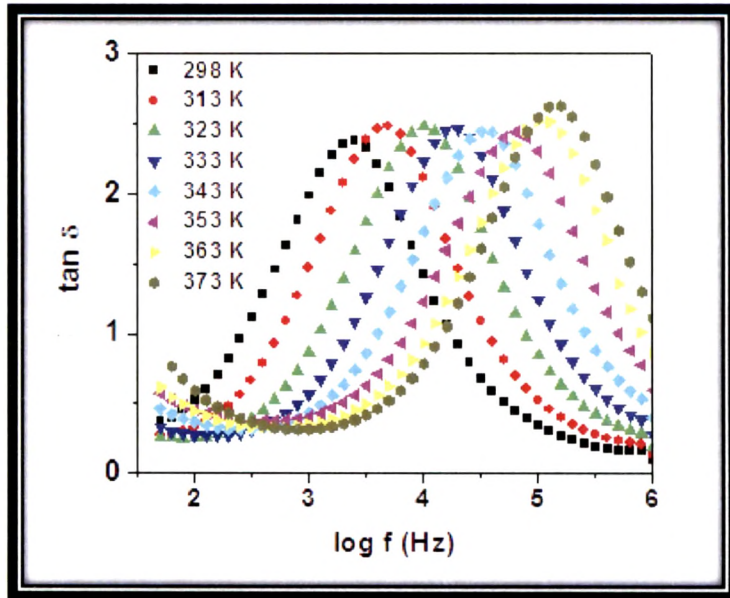


Fig.6.64.  $\tan \delta$  versus  $\log f$  at different temperatures for  $y=50\%$  sample of second series.

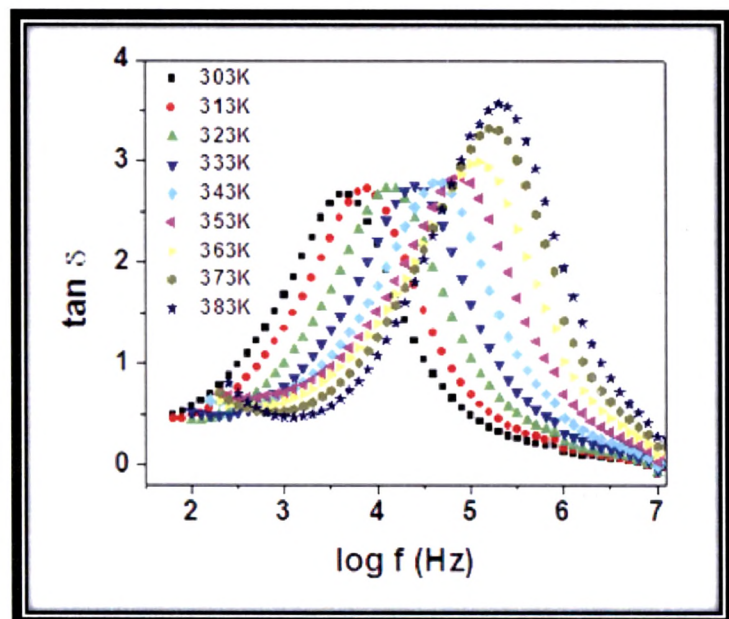


Fig.6.65.  $\tan \delta$  versus  $\log f$  at different temperatures for  $z=55\%$  sample of third series.

dipolar relaxation character of dielectric loss. The dispersion on  $\tan \delta$  with frequency is found to shift towards higher frequencies with increase in temperature. The rapid decrease in  $\tan \delta$  and attaining a constant value at higher frequencies clearly indicates that  $\tan \delta$  is inversely proportional to some power of frequency. The dispersion in  $\tan \delta$  with frequency had been reported for other systems also [32], for example, in phosphate glasses the maximum of the loss tangent increases with increase of temperature whereas in arsenate and molybdate system the maximum of the loss tangent is independent of temperature.

Fig.6.66, shows the  $\tan \delta$  plot for glasses containing different amount of modifier (BaO:1.5 Ag<sub>2</sub>O) in the first series. It is clear from the figure that the frequency of

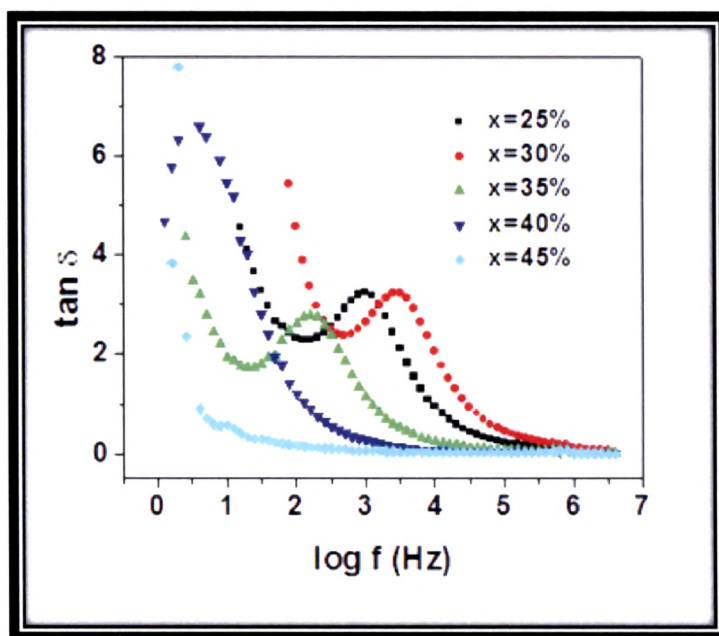


Fig.6.66.  $\log f$  versus  $\tan \delta$  for different samples of first series at 298 K.

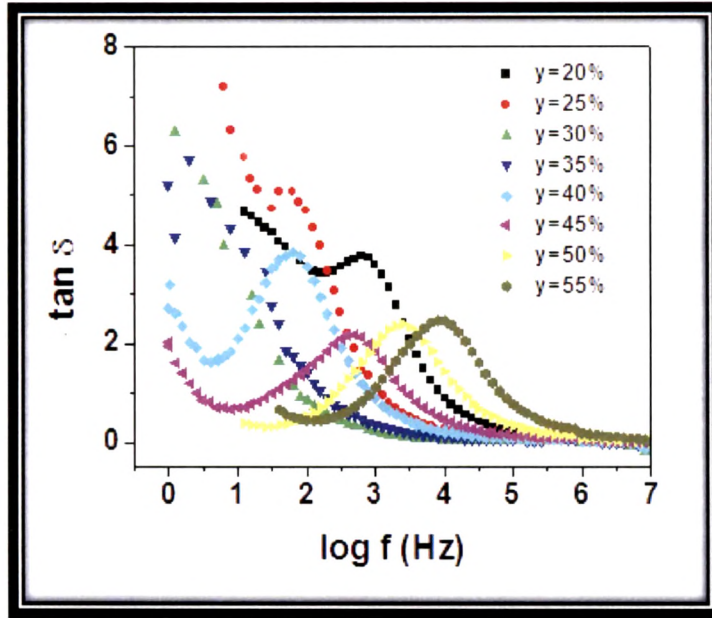


Fig.6.67.  $\log f$  versus  $\tan \delta$  for different samples of second series at 298 K.

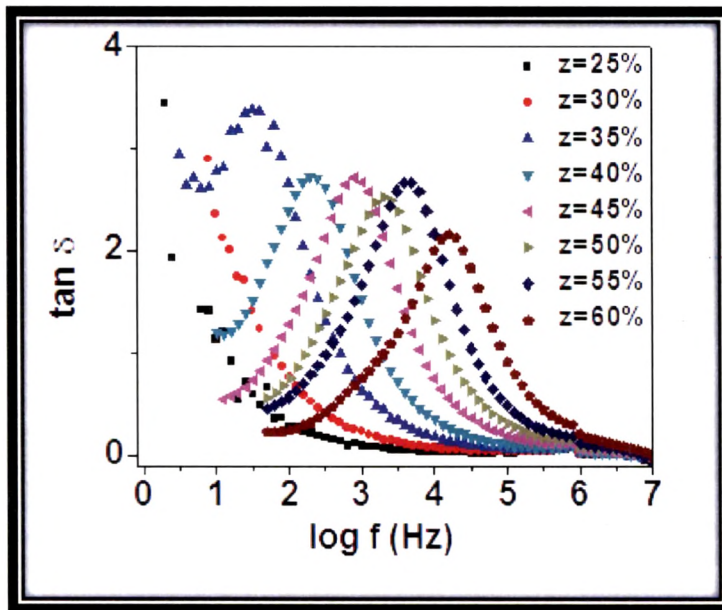


Fig.6.68.  $\tan \delta$  versus  $\log f$  for different samples of third series at 303 K.

tan  $\delta$  peak shifts to low frequency side with the increase in BaO and Ag<sub>2</sub>O content except for x= 30 mol % sample because the conductivity of the samples decreases except at 30 mol% where its value is slightly high. The compositional dependence of tan  $\delta$  in the second series where Ag<sub>2</sub>O is varied with glass former V<sub>2</sub>O<sub>5</sub>, is shown in Fig.6.67, which shows that the peak of tan  $\delta$  shifts towards low frequency side as the amount of y (Ag<sub>2</sub>O mol%) increases from 20 to 30 mol% and after that it shifts towards high frequency side for the samples having more than 30 mol% of Ag<sub>2</sub>O. Such trend can be correlated with the dominance of the type of charge carrier which ultimately help in ascertaining the type of conductivity i.e., electronic or ionic in the system (Fig.4.25 and 5.13). The shifting of tan  $\delta$  peak towards high frequency side is observed in the glass samples of third series, where TeO<sub>2</sub> is changed instead of V<sub>2</sub>O<sub>5</sub> with the increase of Ag<sub>2</sub>O as shown in Fig.6.68. This trend is in perfect correlation with the increase in conductivity and transport number of charge carriers of the samples with increasing Ag<sub>2</sub>O content because of the structural transition of TeO<sub>4</sub> to TeO<sub>3</sub> group, which facilitates easy migration of ions for conduction.

Relaxation time characterizes the motion of an ion between equivalent positions (diffusion independent local jumps) and it is calculated as suggested by Macedo et.al. [10] for a conducting dielectric

$$\tau_{\sigma} = \frac{\epsilon_{\infty} \epsilon_0}{\sigma_{dc}} \quad \dots\dots\dots (6.70)$$

where  $\epsilon_{\infty}$  is the high frequency dielectric constant,  $\epsilon_0$  is the permittivity of free space and  $\sigma_{dc}$  is the dc conductivity of the sample. The plots of dielectric relaxation time against the inverse of temperature for all the samples of first series

x (BaO:1.5 Ag<sub>2</sub>O)- (95-x) V<sub>2</sub>O<sub>5</sub>-5 TeO<sub>2</sub> are shown in Fig. 6.69. It is noted from the figure that  $\tau_\sigma$  exhibits an Arrhenius behavior of the form

$$\tau_\sigma = \tau_0 \exp\left(\frac{E_\tau}{kT}\right) \dots\dots\dots(6.71)$$

where  $\tau_0$  is the pre exponential factor and  $E_\tau$  is the activation energy for conductivity relaxation. From the slope of the above figures the activation energy for conductivity relaxation is calculated. Figure also shows that the relaxation time ( $\tau_\sigma$ ) calculated from Eq.6.70, decreases with increasing temperature, which means

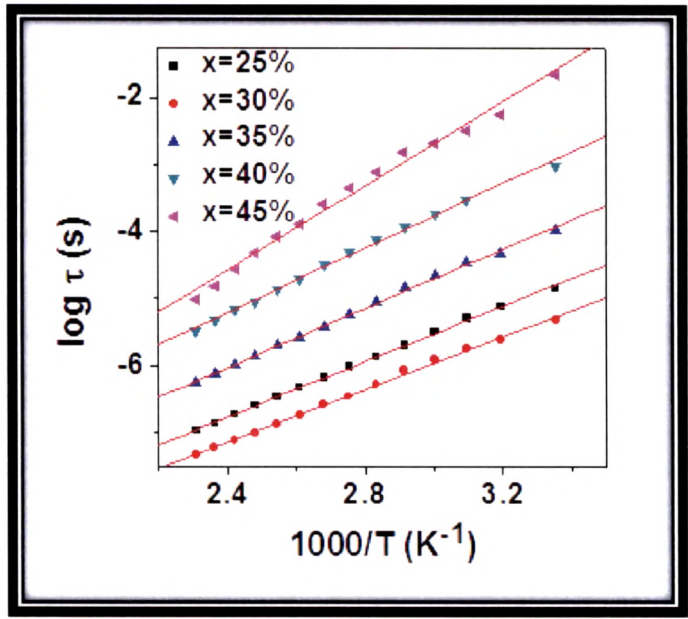


Fig.6.69. log  $\tau$  versus  $1000/T$  plot for all samples of first series.

that the mobility of ions increases with rise in temperature and the heat produced will be dissipated in the surrounding medium causing the increase in conduction

loss. Similarly Fig. 6.70 shows the plot of dielectric relaxation time versus inverse of temperature for second series and that of third series is shown in Fig. 6.71 for all samples at different temperatures. All these plots exhibit Arrhenius behavior and the slope of which gives activation energy for conductivity relaxation.

The compositional dependence of relaxation time ( $\tau_\sigma$ ) and activation energy ( $E_\tau$ ) for the glass samples of first series are shown in Fig.6.72 It is clearly observed from the figure that the relaxation time increases with the modifier content except for 30 mol% sample where its value is slightly low. The results are as expected and discussed earlier for conductivity and hopping frequency (Figs. 5.12 (a) and 6.35). The activation energy ( $E_\tau$ ) increases with modifier except for 30 mol % sample.

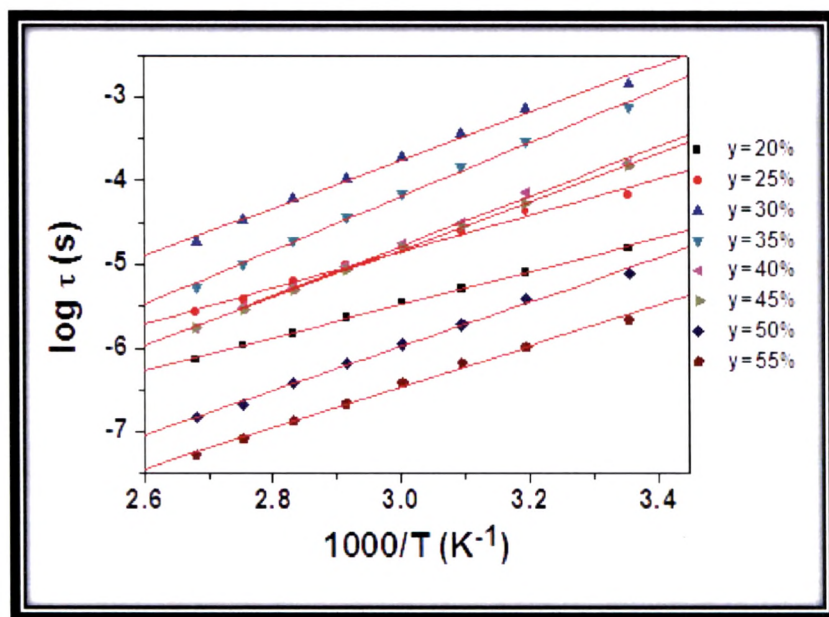


Fig.6.70.  $\log \tau$  versus  $1000/T$  plot for all samples of second series.

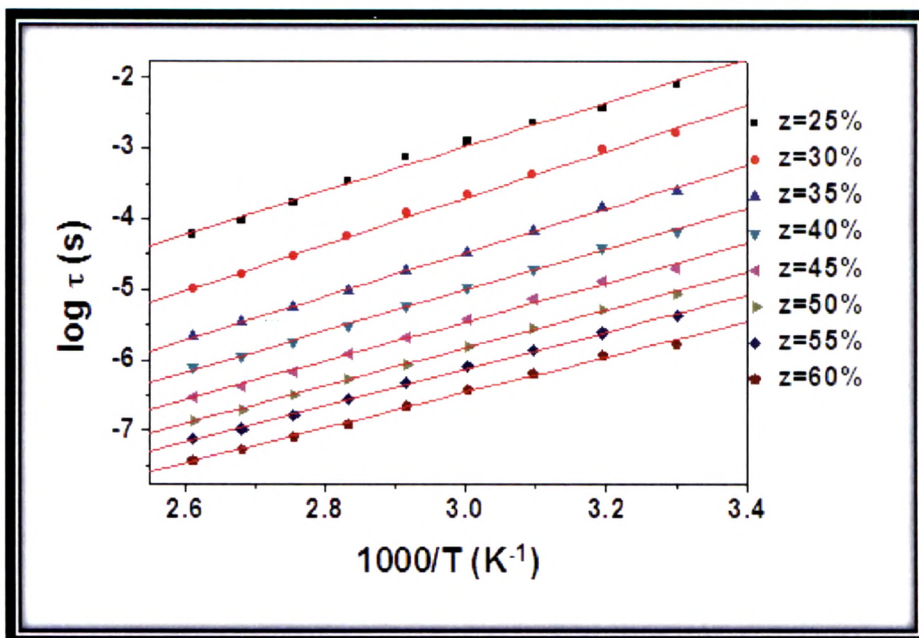


Fig.6.71.  $\log \tau$  versus  $1000/T$  plot for all samples of third series.

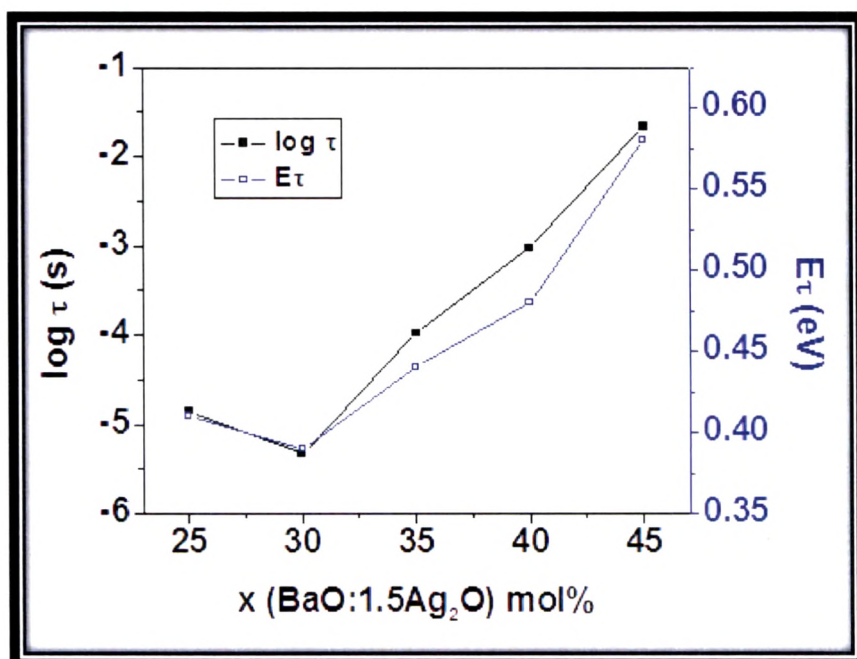


Fig.6.72. Variation of relaxation time and activation energy with the modifier content in first series.

The value of relaxation time with composition for the second series, as shown in Fig.6.73, increases with the addition of  $\text{Ag}_2\text{O}$  upto 30 mol% and after that it decreases continuously. The activation energy calculated by the plots of relaxation time increases upto 35 mol%, thereafter it decreases. The reason for this behavior is clear from conductivity results (Fig.5.13) where upto 30 mol% of  $\text{Ag}_2\text{O}$ , the electronic conductivity dominates and after 30 mol% of  $\text{Ag}_2\text{O}$ , ionic conductivity dominates in the system and a deep minimum in the isotherm of conductivity is observed. The hopping frequency (Fig.6.36) shows minima at 30 mol% of  $\text{Ag}_2\text{O}$  since relaxation time and hopping frequency are inversely proportional to each other.

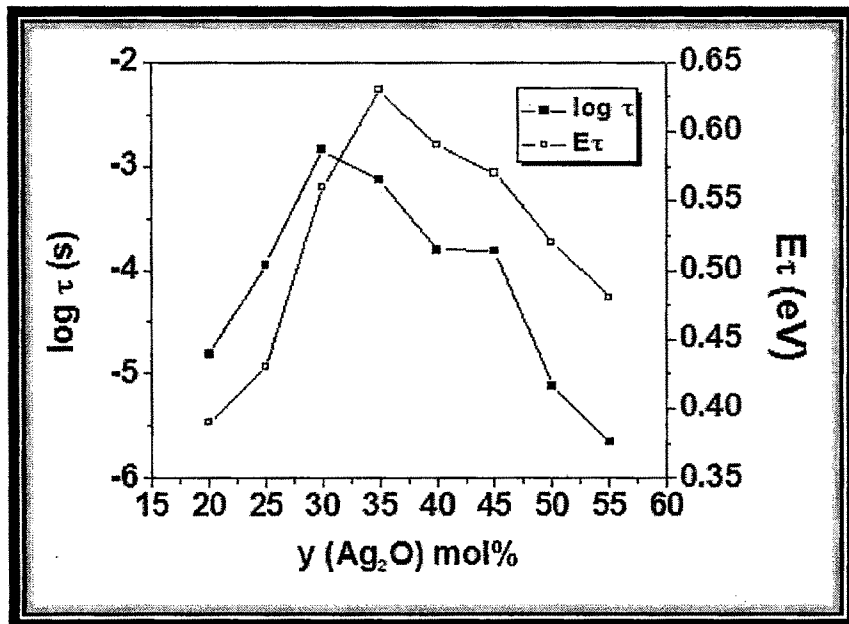


Fig.6.73. Variation of relaxation time and activation energy with modifier  $\text{Ag}_2\text{O}$  in second series.

Now the variation of relaxation time and activation energy with modifier ( $\text{Ag}_2\text{O}$ ) for third series is shown in Fig.6.74. In this series the relaxation time decreases continuously with modifier increase but the activation energy decreases except for 30 mol% where it is slightly high. The activation energies calculated by conductivity and hopping frequency behave similarly as that, calculated by relaxation time, where it decreases continuously except for 30 mol% sample. In all the glass samples of three series, the variation of activation energies, calculated by conductivity ( $E_\sigma$ ), hopping frequency ( $E_h$ ) and relaxation time ( $E_\tau$ ) with composition are observed to be quite close to each other. This suggests that the

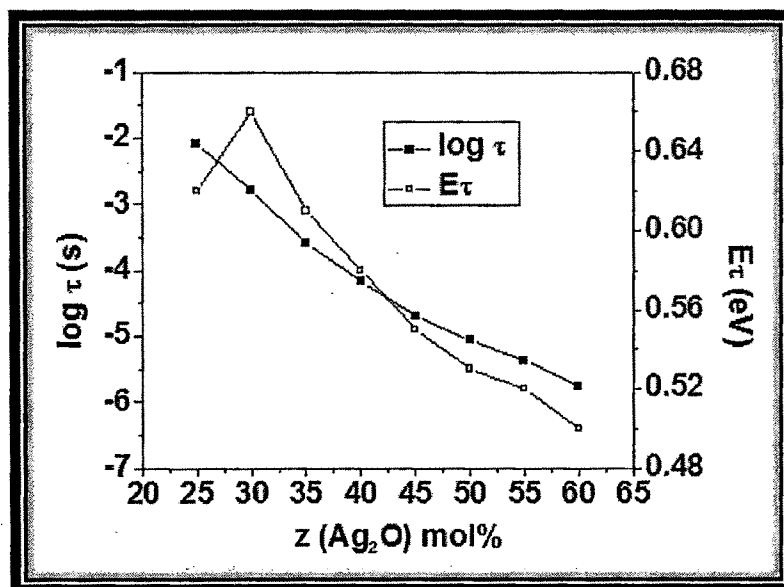


Fig.6.74. Variation of relaxation time and activation energy with modifier  $\text{Ag}_2\text{O}$  in third series.

relaxation time is determined by the flow of charge carriers. Now, it is possible to say that the motion of mobile charge carriers, i.e.,  $\text{Ag}^+$  ions in the present case are responsible for both conductivity and relaxation effect. The Relaxation time, flow of type of charge carriers and behavior of conductivity with composition suggest the mixed conductivity in the present glass system i.e., electronic and/or ionic.

## 6.4 Modulus Analysis:

The dispersion behavior of the conductivity in the frequency domain is more conveniently interpreted in terms of conductivity relaxation time,  $\tau$ , using the electrical modulus,  $M^*=1/\varepsilon^*$  representation [10]. Complex electric modulus  $M^*$  formalism is used very frequently when the relaxation behavior is presumed to be due to the motion of ions or electrons [90]. Although, originally conceived as a formalism to separate space-charge effects from the bulk conductivity, the  $M^*$  representation is now widely used to analyze ionic conductivities by associating a conductivity relaxation time ( $\tau$ ) with the ionic process [90, 91]. The use of modulus formalism in presenting frequency dependent dielectric or conductivity data has the advantage of eliminating any spurious effects due to contacts or interfaces (Maxwell-Wagner effects) [92, 93].

According to Macedo et. al. [10], the electric modulus was defined as the electric analog of the dynamical mechanical modulus and was related to the complex permittivity  $\varepsilon^*(\omega)$  by

$$M^*(\omega) = \left( \frac{1}{\varepsilon^*(\omega)} \right) = \{ \varepsilon'(\omega) - j\varepsilon''(\omega) \} | \varepsilon^*(\omega) |^2 \dots\dots\dots(6.72)$$

$$= M'(\omega) + jM''(\omega)$$

$$= M_\infty \left[ 1 - \int_0^\infty \exp(-j\omega t) \left( -\frac{d\phi(t)}{dt} \right) dt \right] \dots\dots\dots (6.73)$$

where  $M'$  and  $M''$  are the real and imaginary part of the complex modulus  $M^*$  and  $M_\infty=1/\varepsilon_\infty$  is the inverse of high frequency dielectric constant  $\varepsilon_\infty$  [10, 94]. The function  $\phi(t)$  gives the time evolution of the electric field within the materials and  $\omega=2\pi f$  is the angular frequency.

Analysis of electrical relaxation in terms of complex permittivity  $\epsilon^*(\omega)$  gives relaxational parameters, characteristics of the decay of the displacement vector  $\bar{D}$ , under the constraint of constant electric field,  $\bar{E}$  [9]. It has been suggested [10, 90, 94-99] that for electrical relaxation in dielectrics containing a substantial concentration of mobile charges, it is generally more fruitful to focus attention on the decay of electric field  $\bar{E}$  at constant  $\bar{D}$  (displacement vector). If surface charges of an opposite sign are instantaneously placed on opposite faces of an ionic conductor at time zero and then maintained at a constant value, an electric field will arise inside the material which with time will decay to zero due to migration of the mobile ions. The expression for the decay of electric field in time domain can be written as

$$\bar{E}(t) = \bar{E}(0) \phi(t) \quad \dots\dots\dots(6.74)$$

where  $\bar{E}(0)$  denotes the electric field at time  $t=0$  and  $\phi(t)$  is a macroscopic decay function of the general form

$$\phi(t) = \int_0^\infty g(\tau_\sigma) \exp(-t/\tau_\sigma)^\beta d\tau_\sigma \quad \dots\dots\dots(6.75)$$

Thus, 
$$\bar{E}(t) = \bar{E}(0) \int_0^\infty g(\tau_\sigma) \exp(-t/\tau_\sigma)^\beta d\tau_\sigma \quad \dots\dots\dots(6.76)$$

where  $\tau_\sigma$  is an electric field or conductivity relaxation time, and  $g(\tau_\sigma)$  is a normalized density function for relaxation times.

Thus, using Eqs. 6.73 and 6.75, it becomes

$$M^*(\omega) = M_\infty \int_0^\infty g(\tau_\sigma) \left[ \frac{j\omega\tau_\sigma}{(1 + j\omega\tau_\sigma)} \right] d\tau_\sigma \quad \dots\dots\dots(6.77)$$

In glassy materials, the decay function  $\phi(t)$  is found to exhibit non exponential

(i.e., if there is a distribution of relaxation times and  $g(\tau_\sigma)$  is not a delta function) nature. The decay of the electric field due to the migration of mobile ions will then give rise to a non zero frequency dispersion ( $\epsilon_0 - \epsilon_\infty$ ) in the dielectric constant  $\epsilon'$ . In time domain, a good description for the decay function is the so called *stretched exponential* introduced by *Kohlraush-Williams-Watts* (KWW) [100, 101] and is given as

$$\phi(t) = \exp\left(\frac{-t}{\tau_\sigma}\right)^\beta ; \quad 0 < \beta < 1 \quad \dots\dots\dots(6.78)$$

where  $\tau_\sigma$  and  $\beta$  are the parameters of stretched exponential function and are respectively the conductivity relaxation time and the Kohlrausch exponent. The value of  $\beta$  varies from 1 (Debye process) to 0. The smaller is the value of  $\beta$ , the larger is the deviation of the relaxation with respect to a Debye type relaxation. The  $\beta$  parameter has been interpreted either as representatives of a distribution of relaxation times [90, 96] or as characteristic of cooperative motions between charge carriers [99, 102]. Analysis of the impedance data on the modulus formalism assumes importance, as it suppresses the electrode effects occurring at low frequencies [12, 103, 104] and the modulus can also be used for studying conductivity relaxation times [105, 106]. The electric modulus data can be obtained from the complex impedance data according to the relation

$$M^* = M' + j M'' = j\omega C_0 Z^* \quad \dots\dots\dots(6.79)$$

such that  $C_0 = \epsilon_0 \left(\frac{A}{t}\right)$  is the vacuum capacitance,  $Z^*$  is the complex impedance,  $\epsilon_0 = 8.854 \times 10^{-14}$  F/cm is the permittivity of free space,  $A$  and  $t$  are the cross section and thickness of the sample respectively. In the present work, the

impedance data were converted into electrical modulus using the relationship  $M' = \omega C_0 Z'$  and  $M'' = \omega C_0 Z''$  respectively [33, 107] where  $Z'$  and  $Z''$  are the real and imaginary part of the complex impedance respectively.

Fig.6.75 shows the real part of the modulus spectrum for  $x=35$  mol% of (BaO:1.5 Ag<sub>2</sub>O) modifier content in the glass system  $x$  (BaO:1.5Ag<sub>2</sub>O)-(95- $x$ ) V<sub>2</sub>O<sub>5</sub>-5 TeO<sub>2</sub> at different temperatures. Figure shows that,  $M'$  approaches to zero at lower frequencies, which indicates that the electrode polarization make negligible contribution [56] to  $M^*$  and lack of a restoring force for flow of charge under the influence of a steady electric field [10]. It may be ignored when the electric data are analyzed in this form [96]. At higher frequencies  $M'$  reaches a maximum

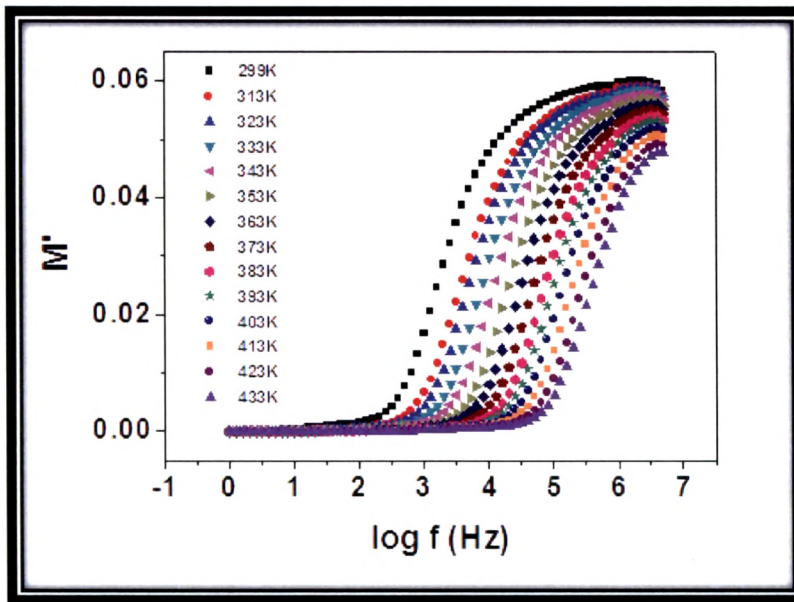


**Fig.6.75.** Variation of  $M'$  with frequency for  $x=35$  mol % of first series at different temperatures.

constant value  $M_\infty$ . At higher temperatures,  $M'$  level off at frequencies higher than that of those at lower temperatures because the relaxation processes are spread over a range of frequencies. Similar frequency dependence of real part of modulus ( $M'$ ) is shown in Fig. 6.76 for  $y=35$  mol % of  $\text{Ag}_2\text{O}$  where only  $\text{Ag}_2\text{O}$  is varied with respect to  $\text{V}_2\text{O}_5$  keeping  $\text{BaO}$  and  $\text{TeO}_2$  as constant in  $10 \text{ BaO}-y \text{ Ag}_2\text{O}-(85-y) \text{ V}_2\text{O}_5-5 \text{ TeO}_2$  glass system and for the sample  $z=45$  mol % of  $\text{Ag}_2\text{O}$  is shown in Fig. 6.77 for the series  $5 \text{ BaO}-z \text{ Ag}_2\text{O} 35 \text{ V}_2\text{O}_5-(60-z) \text{ TeO}_2$  where  $\text{Ag}_2\text{O}$  is varied with respect to  $\text{TeO}_2$ . Other glass compositions also showed the similar characteristics but their frequency of dispersion are different in different glass systems as can be observed in the figures.

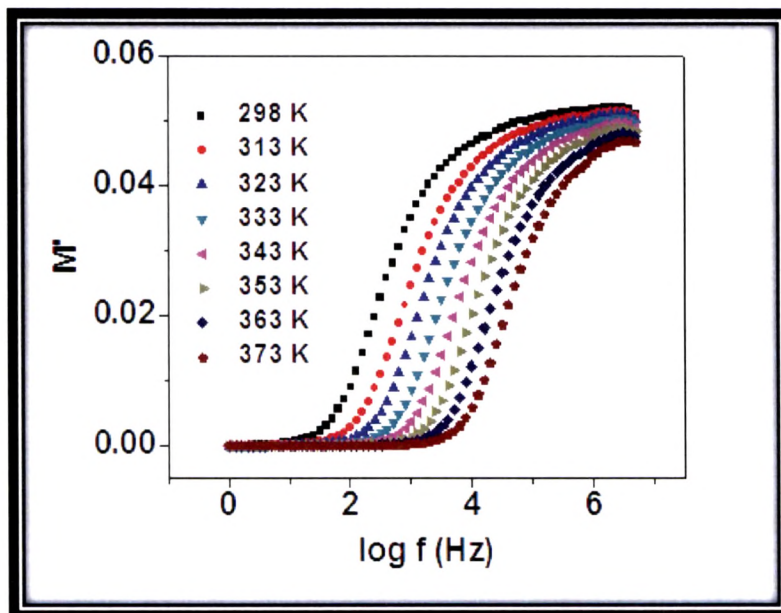
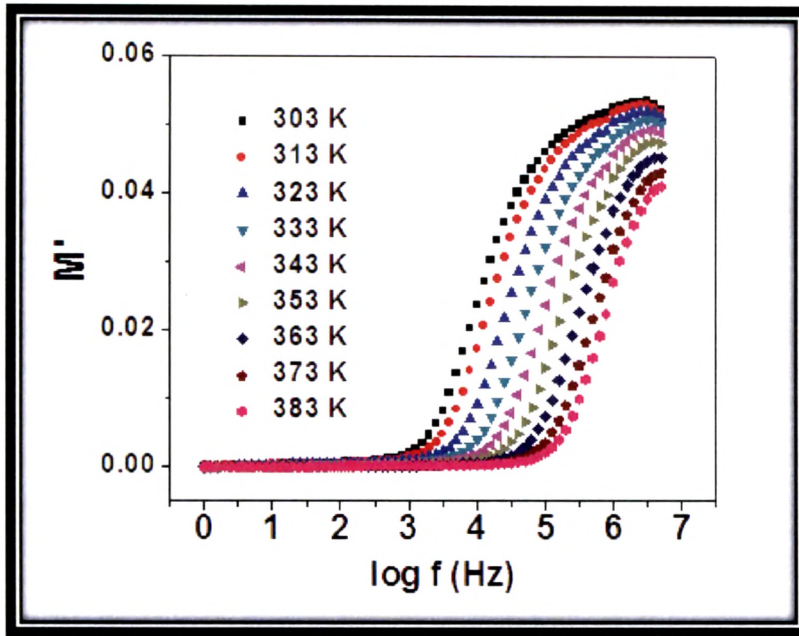
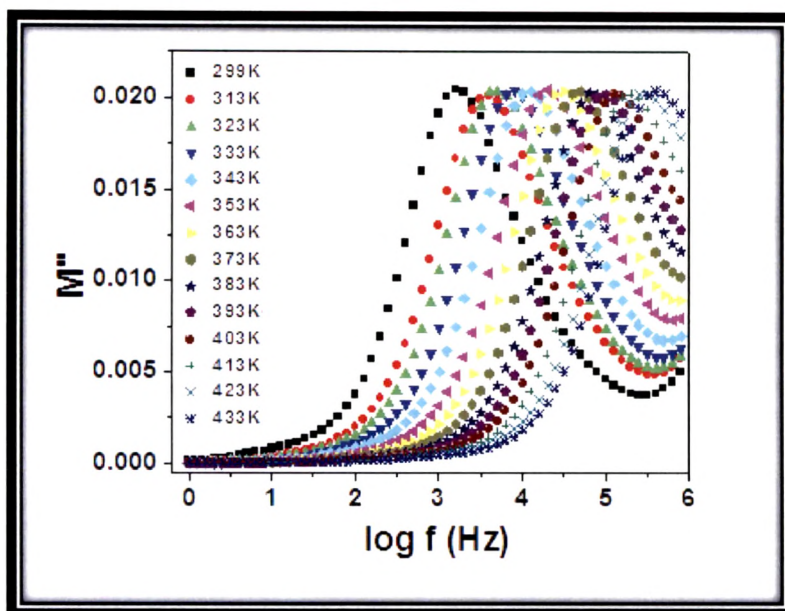


Fig.6.76. Variation of  $M'$  with frequency at different temperatures for  $y=35\%$  sample of second series.



**Fig.6.77. Variation of  $M''$  with frequency for  $z=45\%$  sample of third series at different temperatures.**

Variation of the imaginary part of the modulus ( $M''$ ) with logarithm of frequency at different temperatures is shown in Fig. 6.78 for the sample  $x= 35$  mol % of modifier content for first series. Figure shows a long tail at low frequencies and is due to the large capacitance associated with the electrodes. It is also seen that  $M''$  spectra have an asymmetry with the peak approximately centered in the dispersion region of  $M'$ . The low frequency wing of the peak represents the range of frequencies in which the ions can move over long distances, i.e., ions can perform successful hopping from one site to the neighboring site. On the other hand, corresponding to the high frequency wing of the  $M''$  peak, the ions are spatially



**Fig.6.78. Variation of  $M''$  with frequency at different temperatures for  $x= 35$  mol% sample of first series.**

confined to their potential wells [108] and the ions can make only localized motion with in the wells. Similar variation of the imaginary part  $M''$  of modulus with log frequency at different temperatures is shown in Fig. 6.79 for second series at  $y= 40$  mol % of  $\text{Ag}_2\text{O}$  and in Fig. 6.80 for third series at  $z= 40$  mol % of  $\text{Ag}_2\text{O}$ . It is clear from the above figures that the shape of the spectrum remains constant but the frequency of the modulus maximum  $M''_{\text{max}}$  shifts to higher frequency side with increase in temperature. It may also be noted that the magnitude of  $M''$  peak with temperature is found to be constant. The constancy of the height of the modulus plot suggests the invariance of the dielectric constant and distribution of relaxation times with temperature [109]. The frequency  $\omega_c$ ,

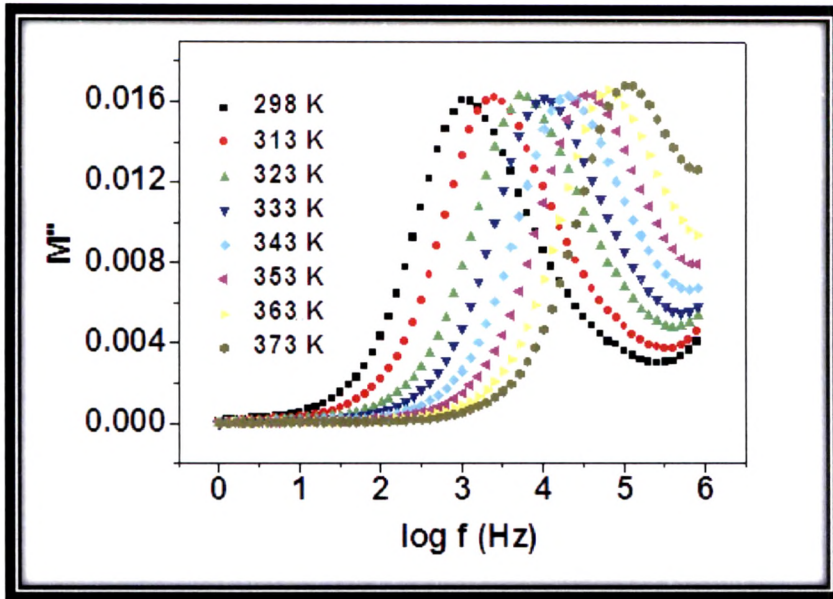


Fig.6.79. Variation of  $M''$  with frequency at different temperatures for  $y=40\%$  sample of second series.

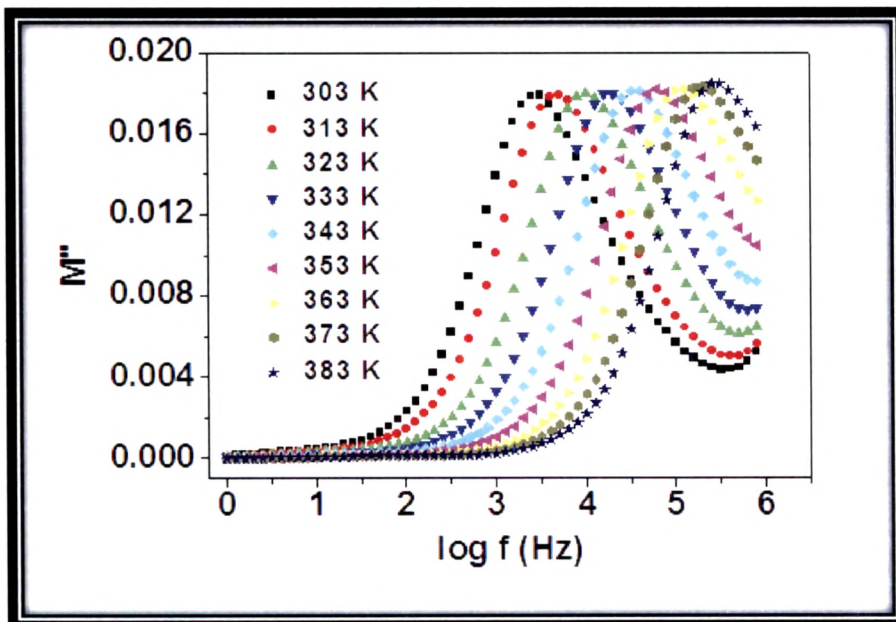


Fig.6.80. Variation of  $M''$  with frequency at different temperatures for  $z=40\%$  sample of third series.

where the maximum in  $M''$  occurs is indicative of the transition from a short range to long range mobility at decreasing frequency and is given by the condition  $\omega_c \tau_c = 1$ , where  $\tau_c$  is the conductivity relaxation time [56, 110, 111]. The variation of  $M'$  and  $M''$  at low and high frequencies can be predicted by the following model proposed by Macedo et. al. [10]

$$\begin{array}{ll} \lim_{\omega \tau_c \ll 1} M' = 0 & \lim_{\omega \tau_c \gg 1} M' = M_s \\ \lim_{\omega \tau_c \ll 1} M'' = 0 & \lim_{\omega \tau_c \gg 1} M'' = 0 \end{array}$$

The result obtained in the present system is in good agreement with the above model. Similar observations are reported in other silver conducting glasses [74, 110, 112].

The Variation of the frequency value at  $M'_{max}$  i.e.,  $f_{max}$  with the composition for first series is shown in Fig.6.81. It is observed from the figure that  $f_{max}$  initially increases for 30 mol% of modifier after that it decreases. The similar behavior is observed in the hopping frequency (Fig.6.35) where it shows slightly high value at 30 mol% sample due to the high conductivity of this sample. Similarly, compositional dependence of the frequency value at  $M'_{max}$  at room temperature for second series is shown in Fig.6.82 where BaO is kept constant and only  $Ag_2O$  is increased with respect to  $V_2O_5$ . In this series  $f_{max}$  decreases upto 30 mol%, after that its value continuously increases for rest of the samples. Similar variation is also observed in conductivity and hopping frequency of this series showing deep minima at 30 mol% in their isotherm due to the change of transport mechanism from electronic to the ionic one. Similarly the variation of  $f_{max}$  with composition in

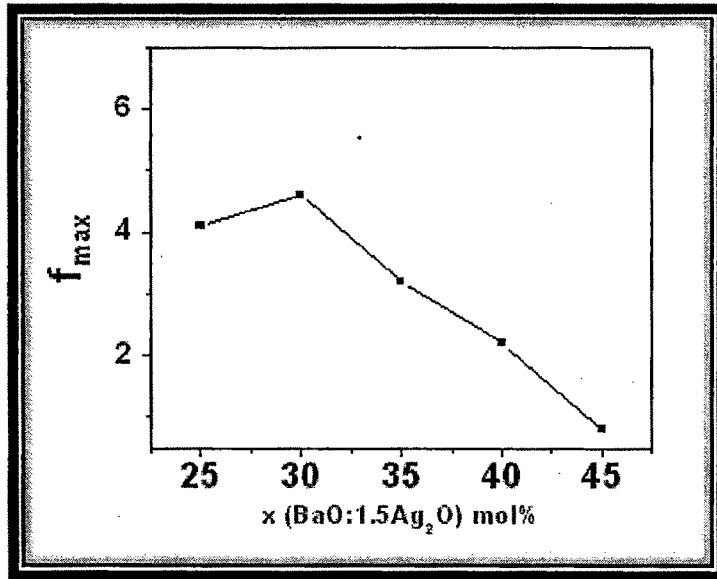


Fig.6.81. Compositional dependence of  $f_{max}$  value with the modifier content in first series.

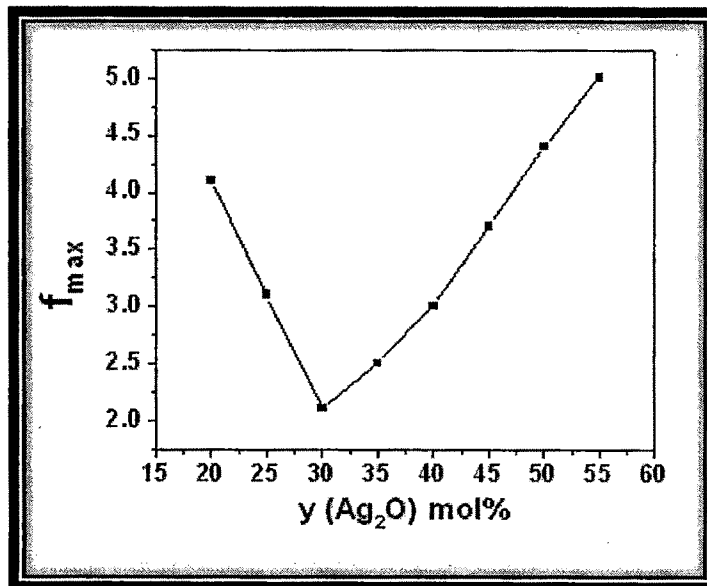
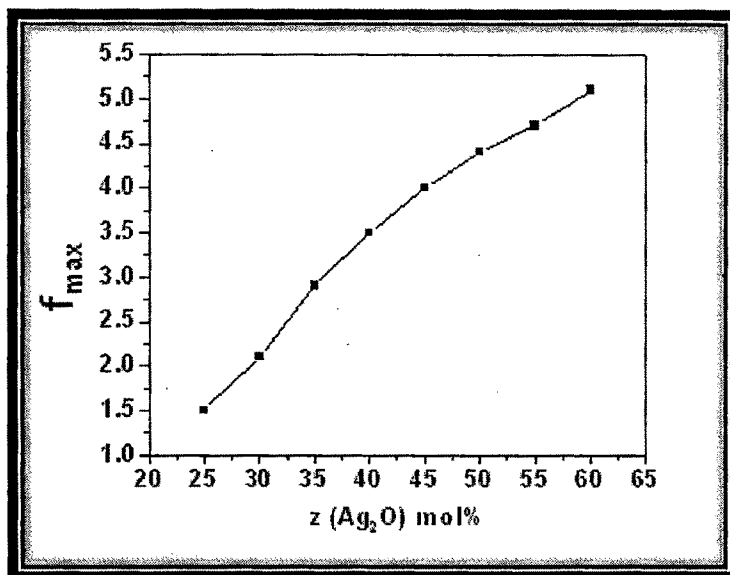


Fig.6.82. Compositional dependence of  $f_{max}$  value with the modifier content in second series.



**Fig.6.83. Compositional dependence of  $f_{max}$  with the modifier content in third series.**

third series where BaO is further decreased in comparison to second series and kept as constant at 5 mol%, is shown in Fig.6.83. Here it is observed from the figure that the  $f_{max}$  value continuously increases in this series as the conductivity also increases with the increase of Ag<sub>2</sub>O. Thus the variation of  $f_{max}$  with the composition in all the three series is similar to that of conductivity and hopping frequency.

The variation of frequency corresponding to  $M_{max}^*$  i.e.,  $f_{max}$  with temperature for the systems  $x=35$  and  $40$  mol % of first series are shown in Fig. 6.84. These plots obey the Arrhenius nature and the activation energies calculated from the modulus spectrum are also comparable to the conductivity values obtained from the impedance spectrum. The calculated values of activation energy  $E_{fmax}$  from

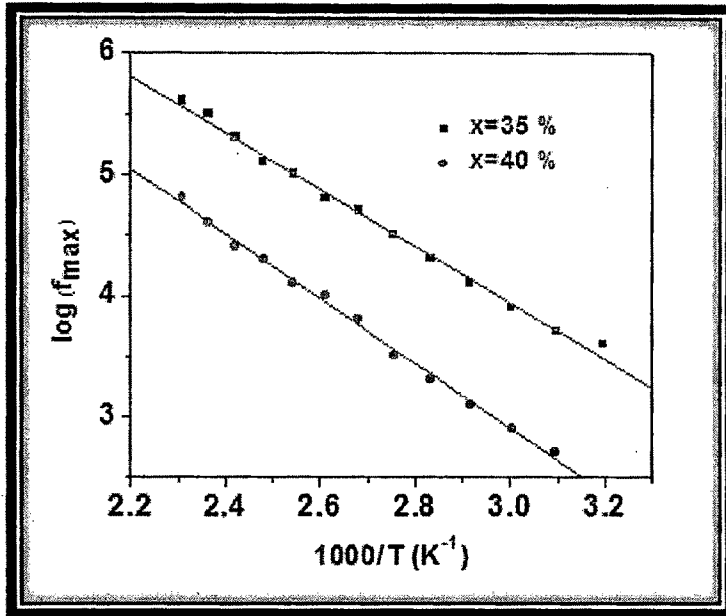


Fig.6.84. Plot of  $\log f_{max}$  vs.  $1000/T$  for first series.

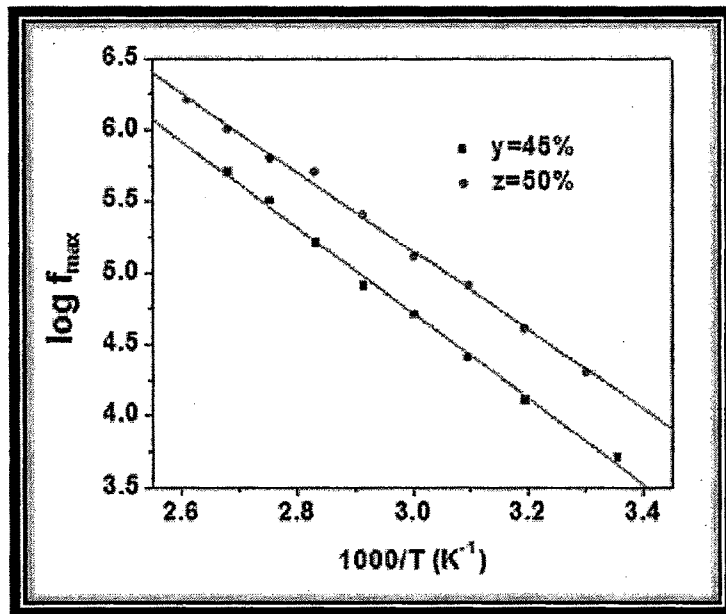


Fig.6.85. Plot of  $\log f_{max}$  vs.  $1000/T$  for  $y=45\%$  sample of second and  $z=50\%$  sample of third series.

modulus spectrum are given in Table.6.3 for three different series. The plot of  $\log f_{max}$  versus  $1000/T$  for  $y= 45$  mol % of second series and  $z= 50$  mol % of third series are shown in Fig. 6.85. The activation energies calculated from the least square straight line fitting of the above Figs.6.84 and 6.85 are also comparable to that obtained from the impedance spectrum. The near value of activation energy obtained from both impedance and modulus spectrum suggests that transport of silver ions in the present system is by a hopping mechanism [109, 113].

A master plot of the modulus isotherms is shown in Fig.6.86 for  $x=35$  mol % of  $(\text{BaO}:1.5 \text{Ag}_2\text{O})$  modifier content in first series  $x (\text{BaO}:1.5\text{Ag}_2\text{O})-(95-x)\text{V}_2\text{O}_5-5\text{TeO}_2$ , where  $M'$  (or  $M''$ ) is scaled by  $M_\infty$  (or  $M'_{max}$ ) and the frequency axis is scaled by the peak frequency  $f_{max}$ , where  $f_{max}$  is frequency corresponding to  $M'_{max}$ .

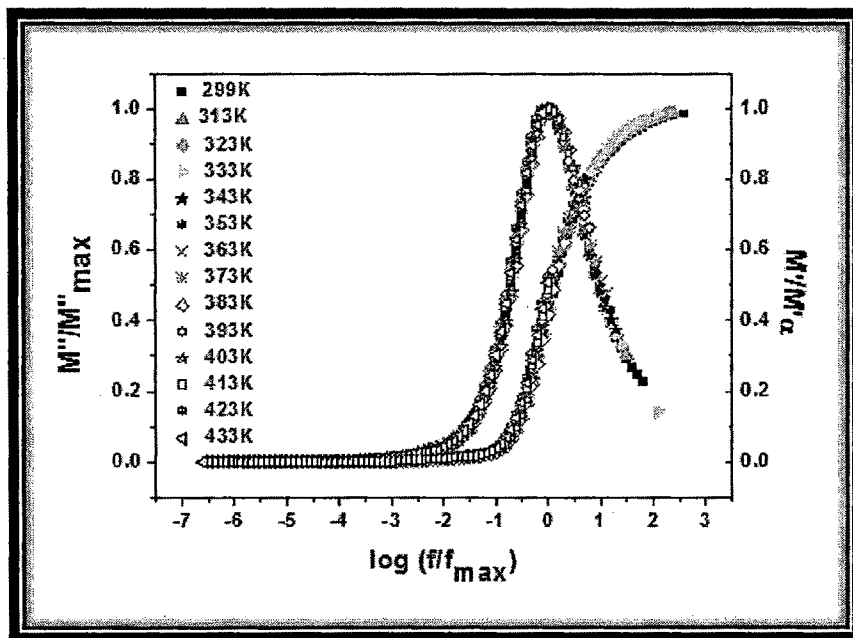


Fig.6.86. Plots of  $M''/M''_{max}$  and  $M'/M'_\infty$  at different temperatures for  $x=35$  % sample of first series.

The near perfect overlap of the data at different temperatures on a single master curve indicates that all the dynamic processes occurring at different frequencies exhibit the same thermal activation energy or in the other way the relaxation mechanism involved is temperature independent. Other glass compositions of this series also showed the similar behavior. Similarly the normalized real and imaginary part of the modulus versus normalized frequency  $\log (f/f_{max})$  for the second series is shown in Fig. 6.87 for  $y= 35$  mol and that of third series is shown in Fig. 6.88 for  $z= 35$  mol %. It can be seen from figures that the plots are clearly super imposable and the data points are found to collapse very well for all the temperatures studied. The super imposition of the plots indicates that the dynamical processes of ion transport are same throughout the range of temperature.

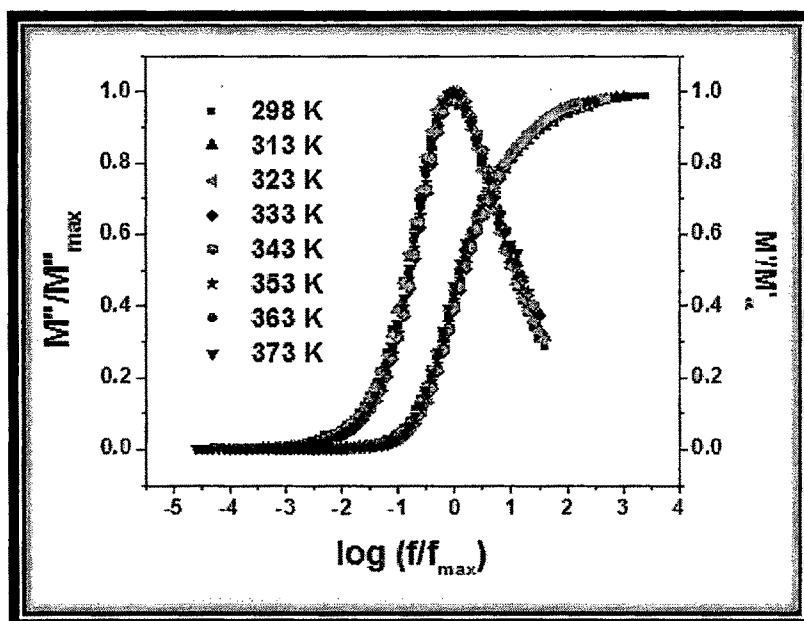
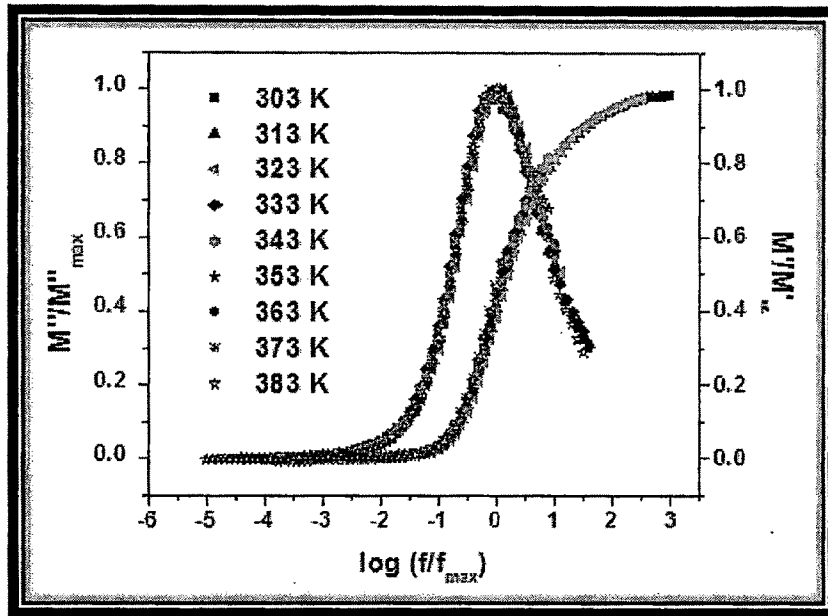


Fig.6.87. Plots of  $M''/M''_{max}$  and  $M'/M'_{\infty}$  at different temperatures for  $y=35\%$  sample of second series.



**Fig.6.88. Plots of  $M''/M''_{max}$  and  $M''/M'_{\infty}$  at different temperatures for  $x=35\%$  sample of third series.**

The scaled spectra of  $M''$  for different compositions of all series at room temperature are shown in Figs. 6.89, 6.90 and 6.91. The curves present high degree of superimposing leading to the same master curve behavior at different compositions. This development suggests a common relaxation mechanism in these glasses for the studied composition range. A remarkable characteristic of this type of data representation is that a direct comparative analysis can be performed for each branch of curves  $M''/M''_{max}$  versus  $\log(f/f_{max})$ . In the same way, any type of dispersion phenomenon can be easily detected. The scaling of the frequency by  $f_{max}$  parameter gives a distribution of  $M''/M''_{max}$  values considering logarithmic representation at around  $(f/f_{max})=1$ . At frequency above

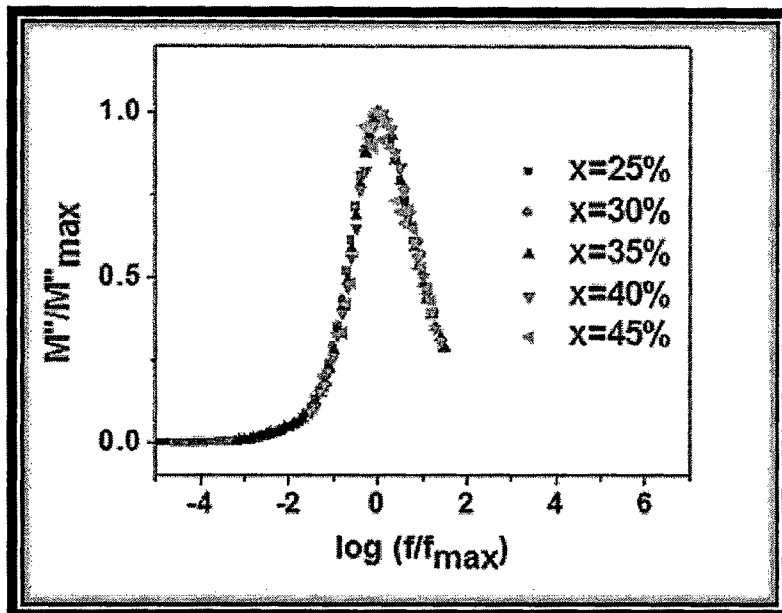


Fig.6.89. Plot of  $M''/M''_{\max}$  vs.  $\log(f/f_{\max})$  at 298 K for different samples of first series.

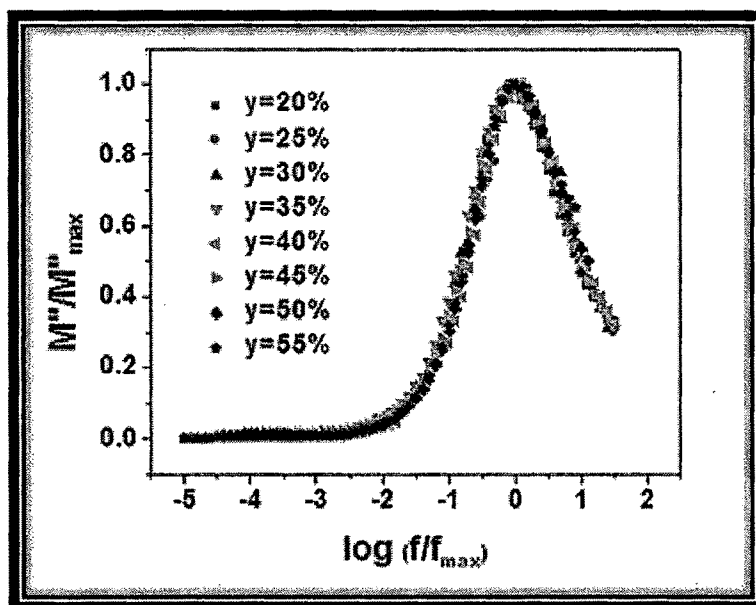


Fig.6.90. Plot of  $M''/M''_{\max}$  vs.  $\log(f/f_{\max})$  at 298 K for different samples of second series.

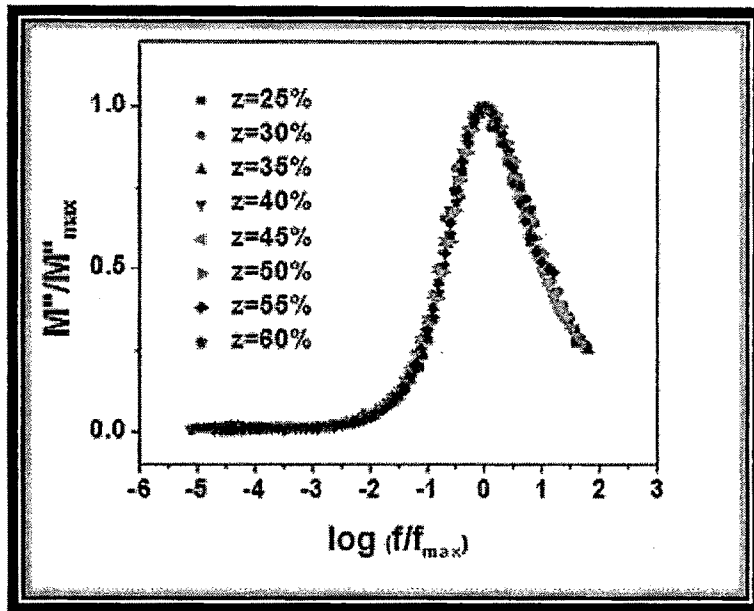


Fig.6.91. Plot of  $M''/M''_{max}$  vs.  $\log(ff_{max})$  at 303 K for different samples of third series.

this value, some degree of dispersion can be observed depending on the glass formulation and temperature of measurement.

The normalized modulus plot is non-symmetric in agreement with the non-exponential behavior of the electrical function which is well described by the Kohlrausch-William-Watts (KWW) exponential function as given in Eq. (6.77) and is known to provide satisfactory fit for the asymmetrical  $M''$  peaks. The value of  $\beta$  can be evaluated by knowing the full width at half height (FWHH) of the

$M''/M''_{max}$  plot, where  $\beta = \frac{1.14}{FWHH}$  value. In first series, the width at half height of

the modulus spectrum for the sample  $x=35$  mol% at different temperatures is close to 1.7 decades and the  $\beta$  results in the value of 0.67. The values of  $\beta$  at room

**Table.6.3: KWW exponential function  $\beta$  and activation energy from modulus plot  $E_{fmax}$  of three different series.**

First series			Second series			Third series		
x (mol%)	$\beta$	$E_{fmax}$ (eV)	y (mol%)	$\beta$	$E_{fmax}$ (eV)	z (mol%)	$\beta$	$E_{fmax}$ (eV)
25	0.63	0.42	20	0.67	0.42	25	0.63	0.65
30	0.67	0.44	25	0.67	0.48	30	0.60	0.65
35	0.67	0.46	30	0.64	0.58	35	0.63	0.62
40	0.71	0.51	35	0.63	0.61	40	0.67	0.60
45	0.54	0.56	40	0.64	0.61	45	0.60	0.58
			45	0.67	0.60	50	0.63	0.55
			50	0.63	0.57	55	0.63	0.53
			55	0.67	0.51	60	0.63	0.50

temperature for other samples of this series are given in Table.6.3. The exponent  $\beta$  generally lies between 0 and 1 and it is widely used to describe different kinds of relaxation processes in amorphous materials. Considering  $\beta$  parameter smaller than 1, some authors [114, 115, 116] have suggested that it can be correlated to a distribution of relaxation times in the material. At low temperatures, the relaxation occurs via isolated non interacting dipoles, becoming more and more Debye like and  $\beta$  values tend towards unity [117] and there is a general tendency of  $\beta$  to decrease with temperature. But in the present study, the values of  $\beta$  seem to level off in the range 0.6 to 0.7, which is found to be insensitive to the variation of both temperature and composition. If the stretched exponent  $\beta$  is sensitive to the variation of temperature and composition then one would have been explained its behavior by considering an approach to treat the stretched exponential behavior as a manifestation of a distribution of relaxation times.

In second series, the width at half height of the modulus spectrum at different temperatures is close to 1.78 decades and the  $\beta$  results in the value of 0.64 for  $y=40$  mol % of  $\text{Ag}_2\text{O}$  while in third series, the width at half height is close to 1.9 decades and the  $\beta$  values of  $z=40$  mol % is 0.6. The  $\beta$  values for all other compositions of these series are given in Table.6.3. Here,  $\beta$  results in a value of 0.6 for the different samples of the different series. The  $\beta$  value obtained for the present glass composition is comparable with those of other  $\text{Ag}^+$  ion conducting glasses [56, 109].

According to Ngai et. al. [99], the  $\beta$  parameter gives the extent to which the mobile ions couple during the conduction processes. The concept of the cooperative motions in a glass is issued from the universal behavior discussed by

Jonscher [43]. It means that jump of a mobile ion in a glass may not be treated as an isolated event i.e., when the ion jumps from one equilibrium position to another, it causes a time dependent movement of other charge carriers in the surroundings, which leads to additional relaxation of the applied field [118]. Therefore, it results the smaller value of  $\beta$  to a more extended cooperative motion between the charge carriers [118]. The non-exponential parameter  $\beta$  obtained from the modulus formalism and the frequency exponent parameter  $n$  obtained from the power law model represent the interaction between the charge carriers. Ngai [119] has proposed that a correlation exists between  $n$  and  $\beta$  namely  $n=1-\beta$ . However, we have not found such a relation for the present glasses. This is because of the fact that the shape of the modulus spectra is influenced by the values of the high frequency dielectric constant [120]. In contrast, the conductivity takes into account the high frequency region of the conductivity spectra.

In case of an ideal circuit, the impedance and modulus spectroscopic plots i.e.,  $Z''$ ,  $M''$  versus  $\log f$  plots are completely super imposable and is given in Eqn. (6.80)

$$Z'' = R \frac{\omega RC}{1+(\omega RC)^2} \quad \text{and} \quad M'' = \frac{C_0}{C} \frac{\omega RC}{1+(\omega RC)^2} \quad \dots\dots\dots(6.80)$$

The Debye like peak shapes in the spectroscopic plots is given by the term,

$$\frac{\omega RC}{1+(\omega RC)^2}$$

in the imaginary parts of both  $Z''$  and  $M''$ . It can be seen that the  $Z''$  peaks are scaled by  $R$  where as the  $M''$  peaks are scaled by  $C_0/C$ . But in the case of practical solid electrolytes, they need to be represented by a series array of  $RC$  elements in order to account for various layers within the material [121, 11]. As a result, there is usually a distribution of relaxation times, in which case the maxima in the impedance and modulus spectra no longer coincide. To understand the non-

Debye behavior of the present system, impedance and modulus spectrum at room temperature have been plotted in Fig. 6.92 for  $x=25$  mol % of (BaO:1.5 Ag<sub>2</sub>O) in first series  $x$  (BaO:1.5 Ag<sub>2</sub>O)- (95- $x$ ) V<sub>2</sub>O<sub>5</sub>-5 TeO<sub>2</sub>. It can be seen from the figure that  $Z''_{\max}$  and  $M''_{\max}$  do not occur at the same frequency and a broadened modulus spectra is obtained which is an indication of the wide distribution of relaxation times. Similar impedance and modulus values with log frequency at room temperature are also shown in Fig. 6.93 for  $y=55$  mol % of Ag<sub>2</sub>O in second series while Fig. 6.94 shows the same plot for  $z=50$  mol % in third series. These curves also show that  $Z''_{\max}$  and  $M''_{\max}$  do not occur at the same frequency, which indicates wide distribution of relaxation times. The above figures also show that the  $Z''$  spectra are broadened on the low frequency side of the peak maximum and

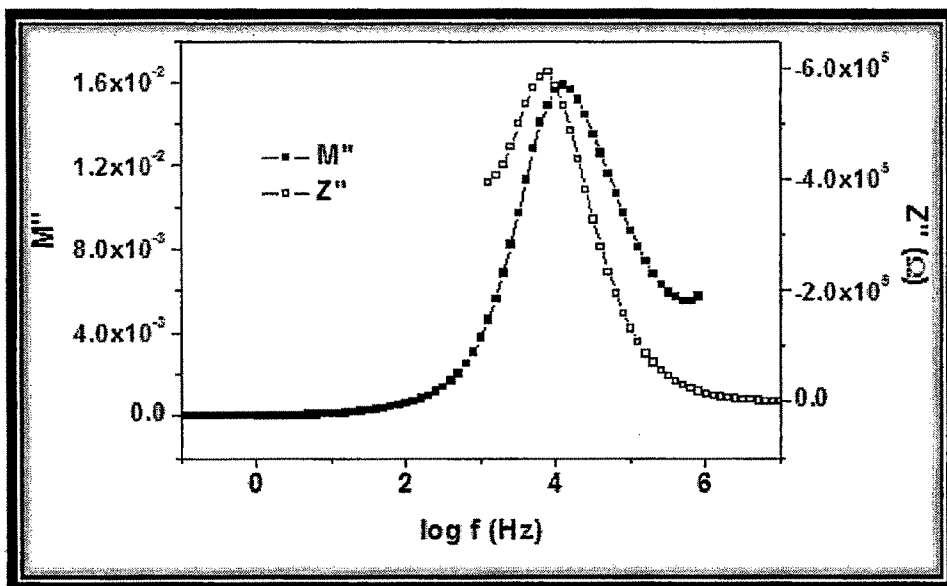


Fig.6.92.  $Z''$  and  $M''$  vs.  $\log f$  plot at 298 K for  $x=25$  mol% sample of first series.

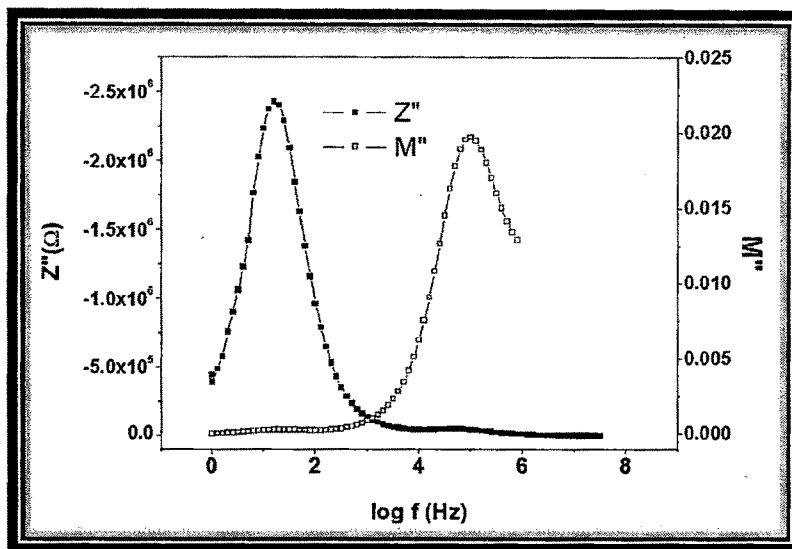


Fig.6.93. Plot of  $Z''$  and  $M''$  vs.  $\log f$  at 298 K for  $y=55\%$  sample of second series.

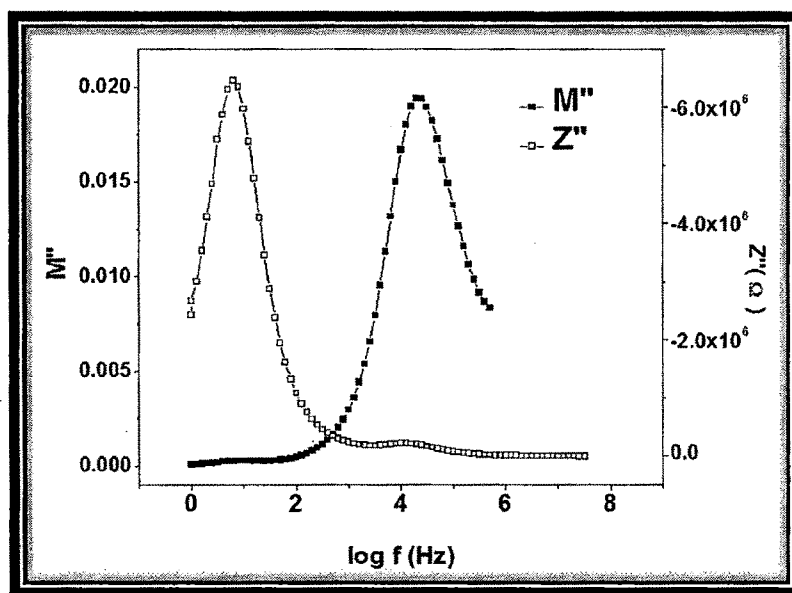


Fig.6.94. Plot of  $M''$  and  $Z''$  vs.  $\log f$  at 303 K for  $z=50\%$  sample of third series.

$M''$  spectra are broadened on the high frequency side. The large rise in  $Z''$  occurring at low frequencies is caused mainly by electrode polarization [122].

#### 6.4.1 Glass decoupling Index:

The glass decoupling index  $R_r(T_g)$  describes the extent to which the conducting ion motion in a given glass can be considered decoupled from the viscous motions of the glassy matrix and is consequently related to the ability of mobile ions to migrate in the glassy electrolytes at  $T_g$  [123, 124]. The decoupling index is defined by Angell [124, 125] as

$$R_r(T_g) = \frac{\langle \tau_s(T_g) \rangle}{\langle \tau_\sigma(T_g) \rangle} \dots\dots\dots(6.81)$$

where  $\langle \tau_s(T_g) \rangle$  and  $\langle \tau_\sigma(T_g) \rangle$  are the average structural and conductivity relaxation times respectively at the glass transition temperature ( $T_g$ ). The conductivity relaxation time  $\tau_\sigma (=1/f_{max})$  is determined from the frequencies at the modulus  $M''$  peak maxima. The decoupling index,  $R_r$  is obtained by extrapolating the  $\log f_{max}$  versus  $1000/T$  curve to  $T_g$  and assuming the structural relaxation time  $\tau_\sigma$  equal to 200 s [109, 110, 111]. The calculated values of  $R_r(T_g)$  for different samples of first series x (BaO:1.5 Ag<sub>2</sub>O)-(95-x) V<sub>2</sub>O<sub>5</sub>- 5TeO<sub>2</sub> are given in Table.6.4. It may be noted from the values in the table that  $R_r(T_g)$  decreases with the increase of modifier content i.e., BaO and Ag<sub>2</sub>O and shows a maximum for x=30 mol % sample. This observation is in agreement with the variation of the conductivity with the modifier content as discussed earlier. The decrease in the calculated values of  $R_r(T_g)$  with the increase in the modifier content suggests that the motion of Ag<sup>+</sup> ions is coupled more and more with the viscous motion of the glass network suggesting a decrease in the conductivity with the increase in the

**Table.6.4: Glass decoupling index values for three different glass series.**

First series		Second series		Third series	
x (mol%)	$R_{\tau}(T_g)$	y (mol%)	$R_{\tau}(T_g)$	z (mol%)	$R_{\tau}(T_g)$
25	$2.52 \times 10^9$	20	$1.26 \times 10^9$	25	$3.99 \times 10^7$
30	$6.32 \times 10^9$	25	$2.52 \times 10^8$	30	$1.59 \times 10^8$
35	$3.99 \times 10^8$	30	$7.96 \times 10^7$	35	$3.99 \times 10^8$
40	$5.02 \times 10^7$	35	$2.00 \times 10^8$	40	$6.32 \times 10^8$
45	$3.17 \times 10^7$	40	$5.02 \times 10^8$	45	$1.00 \times 10^9$
		45	$1.26 \times 10^9$	50	$1.26 \times 10^9$
		50	$3.56 \times 10^9$	55	$1.59 \times 10^9$
		55	$5.64 \times 10^9$	60	$2.52 \times 10^9$

modifier content.

The calculated values of  $R_{\alpha}(T_g)$  for the second series 10 BaO-y Ag<sub>2</sub>O- (85-y) V<sub>2</sub>O<sub>5</sub>-5 TeO<sub>2</sub> are given in Table.6.4 for different samples. Observing the data, it is clear that upto 30 mol % of Ag<sub>2</sub>O,  $R_{\alpha}(T_g)$  decreases with increasing modifier Ag<sub>2</sub>O while above 30 mol % of Ag<sub>2</sub>O, it starts increasing. This suggests that the motion of Ag<sup>+</sup> ions is coupled more and more with the viscous motion of the glass network upto 30 mol % of Ag<sub>2</sub>O, after which, decoupling with the glass network increases with increasing Ag<sub>2</sub>O content. The variation of conductivity is also in agreement with the above result, as it is also decreasing upto 30 mol % and then starts increasing as Ag<sub>2</sub>O further increases. Glass decoupling index  $R_{\alpha}(T_g)$  values for third series at room temperature for different samples increases continuously with increasing Ag<sub>2</sub>O content. It means that the motion of Ag<sup>+</sup> ions is decoupled more and more with the viscous motion of the glass network as we increase Ag<sub>2</sub>O in this glass series. This is also in agreement with the conductivity results, as the conductivity of this series increases continuously with increasing modifier content Ag<sub>2</sub>O. Other Ag<sup>+</sup> ion conducting glasses [124, 114] show high values of  $R_{\alpha}(T_g)$ , in the range of 10<sup>12</sup>, which is quite high than our systems. This means that the motions of the mobile Ag<sup>+</sup> ions are extremely decoupled from the frame work ions whose contribution to the viscosity is dominant.

## References:

- [1] J. E. Bauerle, *J. Phys. Chem. Solids* 30 (1969) 2657.
- [2] J. R. Macdonald (ed.) 1987, *Impedance spectroscopy emphasizing solid state materials and systems* (New York Wiley).
- [3] G. H. Sluyter, A series of papers entitled "Impedance spectroscopy of Galvanic cell", *Rec. Trav. Cbiem*, 79 1092 1101 (1960).
- [4] D. R. Franceschetti, P. C. Shipe, *Solid State Ionics* 11 (1984) 285.
- [5] A. K. Jonscher, J. M. Reau, *J. Mat. Sci.* 13 (1978) 563.
- [6] A. K. Jonscher, *Phys. Thin Films* 11 (1980) 232.
- [7] K. W. Wagner, *Ann d Physik*, 40 (1913) 817.
- [8] J. Schrama, *On the Phenomenological theory of Linear Relaxation Processes*, Ph.D Thesis, (1957), University of Leiden, Netherlands.
- [9] N. G. Mc Crum, B. E. Read, G. Williams, "Anelastic and Dielectric effects in Polymeric Solids" (1967), Wiley London.
- [10] P. B. Macedo, C. T. Moynihan, R. Bose, *J. Phys. Chem. Glasses* 13 (1972) 171-179.
- [11] I. M. Hodge, M. D. Ingram, A. R. West, *J. Electroanal Chem.* 58 (1975) 429-432.

- [12] I. M. Hodge, M. D. Ingram, A. R. West, *J. Electroanal Chem.* 74 (1976) 125-143.
- [13] K. S. Cole, R. H. Cole, *J. Chem. Phys.* 9 (1941) 341-351.
- [14] M. Venkateswarlu, K. N. Reddy, B. Rambabu, N. Satyanarayana, *Solid State Ionics*, 127 (2000) 177-184.
- [15] K. Sebastian, G. H. Frischat, *Phys. Chem. Glasses* 33, 5 (1992) 199.
- [16] K. Hariharan, R. Kaushik, *J. Mater. Sci.* 22(1987) 3335.
- [17] K. Singh, G. Chiodelli, A. Magistris, *J. Power Sources* 58 (1996) 103.
- [18] A. K. Arof, *J. Power Sources* 52 (1994) 129.
- [19] V. C. Veeranna Gowda, R. V. Anavekar, *J. Mater. Sci.* 42 (2007) 3816-3824.
- [20] S. A. Suthanthiraj, V. Matthew, *Ionics* 14 (2008) 79-83.
- [21] A. K. Jonscher, *Dielectric Relaxation in Solids*, Chelsea Dielectric Press, London, 1983.
- [22] A. Hooper, *Application of ac measurement and analysis technique to material research*, AERER, 1980, pp 89-100.
- [23] S. Jayaseelan, P. Murlidharan, M. Venkateswarlu, N. Satyanarayana, *Mater. Chem. Phys.* 87 (2004) 370-377.
- [24] M. R. S. Abouzari, F. Berkemeier, G. Schmitz, D. Wilmer, *Solid State*

- Ionics, 180 (2009) 922-927.
- [25] J. B. Jorcin, M. E. Orazem, N. Pebere, B. Tribollet, *Electrochim. Acta* 51 (2006) 1473.
- [26] F. Berkemeier, M. S. Abouzari, G. Schmitz, *Phys. Rev. B*, 76 (2007) 024205.
- [27] M. Wasiucionek, J. E. Garbarczyk, B. Wnetrzewski, P. Machowski, W. Jakubowski, *Solid State Ionics* 92 (1996) 155-160.
- [28] J. Kawamura, S. Rikito, M. Shinya, M. Shimoji, *Solid State Ionics* 25 (1987) 155.
- [29] M. D. Ingram, *Phys. Chem. Glasses* 28 (1987) 215.
- [30] N. Satyanarayan, A. Karthikeyan, M. Venkateswarlu, *J. Mater. Sci.* 31 (1996) 5471.
- [31] B. V. R. Chowdari, R. Gopalkrishnan, S. H. Goh, K. L. Tan, *J. Mater. Sci.* 23 (1988) 1248.
- [32] M. C. R. Sastri, K. J. Rao, *Solid State Ionics* 44 (1991) 187.
- [33] R. S. Kumar, K. Hariharan, *Mat. Chem. & Phys.* 60 (1999) 28-38.
- [34] R. S. Kumar, K. Hariharan, *Solid State Ionics*, 104 (1997) 227-236.
- [35] T. Nishida, H. Ide, Y. Takashima, T. Yagi, S. Tomariguchi, T. Ishizuka, A.

- Sakai, *J. Mater. Sci.* 24 (1989) 1687-1692.
- [36] S. S. Das, C. P. Gupta, V. Srivastava, *Ionics* 11 (2005) 423.
- [37] R. A. Montani, A. Lorento, M. A. Vincenzo, *Solid State Ionics* 130 (2000) 91-95.
- [38] J. C. Bazan, *Solid State Ionics* 86-88 (1996) 497.
- [39] B. Roling, A. Happe, K. Funke, M. D. Ingram, *Phys. Rev. Lett.* 78 (1997) 2160.
- [40] D. L. Sidebottom, *Phys. Rev. Lett.* 82 (1999) 3653.
- [41] T. B. Schroder, J. C. Dyre, *Phys. Rev. Lett.* 84 (2000) 310.
- [42] A. Ghosh, A. Pan, *Phys. Rev. Lett.* 84 (2000) 2188.
- [43] A. K. Jonscher, *Nature* 267 (1977) 673.
- [44] A. K. Jonscher, *J. Mater. Sci.* 16 (1981) 2037.
- [45] A. S. Nowick, B. S. Lim, A. V. Vaysleyb, *J. Non-Cryst. Solids* 172-174 (1994) 1243.
- [46] H. Jain, J. N. Mundy, *J. Non-Cryst. Solids* 91 (1987) 315.
- [47] M. Ganguli, M. H. Bhat, K. J. Rao, *Mater. Res. Bull.* 34 (1999) 1757.
- [48] K. Funke, *Progr. Solid State Chem.* 22 (1993) 111.
- [49] S. R. Elliot, A. P. Owens, *Philos. Mag. B* 60 (1989) 777.

- [50] P. Maass, J. Petersen, A. Bunde, W. Dietrich, H. E. Roman, *Phys. Rev. Lett.* 66 (1991) 52.
- [51] J. Peterson, W. Dietrich, *Philos. Mag. B* 65 (1992) 231.
- [52] D. P. Almond, G. K. Duncan, A. R. West, *Solid State Ionics* 8 (1983) 159.
- [53] D. P. Almond, A. R. West, *Solid State Ionics*, 9/10 (1983) 277.
- [54] D. P. Almond, A. R. West, *Solid State Ionics*, 11 (1983) 57.
- [55] K. P. Padmasree, D. K. Kanchan, *Mat. Chem. & Phys.*, 91 (2005) 551-557.
- [56] B. V. R. Chowdari, R. Gopalakrishnan, *Solid State Ionics* 23 (1987) 225-233.
- [57] R. A. Huggins, in, *Diffusion in Solids: Recent Development*, Eds. A. S. Nowick and J. J. Burton, Academic Press (1975) 445.
- [58] D. P. Almond, A. R. West, *Nature (London)* 306 (1983) 453.
- [59] E. F. Hairetdinov, N. F. Uvarov, H. K. Patel, S. W. Martin, *Phys. Rev. B* 50 (1994) 13 259.
- [60] B. Roling, M. D. Ingram, M. Lange, K. Funke, *Phys. Rev. B* 56 (1997) 13 619.
- [61] D. L. Sidebottam, P. F. Green, R. K. Brow, *Phys. Rev. B* 56 (1997) 170.
- [62] H. E. Stanley, "Introduction to phase transitions and critical phenomena"  
Oxford University Press, New York, 1971.

- [63] D. L. Sidebottam, Phys. Rev. Lett. 83 (1999) 983.
- [64] A. Ghosh, M. Sural, Europhysics. Lett. 47 (1999) 688.
- [65] K. L. Ngai, J. Chem. Phys. 110 (1999) 10576.
- [66] J. C. Dyre, J. Non-Cryst. Solids 88 (1986) 271.
- [67] S. Bhattacharya, A. Ghosh, J. Chem. Phys. 123 (2005) 124514.
- [68] M. Porto, P. Maass, M. Meyer, A. Bunde, W. Dieterich, Phys. Rev. B 61  
(2000) 6057.
- [69] L. L. Hench, J. K. West, "Principles of Electronic Ceramics" John Wiley &  
Sons, New York, 1990.
- [70] V. Raghvan, Material Science & Engineering"- A First Course", Prentice-  
Hall, New Delhi, 1998.
- [71] S. R. Elliot, Phys. of Amorphous Materials (2<sup>nd</sup> ed.), Longman, New York,  
1990.
- [72] A. K. Jonscher, Phys. D Appl. Phys. 32 R 57 (1999).
- [73] A. K. Jonscher, Phys. State Solidi (a) 32 (1975) 665.
- [74] A. K. Jonscher, J. Mater. Sci. 13 (1978) 553.
- [75] C. P. Smith, "Dielectric behavior and structure", Mc Graw Hill, New York,  
1995.

- [76] N. U. Haque, R. A. Hashmi, M. K. Anis, *J. Non-Cryst. Solids* 175 (1994) 244.
- [77] A. H. Verhof, H. W. den Hartog, *Solid State Ionics* 68 (1994) 305.
- [78] M. Davidovic, T. Cajkoski, D. Cajkovski, V. Likar-Smiljanic, R. Biljic, V. B. Mioc, Z. Nedic, *Solid State Ionics* 147 (2002) 123.
- [79] R. A. Hashmi Noor-Ul Haque, N. Bano, M. K. Anis, *J. Mat. Sci.* 29 (1994) 6615.
- [80] D. L. Sidebottam, B. Roling, K. Funke, *Phys. Rev. B* 63 (2000) 024301-1.
- [81] R. Kaushik, K. Hariharan, S. Radhakrishnan, *J. Appl. Electrochem.* 17 (1987) 813.
- [82] B. V. R. Chowdari, K. Radhakrishnan, *J. Non-Cryst. Solids* 110 (1989) 101.
- [83] B. V. R. Chowdari, R. Gopalakrishnan, *Solid State Ionics* 18 & 19 (1986) 483.
- [84] R. D. Armstrong, K. Taylor, *Electronal. Chem. Interface Electrochem.* 63 (1975) 9.
- [85] J. M. Stevels, in: S. Flugge (Ed.), *Handbuch der Physik*, Springer, Bertin, (1956), pg. 350.
- [86] M. Venkateswarlu, K. N. Reddy, B. Rambabu, N. Satyanarayana, *Solid State*

- Ionics 127 (2000) 177.
- [87] D. K. Durga, N. Veeraiah, *J. Mater. Sci.* 36 (2001) 5625-5632.
- [88] C. K. Suman, K. Prasad, R. N. P. Chowdary, *Mat. Chem. & Phys.* 87 (2003) 140.
- [89] V. Ravi Kumar, N. Veeraiah, *J. Phys. Chem. Solids*, 1 (1998) 91-99.
- [90] C. T. Moynihan, L. P. Boesch, N. L. Laberge, *Phys. Chem. Glasses*, Vol. 14, (1973) 122-125.
- [91] C. A. Angell, *Chem. Rev.* 90 (1990) 523.
- [92] S. R. Elliott, *Physics of Amorphous Materials*, Longman, London (1984).
- [93] S. R. Elliott, *J. Non-Cryst. Solids*, 170 (1994) 97.
- [94] V. Provenzano, L. P. Boesch, V. Volterra, C. T. Moynihan, P. B. Macedo, *J. Am. Ceram. Soc.* 55 (1972) 492.
- [95] C. T. Moynihan, L. P. Boesch, N. L. Laberge, *Phys. Chem. Glasses*, 14, 6 (1974) 639.
- [96] F. S. Howell, R. A. Bose, P. B. Macedo, C. T. Moynihan, *J. Phys. Chem.* 78, 6 (1974) 639-648.
- [97] J. H. Ambrus, C. T. Moynihan, P. B. Macedo, *J. Phys. Chem.* 76, 22 (1972) 3287.

- [98] K. L. Ngai., S.W. Martin., Phys. Rev. B 40 (1989) 10550.
- [99] K. L. Ngai., J. N Mundy, H. Jain, G. Balzer-Jollenbeck, O. Kanert, Phys. Rev. B 39 (1989) 6169.
- [100] R. Kohlraush, Prog. Ann. (Leipzig) 12 (1847) 393.
- [101] G. Willaims, D. C. Watts, Trans. Faraday Soc. 66 (1970) 80.
- [102] K. L. Ngai, H. Jain, Solid State Ionics 18/19 (1986) 362.
- [103] K. C. Shobha, K. J. Rao, Solid State Ionics, 81 (1995) 145-156.
- [104] M. Ganguli, K. J. Rao, J. Non-Cryst. Solids, 243 (1999) 251-267.
- [105] J. M. Reau, X. Y. Jun, J. Senegas, Solid State Ionics, 95 (1997) 191-199.
- [106] S. Ghosh, A. Ghosh, Solid State Ionics, 149 (2002) 67-72.
- [107] A. S. Nowick, B. S. Lim, J. Non-Cryst. Solids 172-174 (1994) 1389-1394.
- [108] J. M. Bobe, J. M. Reau, J. Senegas, M. Poulain, Solid State Ionics, 82 (1995) 39-52.
- [109] J. M. Reau, S. Rossignol, B. Tanguy, J. M. Rojo, P. Herrero, R. M. Rojas, J. Sanz, Solid State Ionics, 74 (1994) 65.
- [110] M. Sural, A. Ghosh, Solid State Ionics, 130 (2000) 259.
- [111] M, Sural, A. Ghosh, Solid State Ionics 120 (1999) 27.
- [112] M. D. Ingram, J. Am. Ceram. Soc. 63 (1980) 248.

- [113] J. Kawamura, M. Shimoji, *Mat. Chem. & Phys.* 23 (1989) 99.
- [114] C. Lin, H. G. K. Sundar, C. A. Angel, *Solid State Ionics* 18-19 (1986) 442.
- [115] H. Naili, N. Zouari, T. Mhiri, A. Daoud, *J. Mol. Struct.* 519 (2000) 143.
- [116] H. K. Patel, S. W. Martin, *Phys. Rev. B* 45 (1992) 10292.
- [117] H. Jain, *J. Non- Cryst. Solids* 131/133 (1991) 961.
- [118] K. L. Ngai, *Comments Solid State Phys.* 9 (1979) 127.
- [119] B. Roling, *Solid State Ionics* 105 (1998) 185.
- [120] A. R. West, D. C. Sinclair, N. Hirose, *J. Electroceram.* 1 (1997) 65.
- [121] H. Takahashi, Y. Hiki, T. Sakuma, Y. Morii, *Solid State Ionics* 90 (1996) 125.
- [122] M. Tachez, R. Mercier, J. P. Malugani, P. Chieux, *Solid State Ionics* 25 (1987) 263.
- [123] K. L. Ngai, *J. Phys. (IV)* C2 (1992) 61.
- [124] C. A. Angell, *Solid State Ionics* 18/19 (1986) 72.
- [125] C. A. Angell, *Solid State Ionics* 9/10 (1983) 3.